NASA TECHNICAL MEMORANDUM

NASA TM X-3129

NASA TM X-3129

EXPERIMENTAL AERODYNAMIC CHARACTERISTICS FOR BODIES OF ELLIPTIC CROSS SECTION AT ANGLES OF ATTACK FROM 0° TO 58° AND MACH NUMBERS FROM 0.6 TO 2.0

Leland H. Jorgensen and Edgar R. Nelson

Ames Research Center

Moffett Field, Calif. 94035

NATIONAL AERONAUTICS AND SPACE ADMINISTRATION • WASHINGTON, D. C. • FEBRUARY 1975

1. Report No.	2. Government Accession No.	3. Recipient's Catalog No.
TM X-3129		

4. Title and Subtitle	5. Report Date
EXPERIMENTAL AERODYNAMIC CHARACTERISTICS FOR BODIES OF ELLIPTIC CROSS SECTION AT ANGLES OF ATTACK FROM 0° TO 58° AND MACH NUMBERS FROM 0.6 TO 2.0	February 1975
	6. Performing Organization Code

7. Author(s)	8. Performing Organization Report No.
Leland H. Jorgensen and Edgar R. Nelson	A-5756
	10. Work Unit No.
	505-06-81

9. Performing Organization Name and Address	11. Contract or Grant No.
NASA Ames Research Center Moffett Field, Calif. 94035 and ARO, Inc., Moffett Field, Calif. 94035	

12. Sponsoring Agency Name and Address	13. Type of Report and Period Covered
National Aeronautics and Space Administration Washington, D. C., 20546	Technical Memorandum
	14. Sponsoring Agency Code

15. Supplementary Notes

16. Abstract

An experimental investigation was conducted in the Ames 6- by 6-Foot Wind Tunnel to measure the static aerodynamic characteristics for two bodies of elliptic cross section and for their equivalent body of revolution. The equivalent body of revolution had the same length and axial distribution of cross-sectional area as the elliptic bodies. It consisted of a tangent ogive nose of fineness ratio 3 followed by a cylinder with a fineness ratio of 7. For the first body of elliptic cross section, the ratio of the semimajor axis to semiminor axis was held constant at 2 all along the body length. For the second elliptic body the nose was unchanged, but the aftersection was changed as follows: The cross-sectional axis ratio a/b was decreased from 2 to 1 over an axial distance of about 1.66 diam. Then, at this position, the a,b axis system was rotated 90°, and the a/b ratio was increased back to 2 over the next 2.34 diam in length. Over the last length of three body diam, this rotated a/b ratio was held constant at 2.

All bodies were tested at Mach numbers of 0.6, 0.9, 1.2, 1.5, and 2.0 at angles of attack from 0° to 58°. The Reynolds numbers, based on base diameter, were 2.2×10^5, 4.3×10^5, and 6.5×10^5 at $M = 0.6$ and 0.9 and 3.8×10^5 at $M = 1.2$, 1.5, and 2.0. The elliptic bodies were tested at roll angles of 0° (flattest side of nose pitching against the flow) and 90°.

The data demonstrate that the aerodynamic characteristics can be significantly altered by changing the body cross section from circular to elliptic and by rolling the body from 0° to 90°. For example, the first elliptic body (with a constant cross-sectional axis ratio of 2) developed at zero roll about twice the normal force developed by the equivalent body of revolution. At some angles of attack greater than about 25°, side forces and yawing moments were measured in spite of the fact that the bodies were tested at zero angle of sideslip. The side-force and yawing-moment coefficients decreased with an increase in Mach number and essentially disappeared for all the bodies at Mach numbers greater than 1.2. From the standpoint of reducing undesirable side forces at high angles of attack, it is best to have the flattest side of the nose of the elliptic bodies pitching against the stream crossflow. The effect of Reynolds number was also the least significant for both elliptic bodies when the flattest side of the nose was pitched against the stream crossflow.

17. Key Words (Suggested by Author(s))	18. Distribution Statement
High angle-of-attack aerodynamics Elliptic cross sections Body aerodynamics	Unclassified—Unlimited STAR Category - 02

19. Security Classif. (of this report)	20. Security Classif. (of this page)	21. No. of Pages	22. Price*
Unclassified	Unclassified	81	$4.75

*For sale by the National Technical Information Service, Springfield, Virginia 22151

NOMENCLATURE

All forces and moments are referred to the body axis coordinate system. Because the data are computer plotted, both the conventional symbol and the plot symbol are given.

Symbol	Plot symbol	Definition
A_r		reference area = body base area = 34.26 cm^2 (5.31 in.^{2})
a,b		semimajor and semiminor axes of elliptic cross section
C_A	CA	axial-force coefficient, $C_{A_{bal}} - C_{A_{base}}$
$C_{A_{bal}}$		balance axial-force coefficient, $\frac{F_A}{qA_r}$
$C_{A_{base}}$		base-pressure force coefficient, $\frac{(p - p_{base})}{q}$
C_m		pitching-moment coefficient about balance center $4d$ from body base, $\frac{\text{pitching moment}}{qA_rX}$
C_N	CN	normal-force coefficient, $\frac{F_N}{qA_r}$
C_n	CYN	yawing-moment coefficient about balance center $4d$ from body base, $\frac{\text{yawing moment}}{qA_rX}$
C_Y	CY	side-force coefficient, $\frac{F_Y}{qA_r}$
d		body base diameter, 6.60 cm (2.60 in.)
F_A,F_N,F_Y		axial, normal, and side force, respectively
ℓ		body length
ℓ_N		nose length
M	MACH	free-stream Mach number
p		free-stream static pressure

p_{base}		base pressure
q		free-stream dynamic pressure
$\frac{Re}{L}$		unit Reynolds number, million/m
Re	RE	Reynolds number based on d
X		reference length = d = 6.60 cm (2.60 in.)
$\frac{x_{ac_N}}{d}$	XACN/D	distance (in diam) from body base to aerodynamic force center in normal-force plane, $\left(\frac{C_m}{C_N}+\frac{x_m}{X}\right)$
x_m		distance from body base to balance moment reference = $4d$ = 26.42 cm (10.40 in.)
α	ALPHA	angle of attack, deg
ϕ	PHI	angle of bank about body longitudinal axis, deg

Configuration Code

Symbol	Plot symbol	Component
B_1	B1	basic circular body (tangent ogive nose of fineness ratio 3 with cylinder aftersection of fineness ratio 7)
B_2	B2	body with elliptic cross section of constant $\frac{a}{b}$ = 2
B_3	B3	body with elliptic cross section of variable $\frac{a}{b}$
$\phi = 0°$	PHI = 0	body banked 0° about longitudinal axis (see fig. 1)
$\phi = 90°$	PHI = 90	body banked 90° about longitudinal axis (see fig. 1)

EXPERIMENTAL AERODYNAMIC CHARACTERISTICS FOR BODIES OF ELLIPTIC CROSS SECTION AT ANGLES OF ATTACK FROM 0° TO 58° AND MACH NUMBERS FROM 0.6 TO 2.0

Leland H. Jorgensen and Edgar R. Nelson*

Ames Research Center

SUMMARY

An experimental investigation was conducted in the Ames 6- by 6-Foot Wind Tunnel to measure the static aerodynamic characteristics for two bodies of elliptic cross section and for their equivalent body of revolution. The equivalent body of revolution had the same length and axial distribution of cross-sectional area as the elliptic bodies. It consisted of a tangent ogive nose of fineness ratio 3 followed by a cylinder with a fineness ratio of 7. For the first body of elliptic cross section, the ratio of the semimajor axis to semiminor axis was held constant at 2 all along the body length. For the second elliptic body the nose was unchanged, but the aftersection was changed as follows: The cross-sectional axis ratio a/b was decreased from 2 to 1 over an axial distance of about 1.66 diam. Then, at this position, the a,b axis system was rotated 90°, and the a/b ratio was increased back to 2 over the next 2.34 diam in length. Over the last length of three body diam, this rotated a/b ratio was held constant at 2.

All bodies were tested at Mach numbers of 0.6, 0.9, 1.2, 1.5, and 2.0 at angles of attack from 0° to 58°. The Reynolds numbers, based on base diameter, were 2.2×10^5, 4.3×10^5, and 6.5×10^5 at $M = 0.6$ and 0.9 and 3.8×10^5 at $M = 1.2$, 1.5, and 2.0. The elliptic bodies were tested at roll angles of 0° (flattest side of nose pitching against the flow) and 90°.

The data demonstrate that the aerodynamic characteristics can be significantly altered by changing the body cross section from circular to elliptic and by rolling the body from 0° to 90°. For example, the first elliptic body (with a constant cross-sectional axis ratio of 2) developed at zero roll about twice the normal force developed by the equivalent body of revolution, whereas at 90° roll it developed only about half the normal force.

At some angles of attack greater than about 25°, side forces and yawing moments were measured in spite of the fact that the bodies were tested at zero angle of sideslip. The side-force and yawing-moment coefficients decreased with an increase in Mach number and essentially disappeared for all the bodies at Mach numbers greater than 1.2.

From the standpoint of reducing undesirable side forces at high angles of attack, it was best to have the flattest side of the nose of the elliptic bodies pitching against the stream crossflow. The effect of Reynolds number was also the least significant for both elliptic bodies when the flattest side of the nose was pitched against the stream crossflow.

---

*Project Engineer, ARO, Inc., Moffett Field, Calif. 94035.

INTRODUCTION

High angle-of-attack aerodynamics is increasing in importance because of the demand for greater maneuverability of missiles and military aircraft. There is great need for experimental force and moment data for bodies of circular and noncircular cross section alone and with lifting surfaces at Mach numbers from subsonic to supersonic.

This report presents experimental force and moment data for bodies of elliptic cross section at angles of attack from 0° to 58° and at Mach numbers from 0.6 to 2.0. Data were presented for some similar bodies in 1958 (ref. 1), but the results were limited to angles of attack less than 20° and Mach numbers from 2 to 4.

TEST FACILITY

The experimental investigation was conducted in the Ames 6- by 6-Foot Wind Tunnel, a variable pressure, continuous flow, closed return type facility. The nozzle ahead of the test section consists of an asymmetric sliding block that permits a continuous variation of Mach number from 0.6 to 2.3. The test section has a perforated floor and ceiling to remove boundary layer for transonic testing.

MODELS AND BALANCE

The dimensions of the three models tested are shown in figure 1(a), and the planform views of the models as they were oriented (in five different configurations) for the tests are shown in figure 1(b). The basic circular body B_1 consisted of a circular-arc tangent ogive nose of fineness ratio 3 followed by a cylindrical aftersection of fineness ratio 7. Bodies B_2 and B_3 had elliptic cross sections, and these bodies had the same length and axial distribution of cross-sectional area as B_1. Hence, the fineness ratio of $\ell/d = 10$ for B_1 was also the equivalent fineness ratio for B_2 and B_3, and all bodies had equal volumes. For B_2, the ratio of the semimajor to the semiminor cross-section axis, $a/b = 2$, was held constant along the body length. Bodies B_1 and B_2 were investigated in 1958 (ref. 1) for angles of attack from about 0° to 20° and Mach numbers from 2 to 4. Body B_3, which was new to the present investigation, consisted of the same nose shape as B_2 but had an afterbody section of variable a/b over four body diameters in length and a constant $a/b = 2$ over the rear three body diameters (see fig. 1(a)).

Bodies B_1 and B_2 were constructed of stainless steel, and B_3 was constructed of aluminum. Photographs of B_3 are shown in figure 2. All models were sting mounted through the base on a six-component strain-gage "Task" balance. The balance force center was located inside each body 4 diam forward of the base.

TESTS AND DATA REDUCTION

All configuration arrangements shown in figure 1(b) were tested at angles of attack from 0° to about 58°. Two model support setups were used – one for $\alpha = 0°$ to about 27°, and the other for $\alpha = 27°$ to 58°. Photographs of these setups are shown in reference 2.

The models were tested at the following Mach numbers and Reynolds numbers:

M	$Re \times 10^{-6}$ (m)	$Re \times 10^{-6}$ (ft)	$Re \times 10^{-5}$ (based on d)
0.6, 0.9	3.28	1.0	2.3
0.6, 0.9	6.56	2.0	4.3
0.6, 0.9	9.84	3.0	6.5
1.2, 1.5, 2.0	5.74	1.75	3.8

Six-component aerodynamic force and moment data were measured at each test condition, and all data were reduced to coefficient form and referred to the body axis coordinate system. The average base pressure from four base pressure tubes (at sides, top, and bottom of base) was used to compute the base drag, which was subtracted from the total axial-force balance measurement, so that the data presented are for forces ahead of the body base. Rolling-moment coefficients were generally negligible and are omitted from this report. Normal-force aerodynamic centers were computed from the normal-force and pitching-moment coefficients and are presented in lieu of the pitching-moment coefficients.

RESULTS AND DISCUSSION

Experimental results (figs. 3 through 24) show the effects of elliptic cross section with constant a/b along the body length, elliptic cross section with variable a/b along the body length, Reynolds number, and Mach number. Each effect is discussed briefly with the aid of plots of C_N, x_{ac_N}/d, C_Y, C_Y/C_N, and C_n versus α for $\alpha = 0°$ to 60°. Plots of C_A versus α are also presented but are not discussed. Because the models were sting supported from the rear, it is likely that the C_A data include effects of support interference.

Effect of Elliptic Cross Section with Constant a/b

In figures 3 through 7, data are presented for body B_2 which has an elliptic cross section with constant $a/b = 2$ along the entire length. The aerodynamic characteristics for B_2, oriented in roll both at $\phi = 0°$ and 90°, are compared with those for B_1, the equivalent body of revolution. The data are for the highest test Reynolds numbers, $Re = 6.5 \times 10^5$ at $M = 0.6$ and 0.9 (figs. 3 and 4) and $Re = 3.8 \times 10^5$ at $M = 1.2$, 1.5, and 2.0 (figs. 5–7).

As expected, changes in a/b and ϕ cause significant changes in most of the aerodynamic characteristics throughout the high α range. For example, values of C_N are about twice as large for B_2 ($a/b = 2$) at $\phi = 0°$ as for B_1 ($a/b = 1$). With B_2 at $\phi = 90°$, however, the values of C_N are roughly half those for B_1. At α less than about 30°, the aerodynamic centers (x_{ac_N}/d) are

considerably farther forward on B_2 at $\phi = 90°$ than at $\phi = 0°$, but at higher α they lie at about the same location.

At all Mach numbers and angles of attack, the side-force coefficients are generally quite small or negligible for B_1 and for B_2 at $\phi = 0°$. For B_2 at $\phi = 90°$ and M up to 1.2, however, values of C_Y become significantly large at some of the higher angles of attack. At $M = 0.6$, for example, C_Y is more than twice that of C_N at $\alpha = 50°$. Generally, with an increase in M from 0.6 to 1.2, the maximum values of C_Y decrease; at $M = 1.5$ and 2.0, all values of C_Y are essentially zero throughout the α range. This side-force phenomenum at high angles of attack appears to be associated primarily with subsonic flow.

Effect of Elliptic Cross Section with Variable a/b

In figures 8 through 12, data are presented for body B_3 which has an elliptic cross section with variable a/b over part of the body length (see figs. 1 and 2). The aerodynamic characteristics for B_3, oriented in roll both at $\phi = 0°$ and 90°, are compared with those for B_1, the equivalent body of revolution. As in the previous figures, the data are for the highest test Reynolds number at each Mach number.

At all Mach numbers and angles of attack, B_3 at $\phi = 90°$ develops the greatest normal force, and the aerodynamic force center is the most rearward. With B_3 at $\phi = 0°$, the aerodynamic center is much more forward.

Large side forces and yawing moments developed only for B_3 at $\phi = 90°$ and at Mach numbers less than about 1.2 or 1.5. For example, at $M = 0.6$, (fig. 8), the maximum C_Y is about 40 percent of C_N (at $\alpha \approx 38°$), whereas at $M = 1.2$ (fig. 10), the maximum C_Y is only about 20 percent of C_N (at $\alpha \approx 27$). At $M = 1.5$, the maximum side force is near zero. Therefore, from the standpoint of reducing undesirable side forces at high α, it is best to have the flattest side of the nose (major axis, a) pitching perpendicular to the stream crossflow. This was also shown to be true for body B_2.

Effect of Reynolds Number

In figures 13 through 22, data are presented which show the effect of Reynolds number for the configurations at $M = 0.6$ and 0.9. The Reynolds numbers are 2.2×10^5, 4.3×10^5, and 6.5×10^5 based on body base diameter.

Body (B_1) with circular cross section.– For B_1, Reynolds number Re has a significant effect on the variation of C_N and x_{ac_N}/d with α at $M = 0.6$ (fig. 13). At the higher angles of attack, C_N generally decreases with an increase in Re. The effect at $M = 0.9$, however, is smaller (fig. 14). At first observation, it might be surprising that there would be this effect at $M = 0.6$ but not so much at $M = 0.9$ for such a small range of Reynolds numbers. An explanation probably can be made on the basis of crossflow theory (e.g., ref. 3 or 4). From the theory, for crossflow Mach numbers ($M \sin \alpha$) less than critical (about 0.4), a change in crossflow Reynolds number ($Re \sin \alpha$) from about 2×10^5 to 5×10^5 can decrease the crossflow drag coefficient significantly and hence the normal

force. In the present investigation, for $M = 0.6$ the crossflow Mach numbers were subcritical over most of the α range, and the crossflow Reynolds numbers ranged from subcritical (less than about 2×10^5 throughout the entire α range for $Re = 2.2\times10^5$) to supercritical (greater than about 2×10^5 throughout most of the α range for $Re = 6.5\times10^5$). For this situation, crossflow theory predicts a decrease in C_N at high α with an increase in Reynolds number from 2.2×10^5 to 6.5×10^5. Crossflow theory, however, predicts little or no effect at $M = 0.9$, since the crossflow Mach number is supercritical (greater than about 0.4) for $\alpha > 30°$.

The effect of Reynolds number on the side-force and yawing-moment coefficients also appears to be more significant at $M = 0.6$ than at $M = 0.9$. Presently, this side-force phenomenon is not well understood.

Body (B_2) with elliptic cross section of constant $a/b = 2$.— For B_2 at $\phi = 0°$, Reynolds number does not significantly affect the aerodynamic characteristics (figs. 15 and 16). However, at $M = 0.6$, there is a small decrease in C_N with an increase in Re from 4.3×10^5 to 6.5×10^5 over the α range from about 25° to 50° (fig. 15).

For B_2 at $\phi = 90°$, the Reynolds number effects the aerodynamic characteristics more significantly (figs. 17 and 18). The effects on aerodynamic force center and side force are particularly significant but are not understood at present.

Body (B_3) with elliptic cross section of variable a/b.— As for B_2 at $\phi = 0°$, the Reynolds number does not significantly affect the aerodynamic characteristics for B_3 at $\phi = 0°$ (figs. 19 and 20). As for B_2 at $\phi = 90°$, there are some significant effects for B_3 at $\phi = 90°$ (figs. 21 and 22).

Both B_2 and B_3 have the same nose shape and flow orientation at $\phi = 0°$, and it is thus apparent that, from the standpoint of resisting changes in the aerodynamic characteristics due to Reynolds number, this nose shape performs best when oriented at $\phi = 0°$.

Effect of Mach Number

In Figures 23 and 24, data are presented which demonstrate the effect of Mach number on the aerodynamic characteristics for B_1 and B_2 at $\phi = 0°$. For the data at $M = 0.6$ and 0.9, the Reynolds number is 6.5×10^5, and for $M = 1.2, 1.5$, and 2.0, the Reynolds number is 3.8×10^5.

For both configurations the values of C_N at the higher angles of attack ($\alpha > 40°$) increase considerably from $M = 0.6$ to 1.2. Then, with a further increase in M to 2.0, there is generally a small decrease or little change in C_N. This trend is in accord with that which would be expected from crossflow theory (ref. 3).

The side-force and yawing-moment plots show that the side-force phenomenon at α greater than about 25° is essentially associated with subsonic Mach numbers. However, the values of C_Y (CY) and C_n (CYN) are small for these configurations at all test Mach numbers.

CONCLUSIONS

1. As expected, a change in body cross section from circular to elliptic ($a/b = 2$) and variation in body roll angle caused significant changes in most of the aerodynamic characteristics. For example, values of normal-force coefficient for an elliptic body of $a/b = 2$ at $\phi = 0°$ were about twice those for the equivalent circular body. At $\phi = 90°$ they were about one half.

2. At some angles of attack greater than about 25°, side forces and yawing moments were measured in spite of the fact that the bodies were tested at zero angle of sideslip. The side-force and yawing-moment coefficients generally decreased with an increase in Mach number and essentially disappeared for all the bodies at supersonic Mach numbers above 1.2.

3. At all test Mach numbers and angles of attack, the side-force coefficients were generally small or negligible for the circular body and the elliptic bodies at $\phi = 0°$. With the elliptic bodies at $\phi = 90°$, however, some values of side-force coefficient became as large as twice the values of normal-force coefficient at the same high angles of attack.

4. From the standpoint of reducing undesirable side forces at high angles of attack, it was found best to have the flattest side of the elliptic body nose pitching against the stream crossflow.

5. The effect of Reynolds number was also the least significant for the elliptic bodies when the flattest side of the nose was pitched against the stream crossflow.

6. There were significant effects of Reynolds number measured for the equivalent body of revolution, and the trends in the effects on the normal-force coefficients at high α were in agreement with expectations from crossflow theory.

Ames Research Center
National Aeronautics and Space Administration
Moffett Field, Calif., 94035, September 26, 1974

REFERENCES

1. Jorgensen, Leland H.: Inclined Bodies of Various Cross Sections at Supersonic Speeds. NASA MEMO 10-3-58A, 1958.

2. Jorgensen, Leland H.; and Nelson, Edgar R.: Experimental Aerodynamic Characteristics for a Cylindrical Body of Revolution With Various Noses at Angles of Attack from 0° to 58° and Mach Numbers from 0.6 to 2.0. NASA TM X-3128, 1974.

3. Jorgensen, Leland H.: Prediction of Static Aerodynamic Characteristics for Space-Shuttle-Like and Other Bodies at Angles of Attack From 0° to 180°. NASA TN D-6996, 1973.

4. Jorgensen, Leland H.: A Method for Estimating Static Aerodynamic Characteristics for Slender Bodies of Circular and Noncircular Cross Section Alone and With Lifting Surfaces at Angles of Attack From 0° to 90°. NASA TN D-7228, 1973.

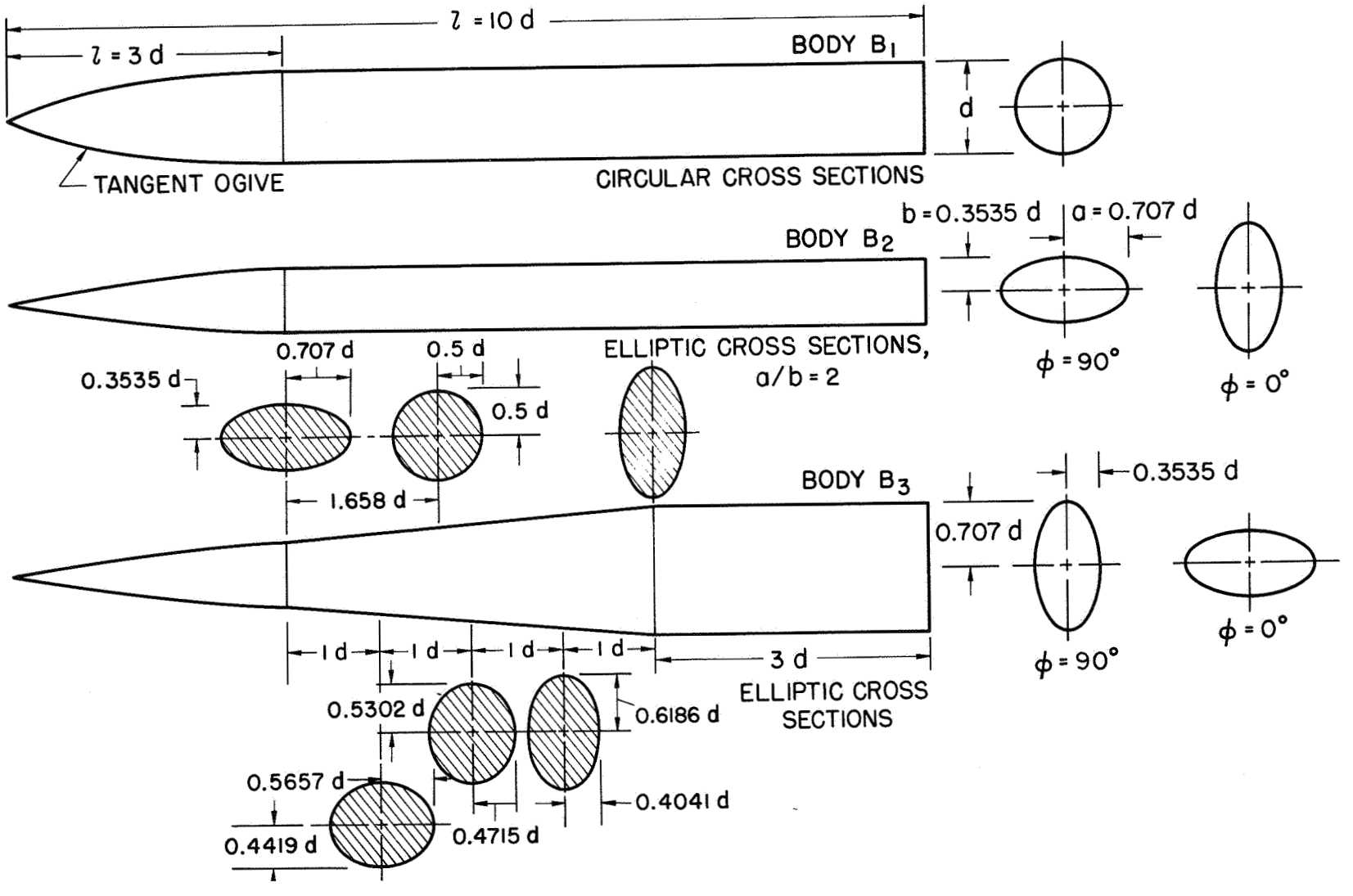

(a) Model dimensions with $d = 6.6$ cm (2.6 in.)

Figure 1.– Model dimensions and planform views of configurations tested.

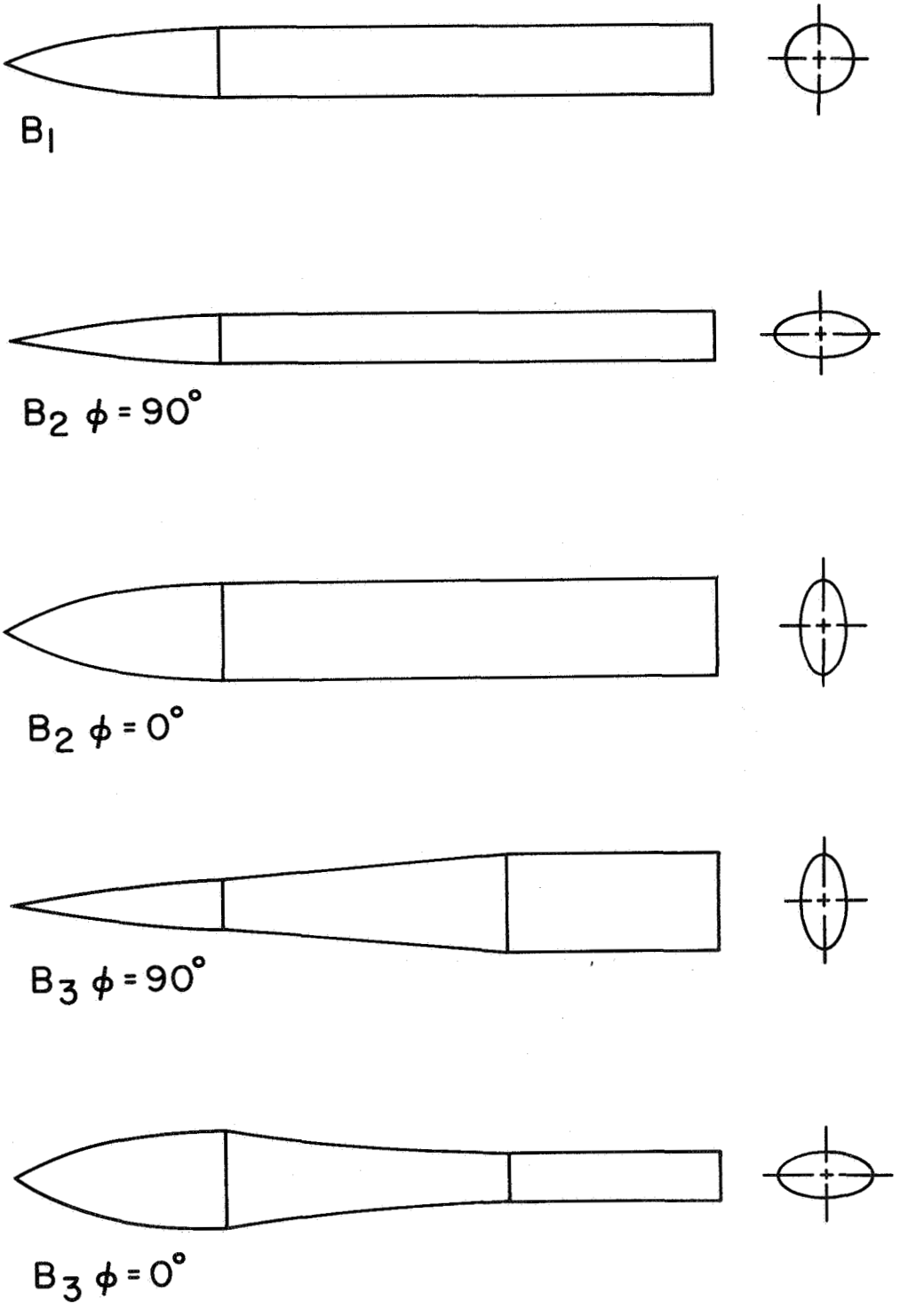

(b) Planform views of configurations tested.

Figure 1.– Concluded.

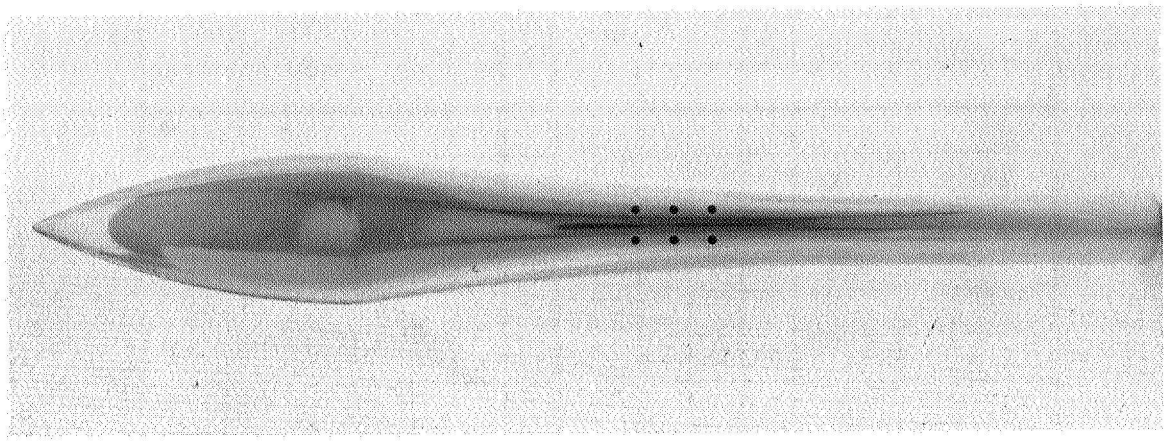

(a) Planform view of B_3 at $\phi = 0°$

Figure 2.– Photographs of aluminum body B_3.

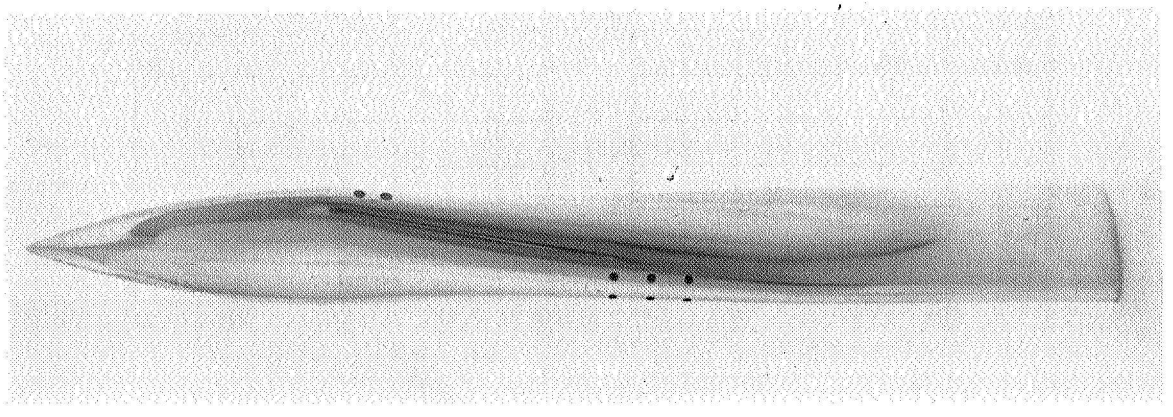

(b) Three-quarter view

Figure 2.– Concluded.

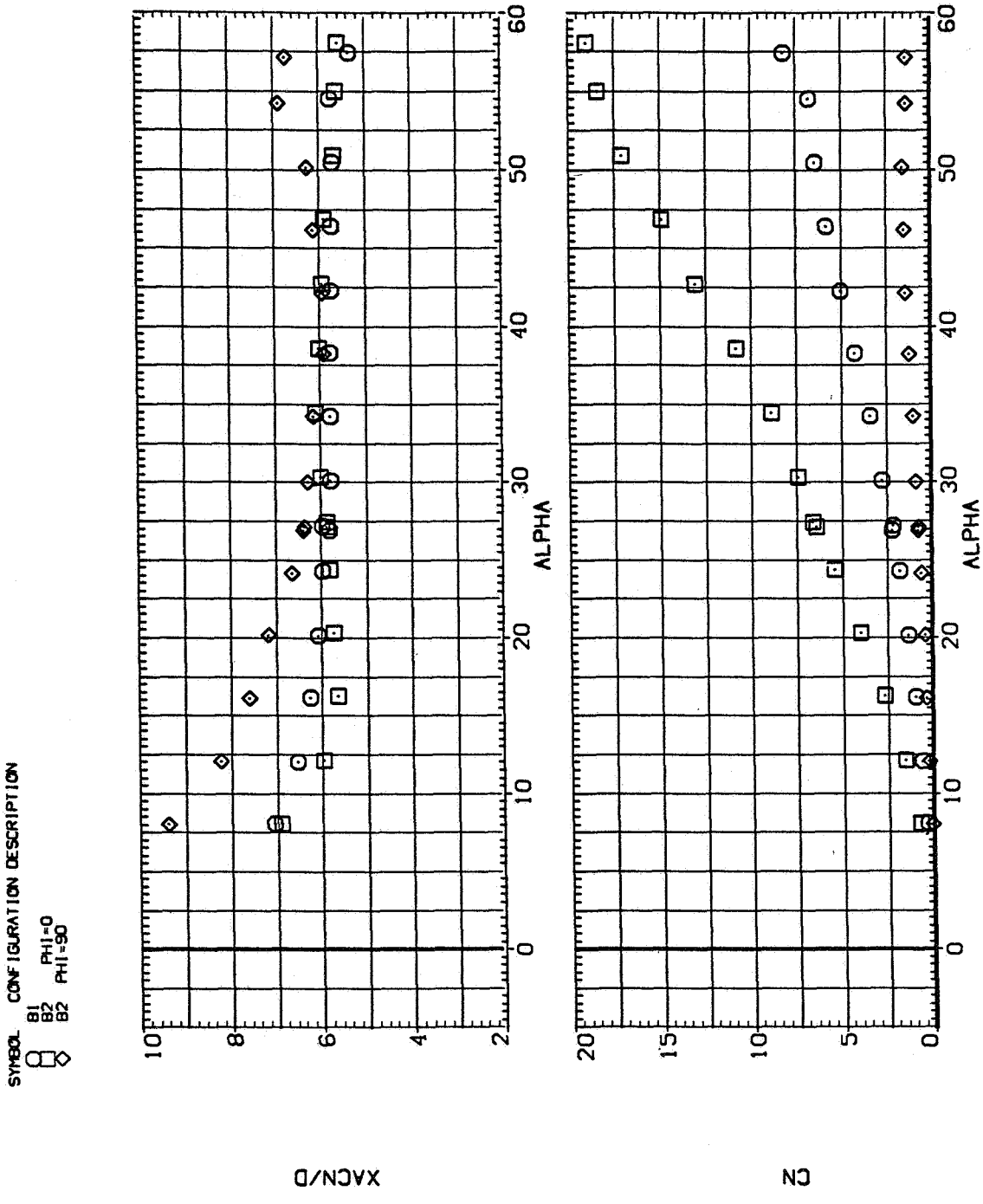

(a) x_{ac_N}/d and C_N versus α

Figure 3.– Effect of elliptic cross section with constant a/b; $M = 0.6$, $Re = 6.5 \times 10^5$.

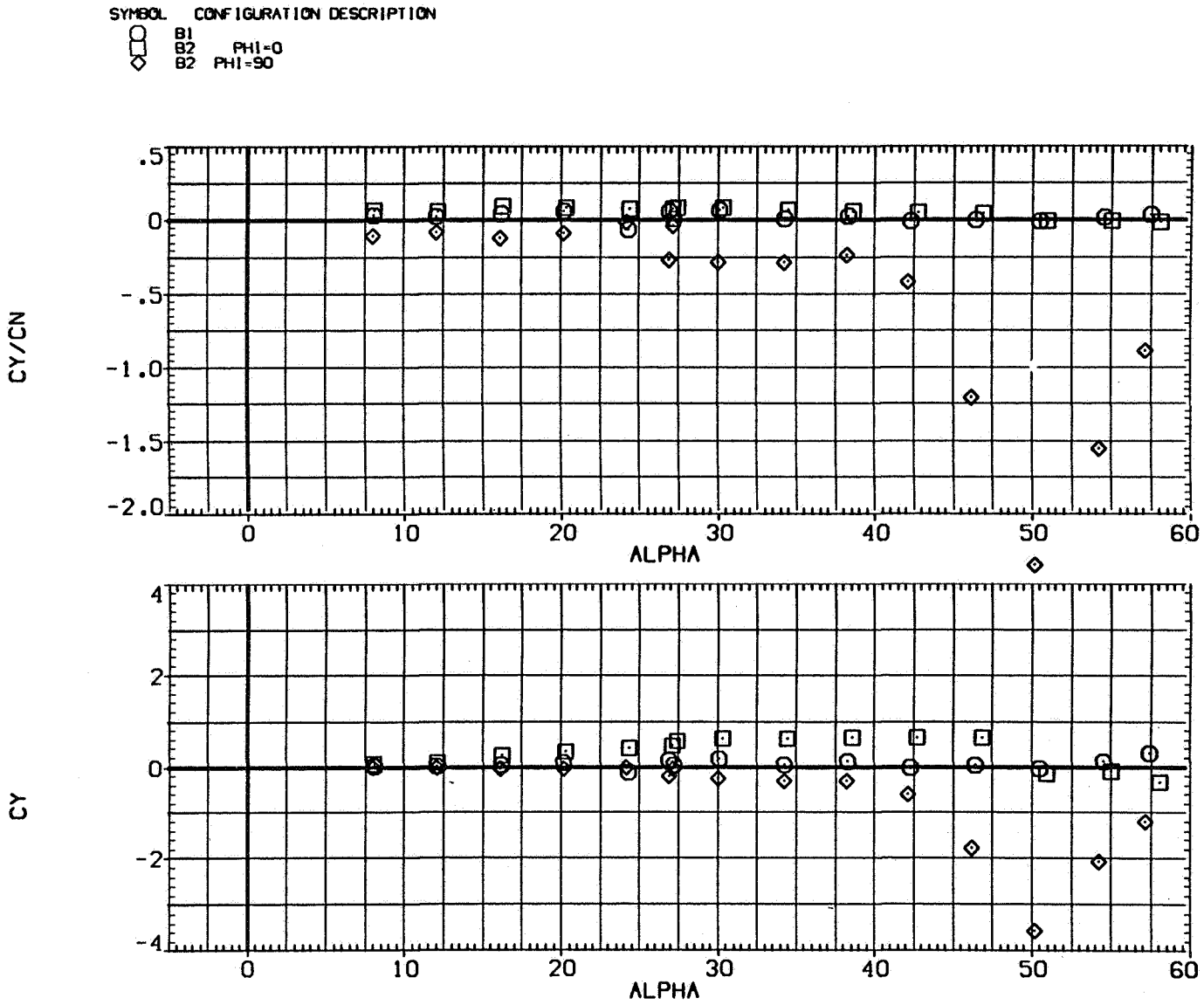

(b) C_Y/C_N and C_Y versus α

Figure 3.– Continued.

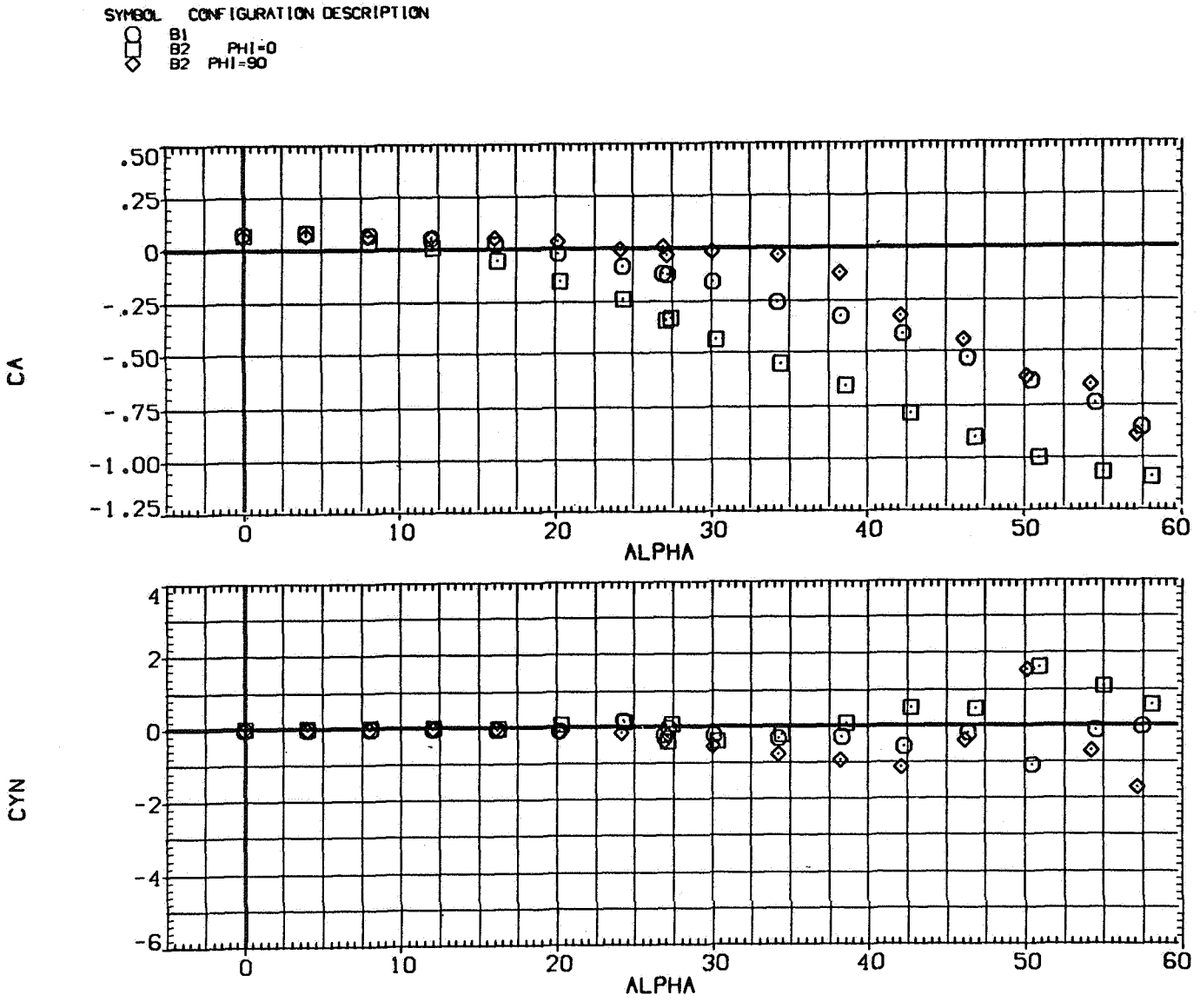

(c) C_A and C_n versus α

Figure 3.– Concluded.

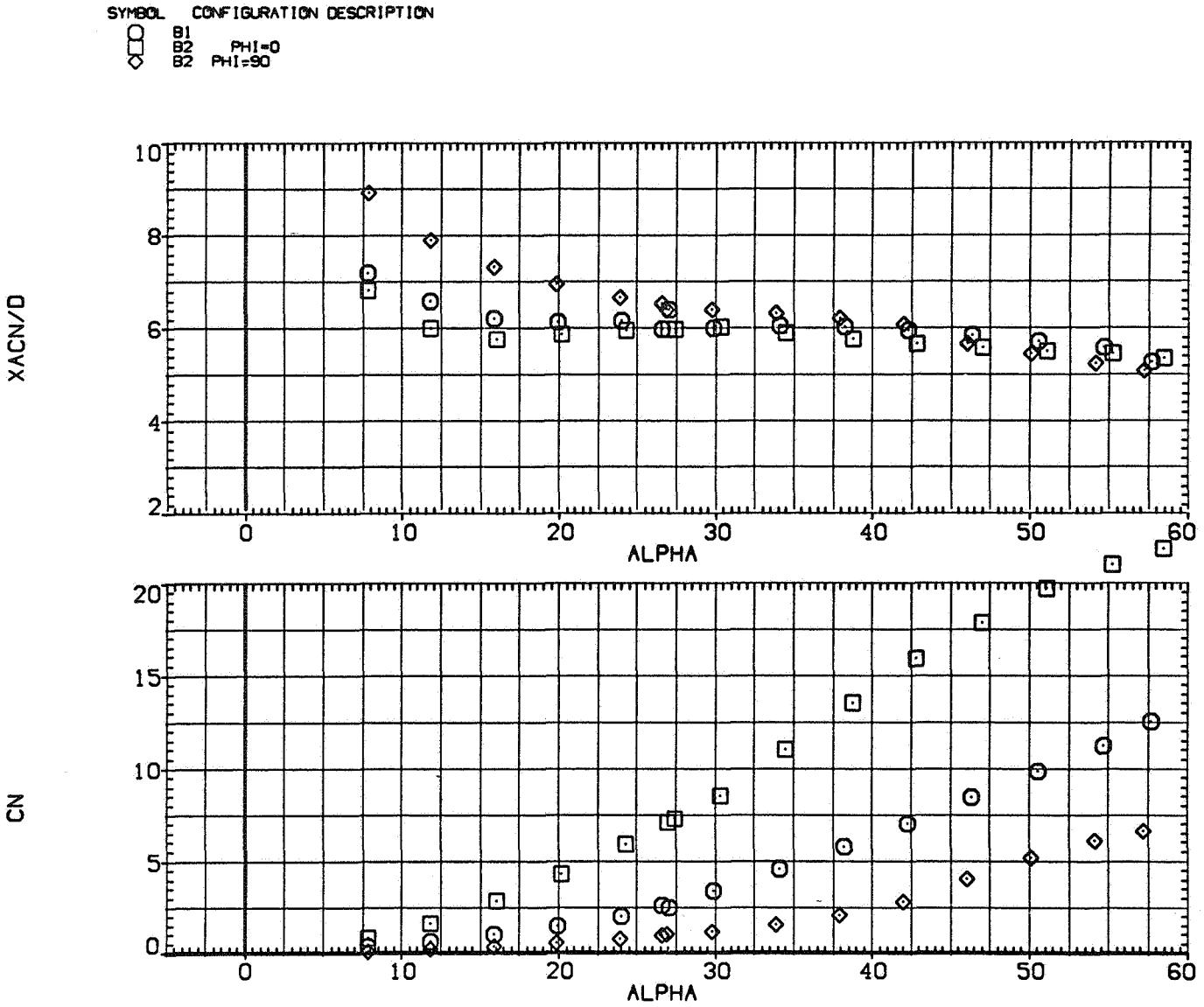

(a) x_{ac_N}/d and C_N versus α

Figure 4.— Effect of elliptic cross section with constant a/b; $M = 0.9$, $Re = 6.5 \times 10^5$.

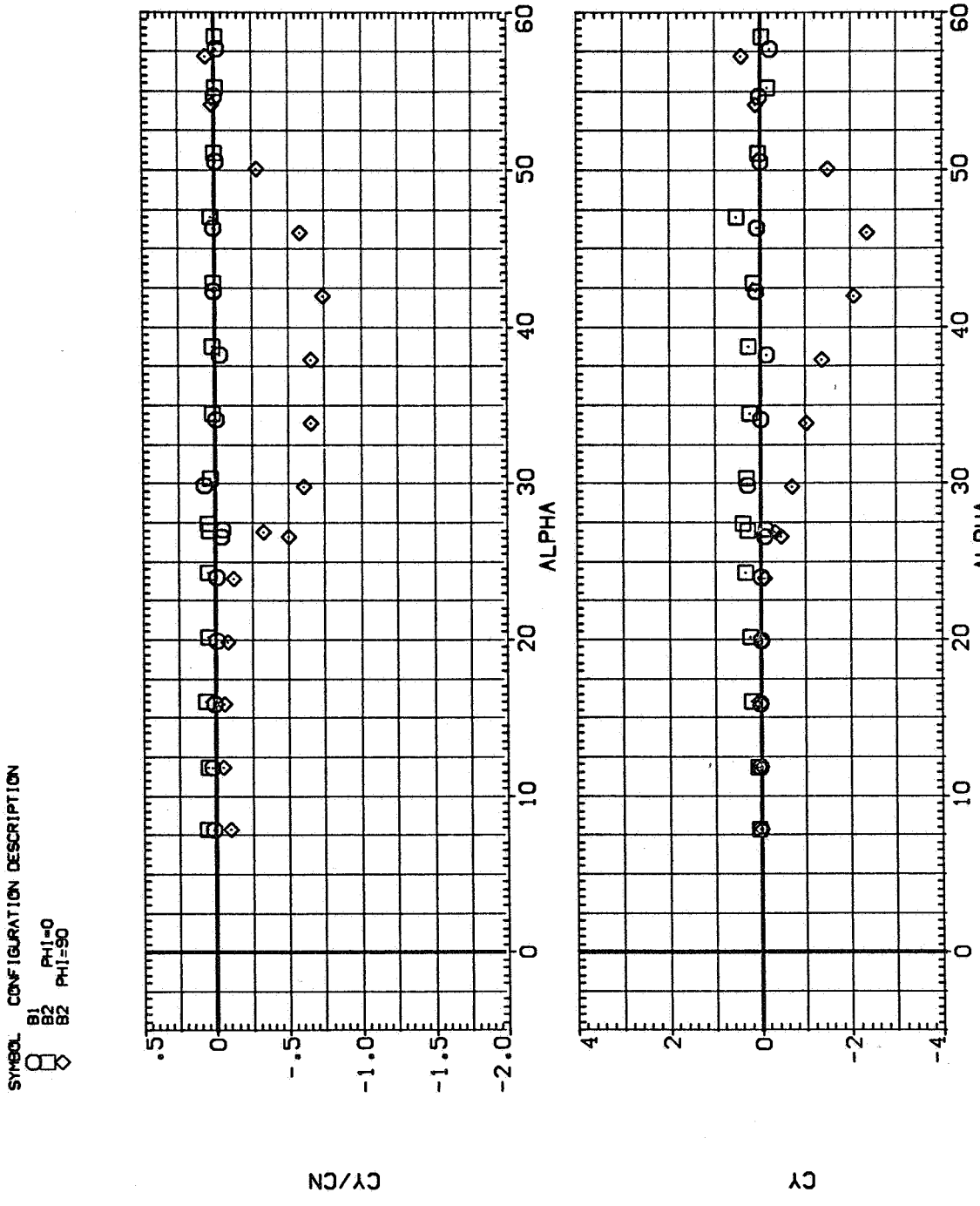

(b) C_Y/C_N and C_Y versus α

Figure 4.– Continued.

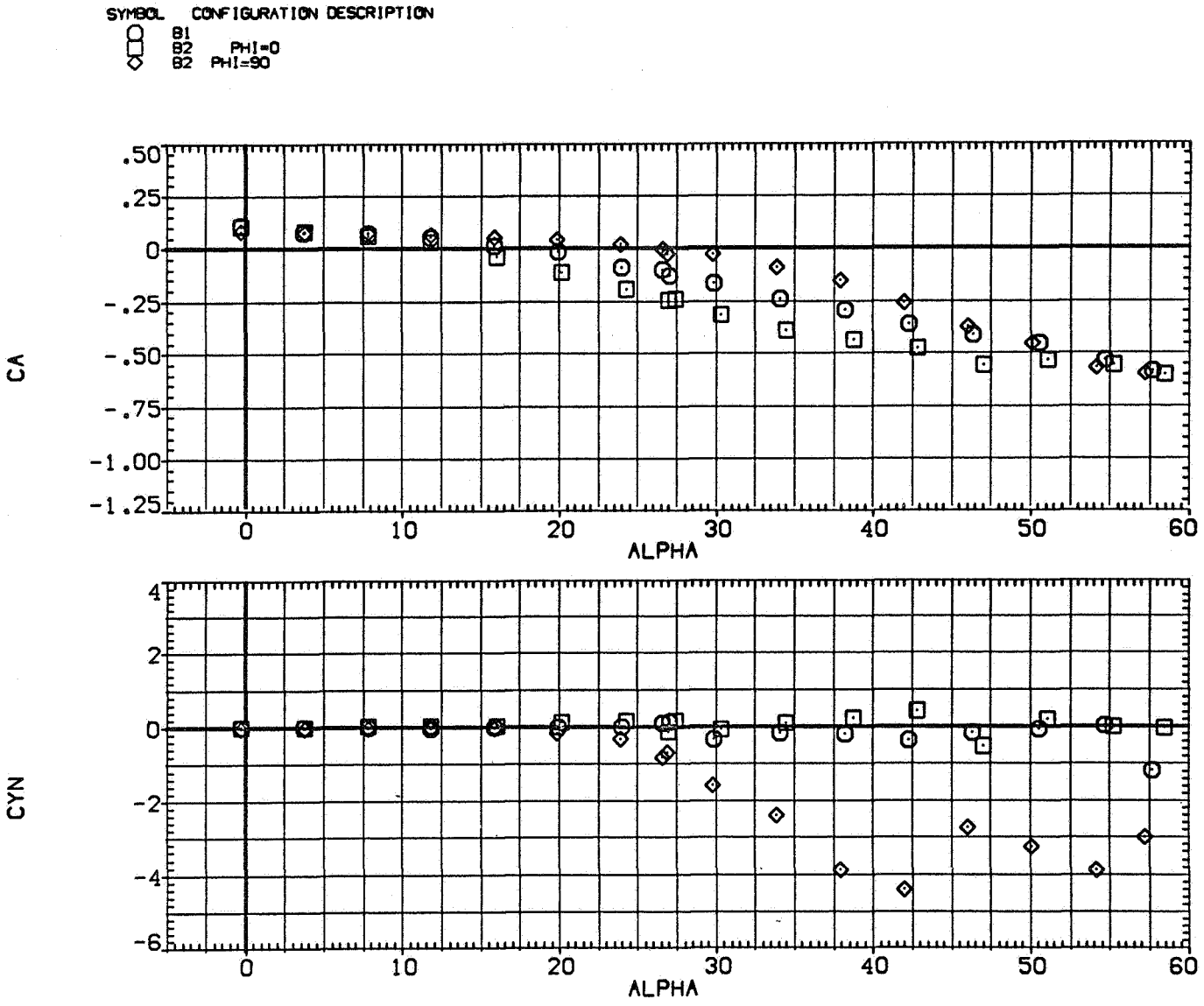

(c) C_A and C_n versus α

Figure 4.– Concluded.

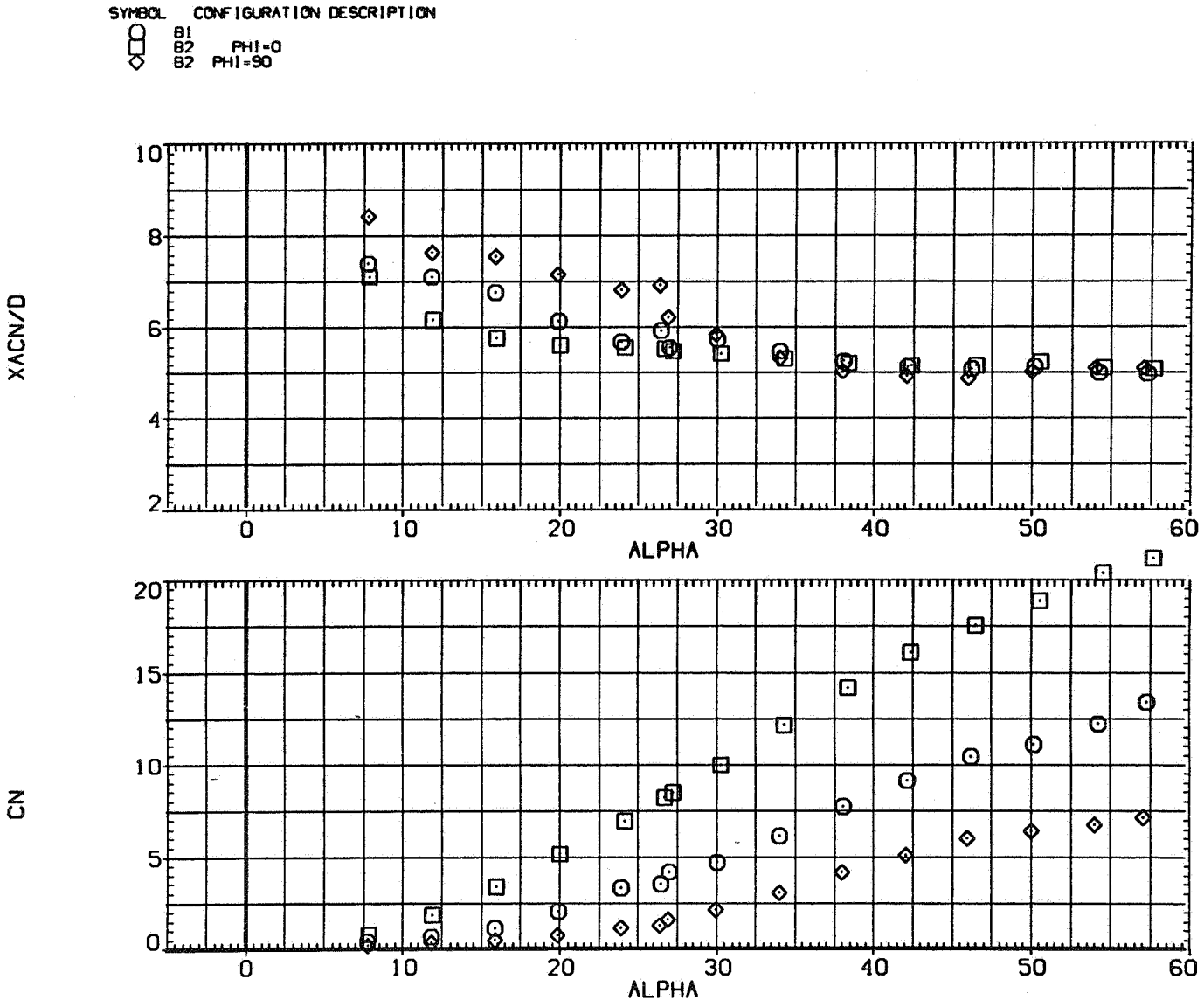

(a) x_{ac_N}/d and C_N versus α

Figure 5.– Effect of elliptic cross section with constant a/b; $M = 1.2$, $Re = 3.8 \times 10^5$.

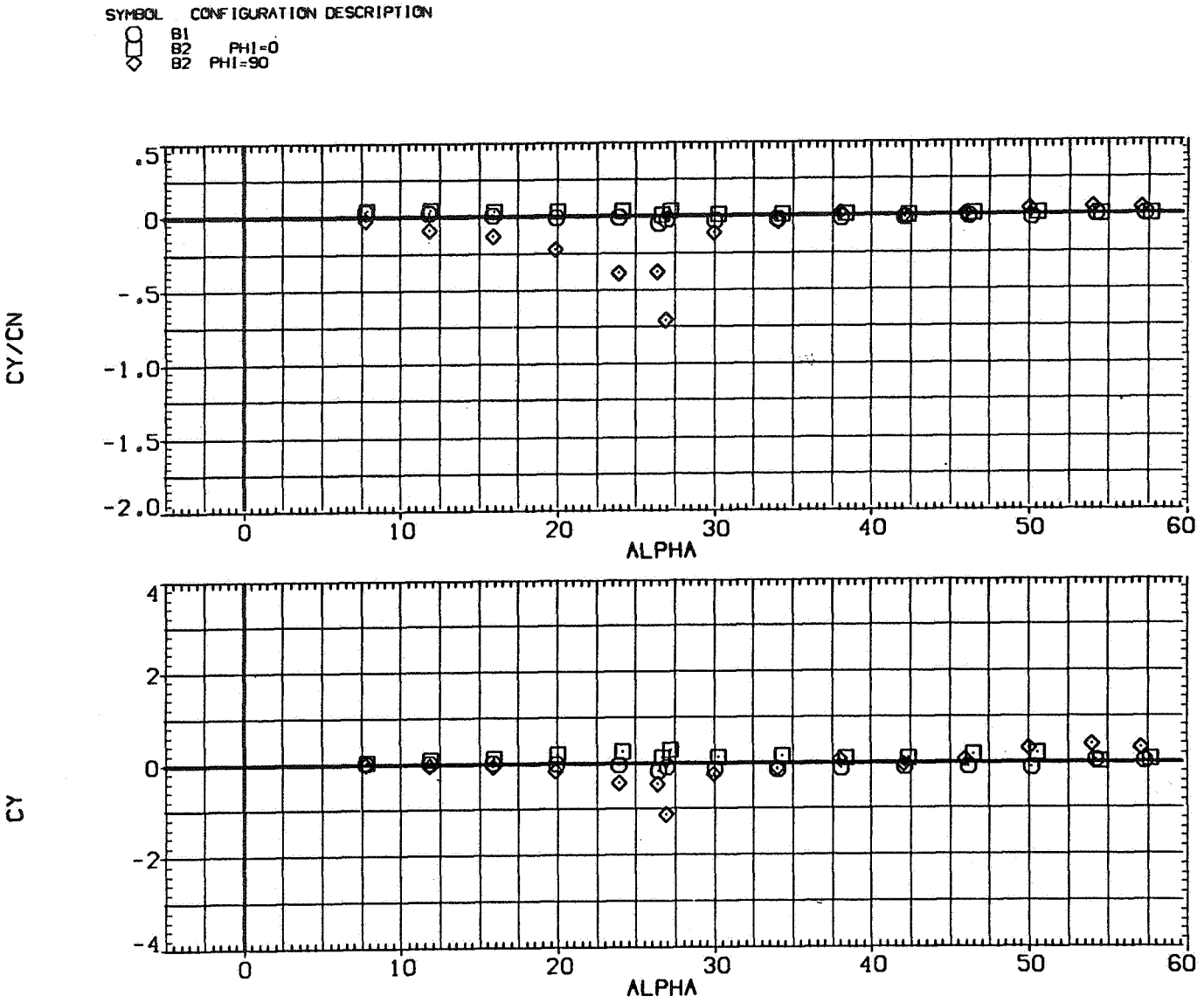

(b) C_Y/C_N and C_Y versus α

Figure 5.– Continued.

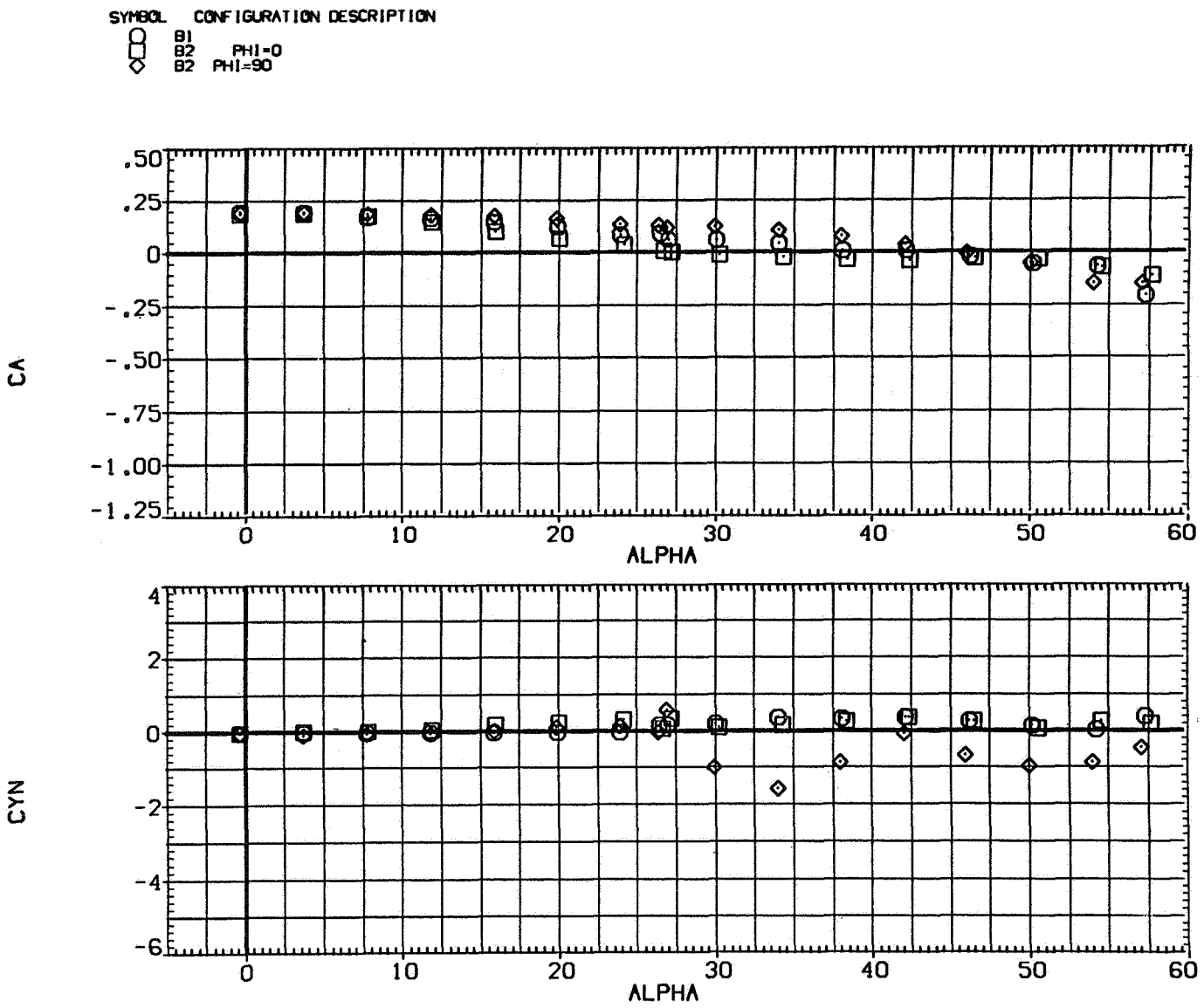

(c) C_A and C_n versus α

Figure 5.– Concluded.

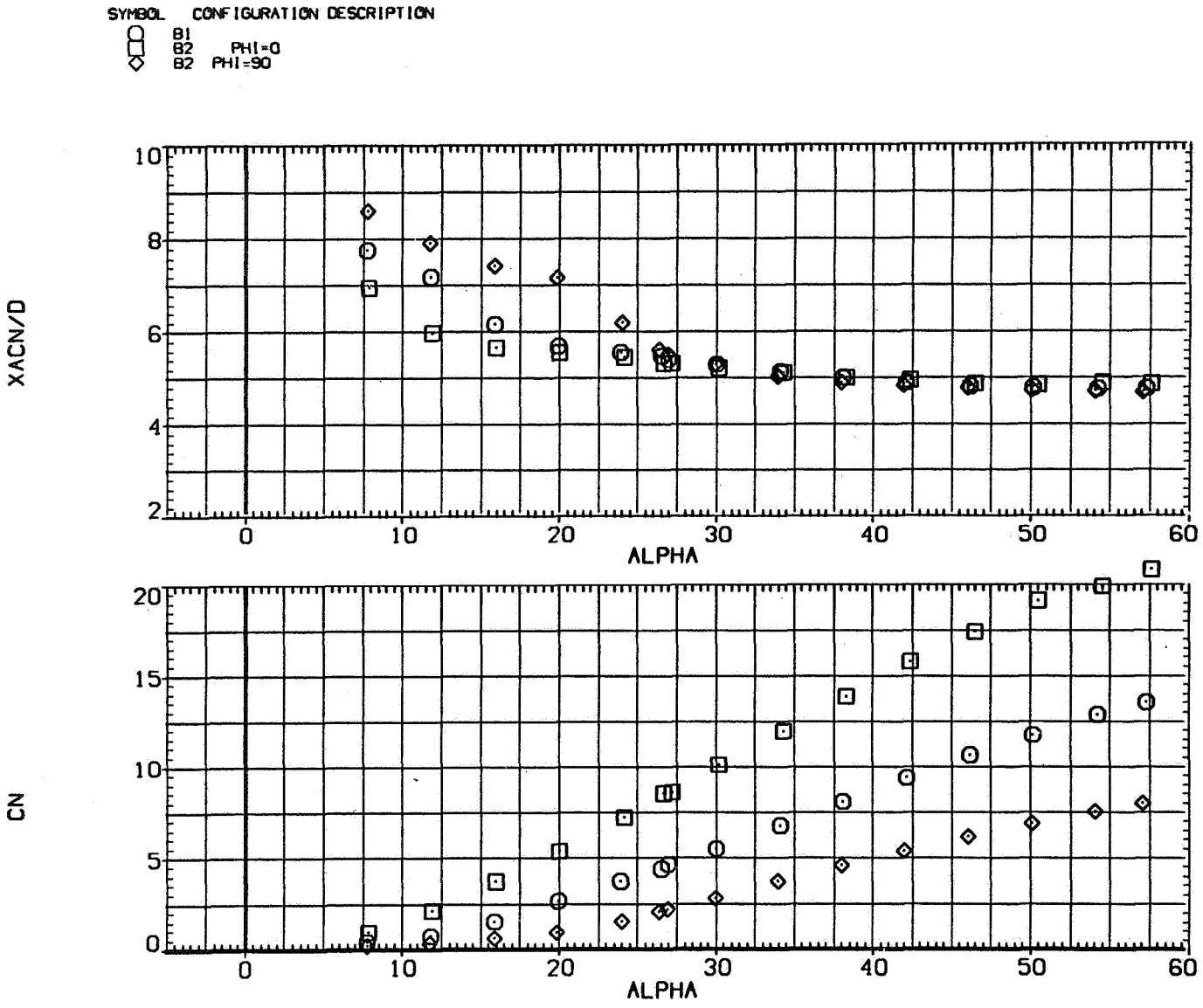

(a) x_{ac_N}/d and C_N versus α

Figure 6.– Effect of elliptic cross section with constant a/b; $M = 1.5$, $Re = 3.8\times10^5$.

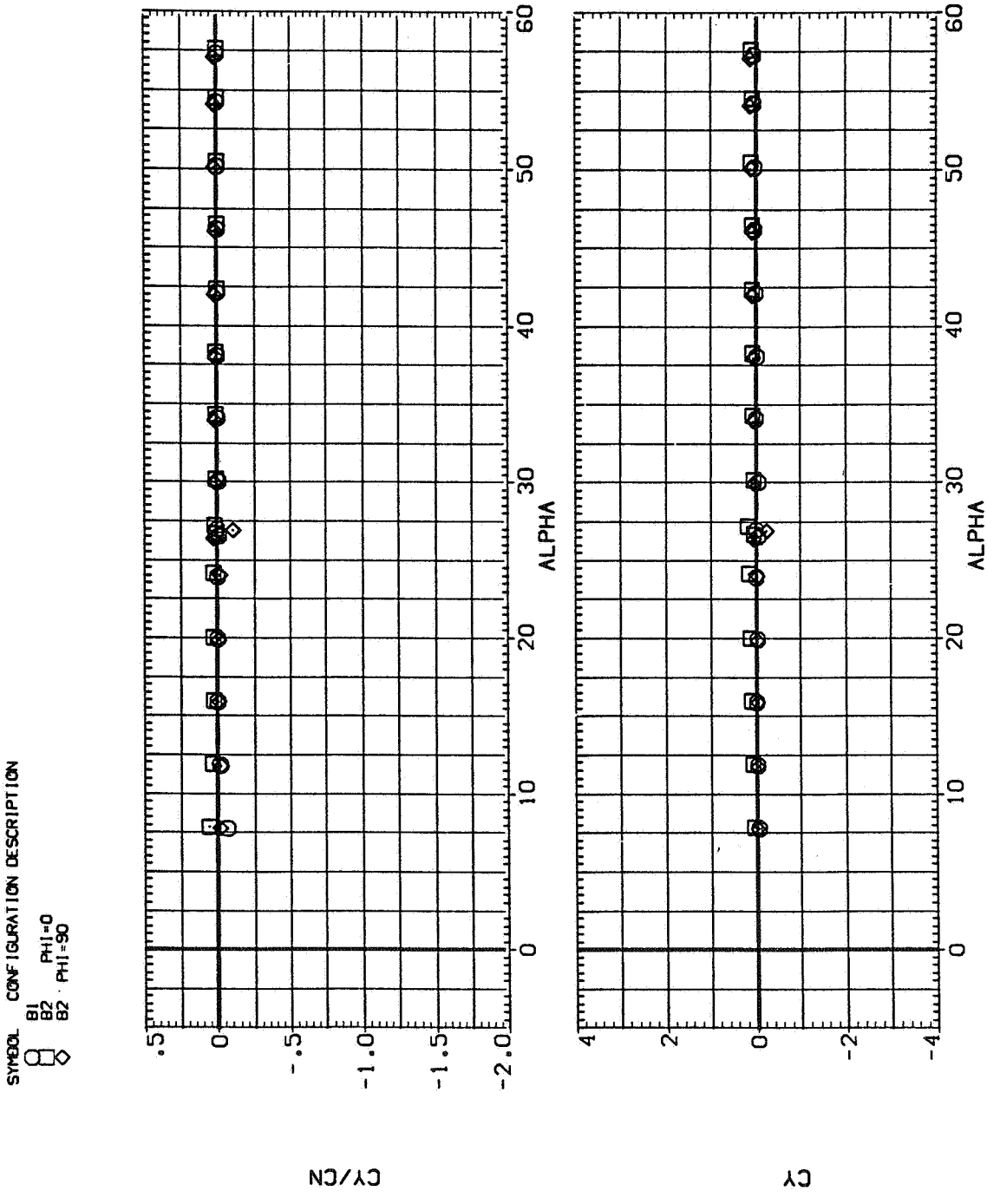

(b) C_Y/C_N and C_Y versus α

Figure 6.– Continued.

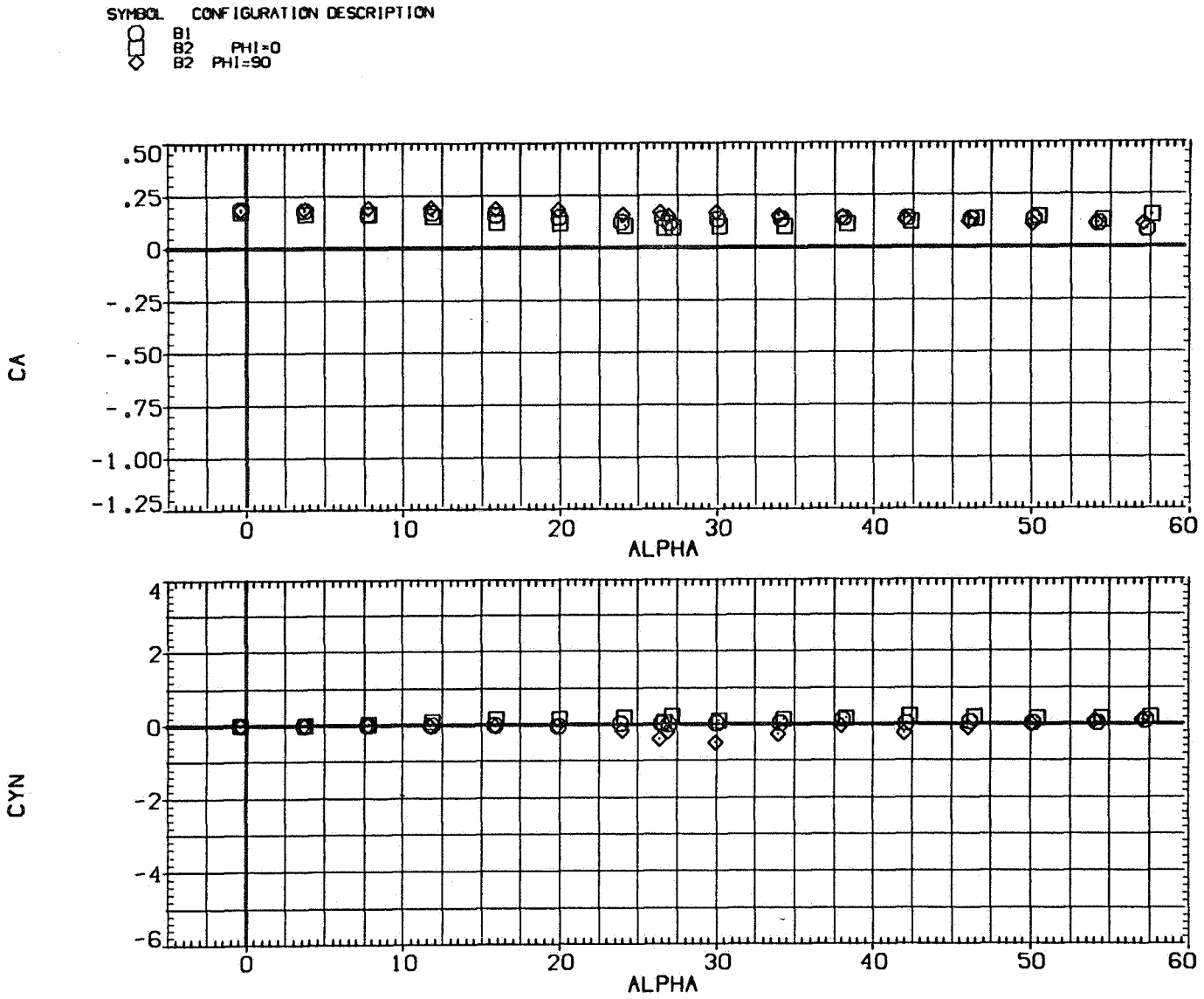

(c) C_A and C_n versus α

Figure 6.– Concluded.

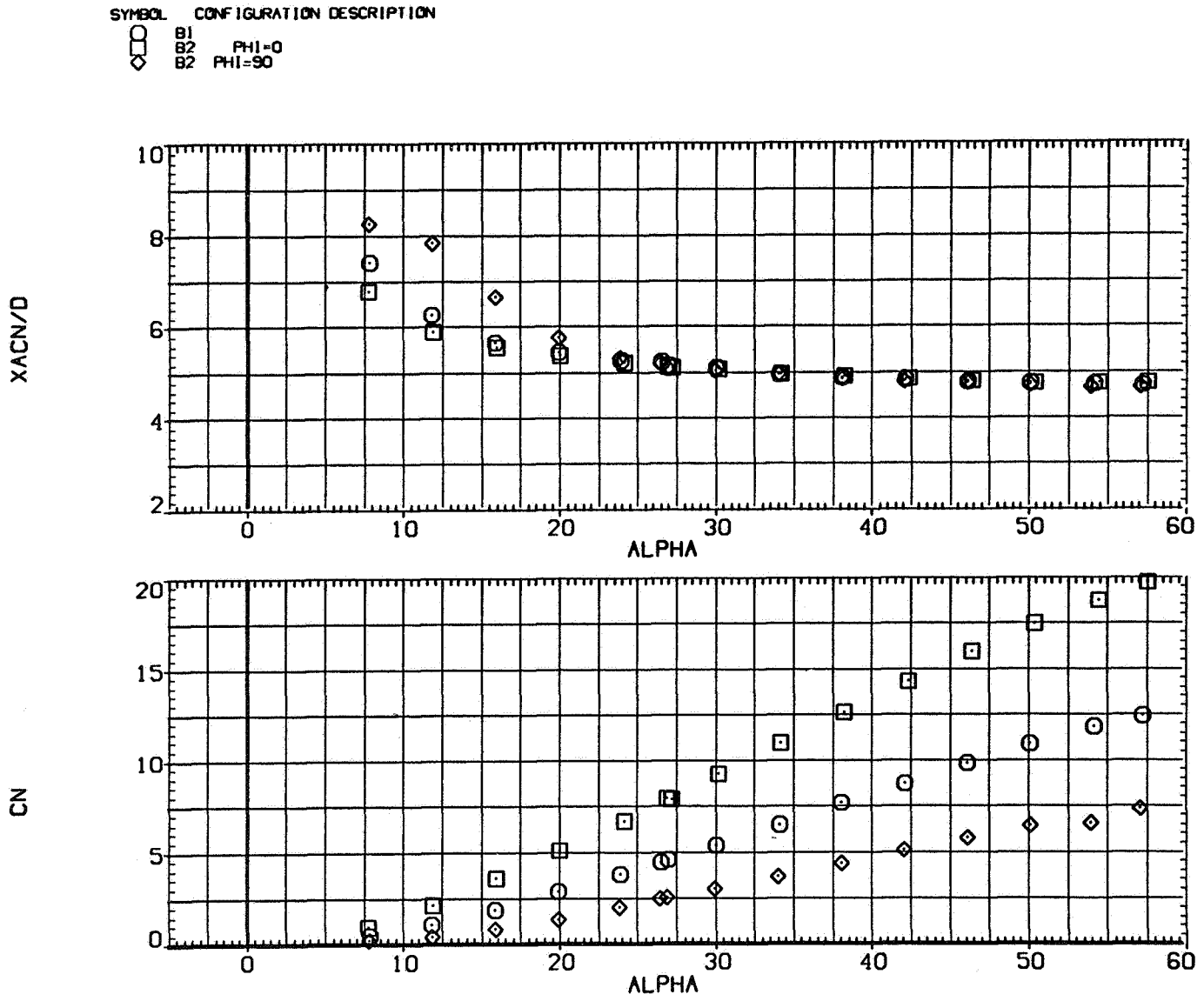

(a) x_{ac_N}/d and C_N versus α

Figure 7.– Effect of elliptic cross section with constant a/b; $M = 2.0$, $Re = 3.8 \times 10^5$.

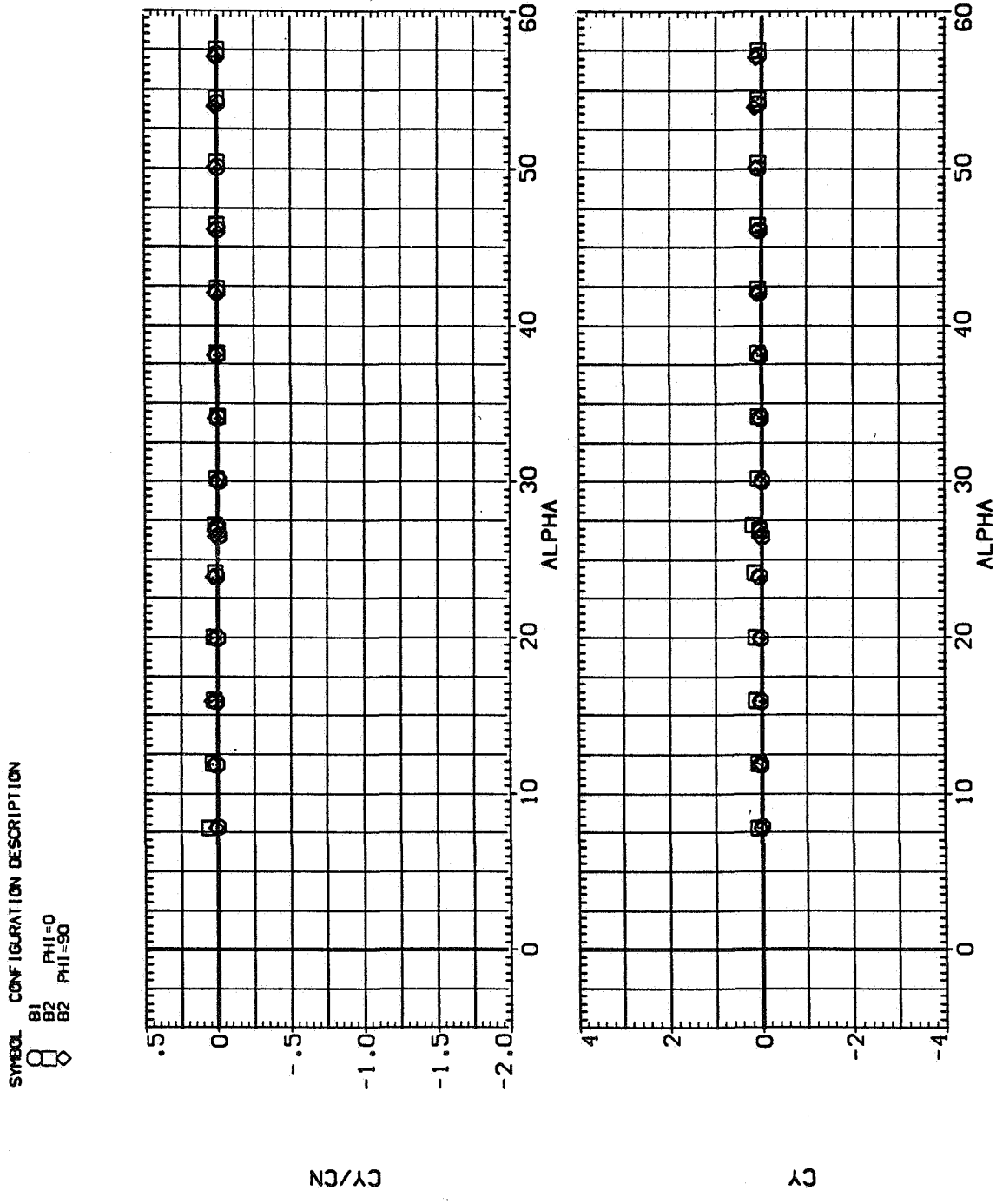

(b) C_Y/C_N and C_Y versus α

Figure 7 — Continued.

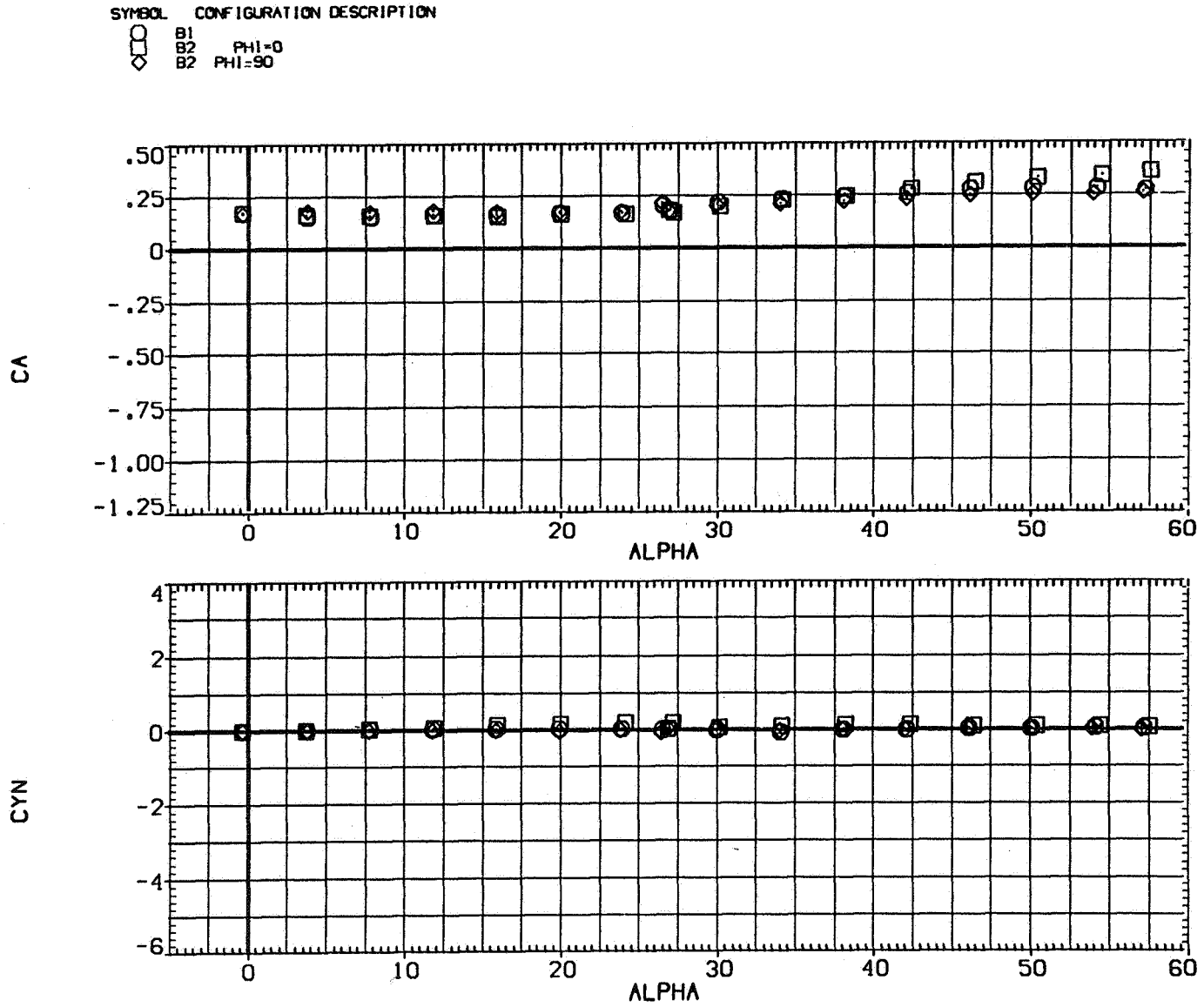

(c) C_A and C_n versus α

Figure 7.– Concluded.

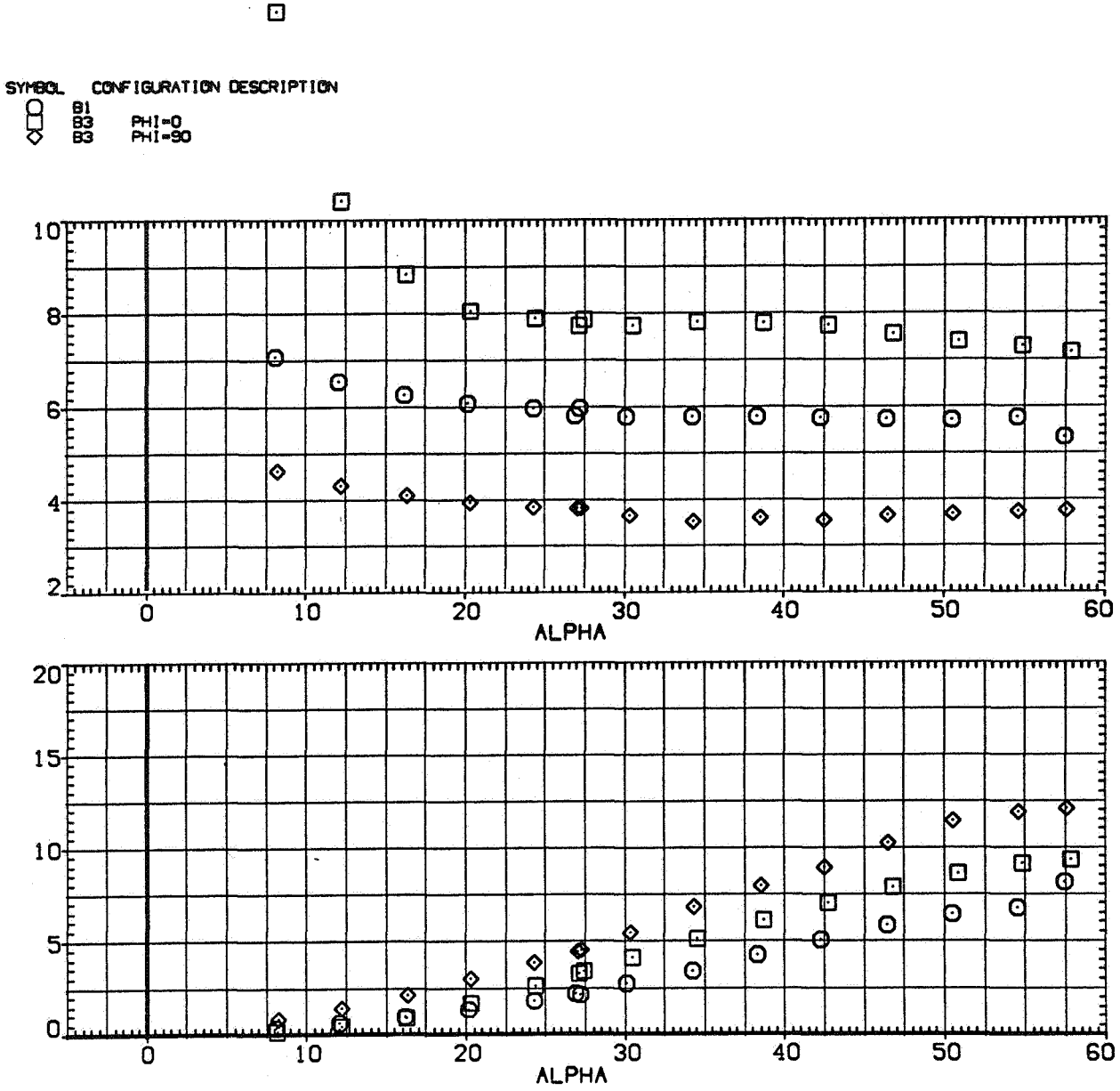

(a) x_{ac_N}/d and C_N versus α

Figure 8.— Effect of elliptic cross section with variable a/b; $M = 0.6$, $Re = 6.5 \times 10^5$.

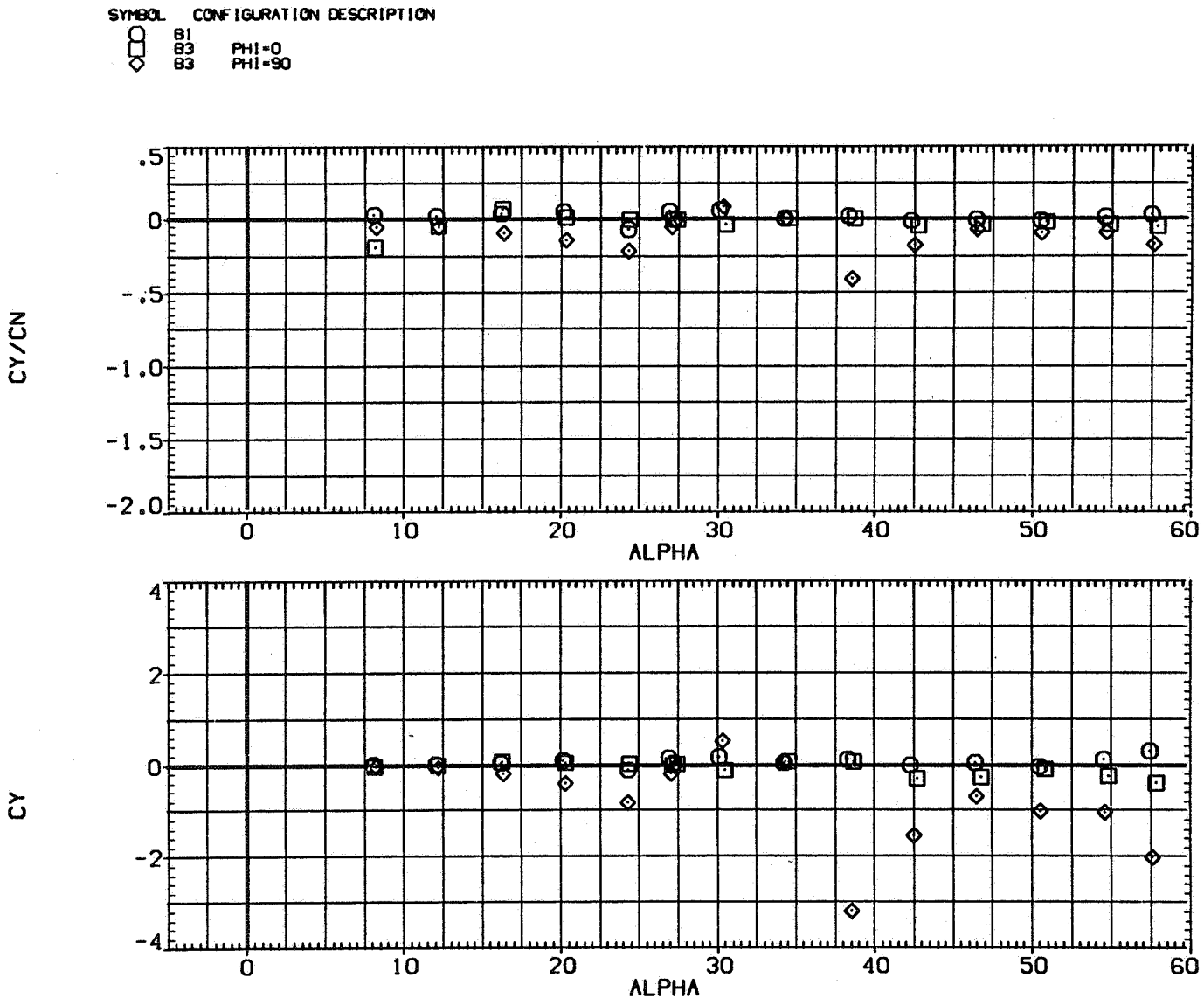

(b) C_Y/C_N and C_Y versus α

Figure 8.– Continued.

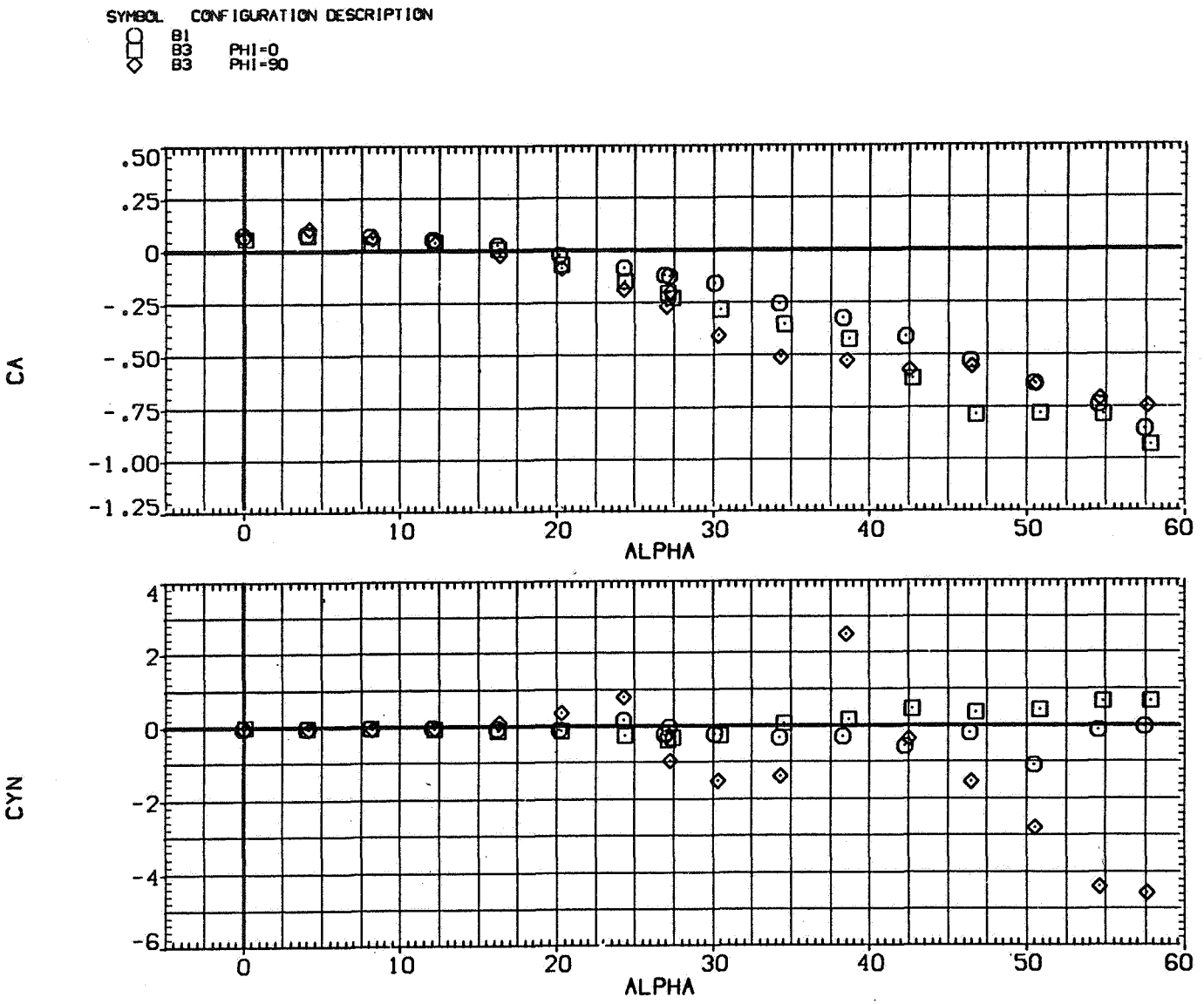

(c) C_A and C_n versus α

Figure 8.– Concluded.

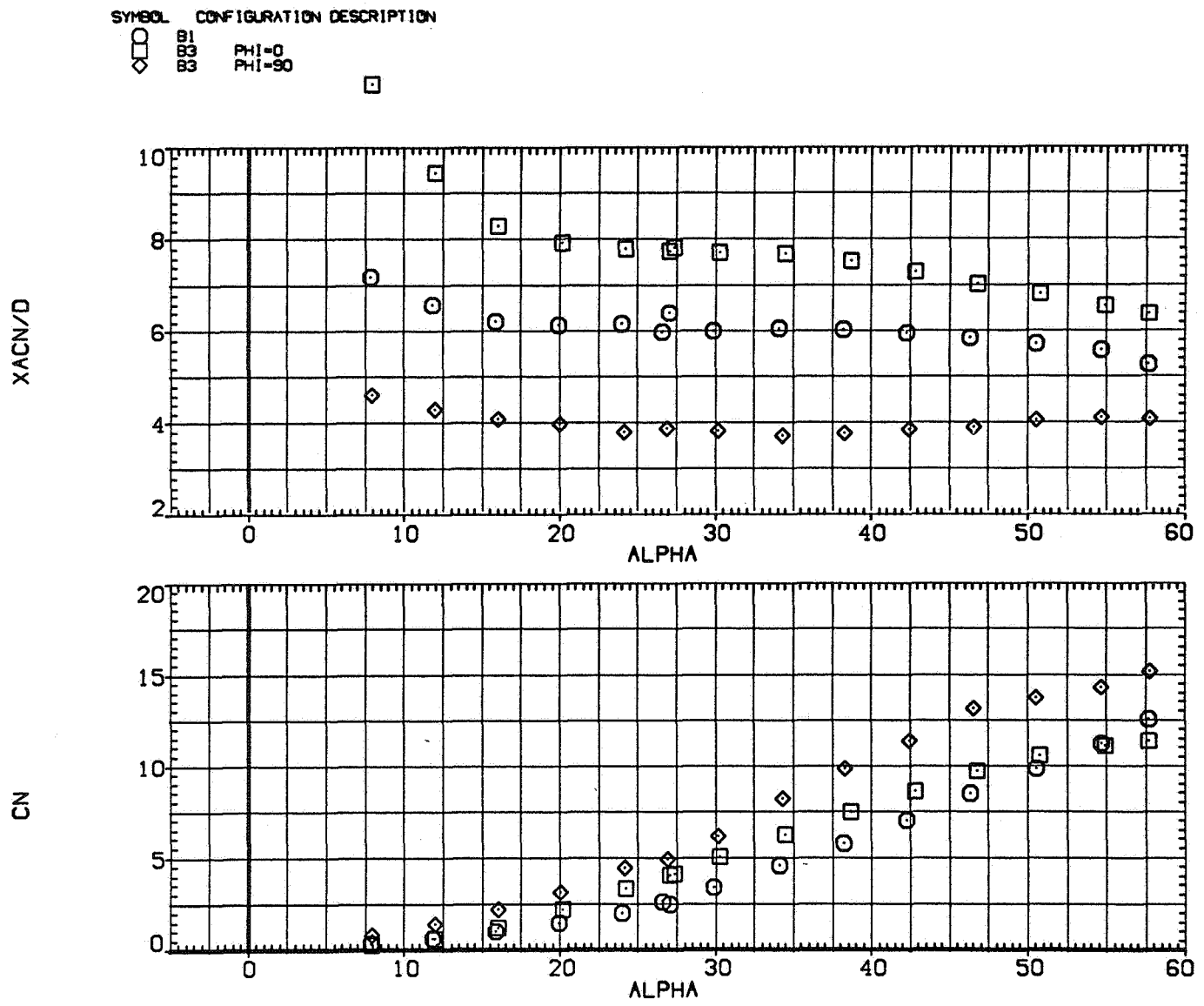

(a) x_{ac_N}/d and C_N versus α

Figure 9.-- Effect of elliptic cross section with variable a/b; $M = 0.9$, $Re = 6.5 \times 10^5$.

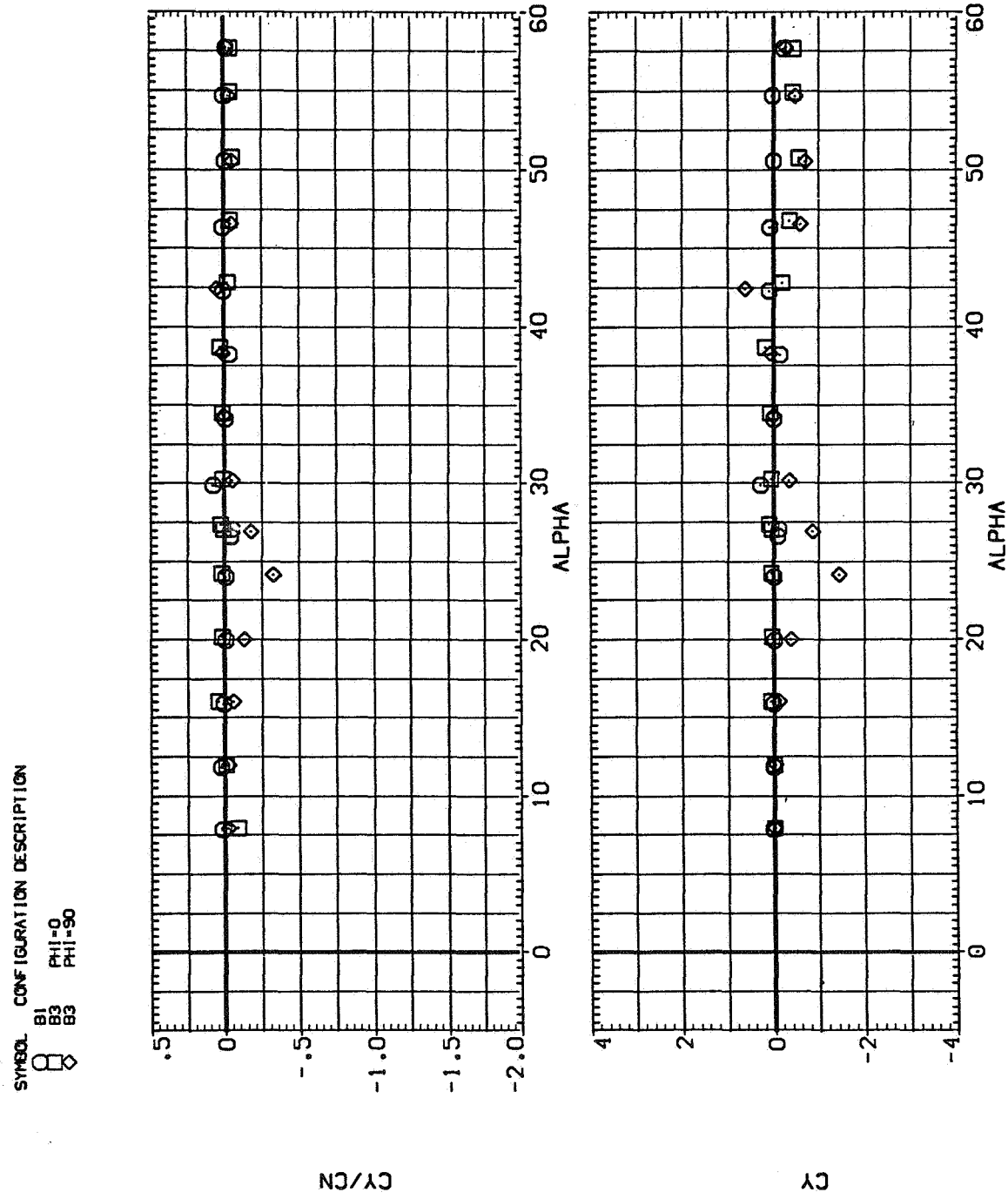

(b) C_Y/C_N and C_Y versus α

Figure 9.– Continued.

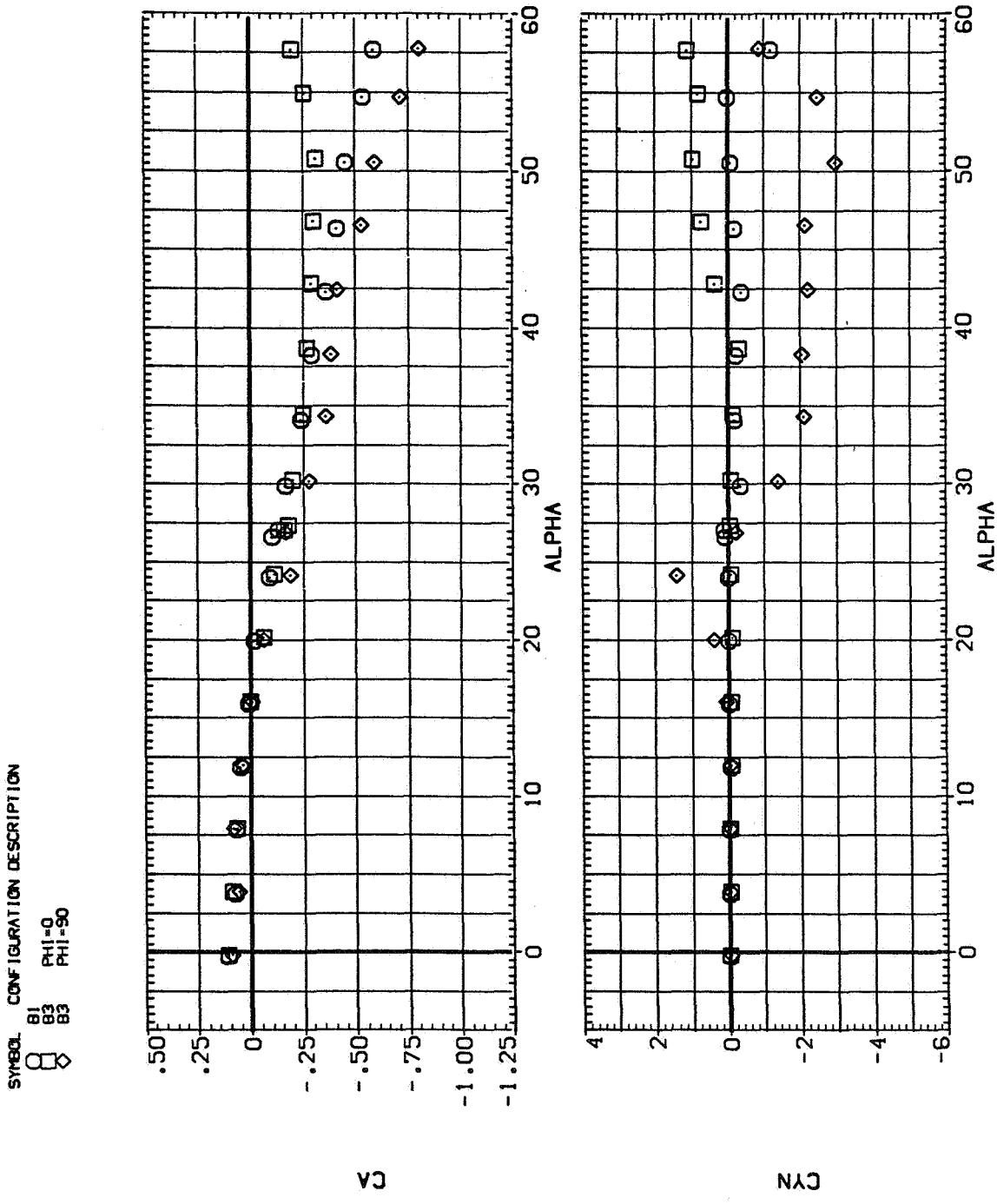

(c) C_A and C_n versus α

Figure 9.– Concluded.

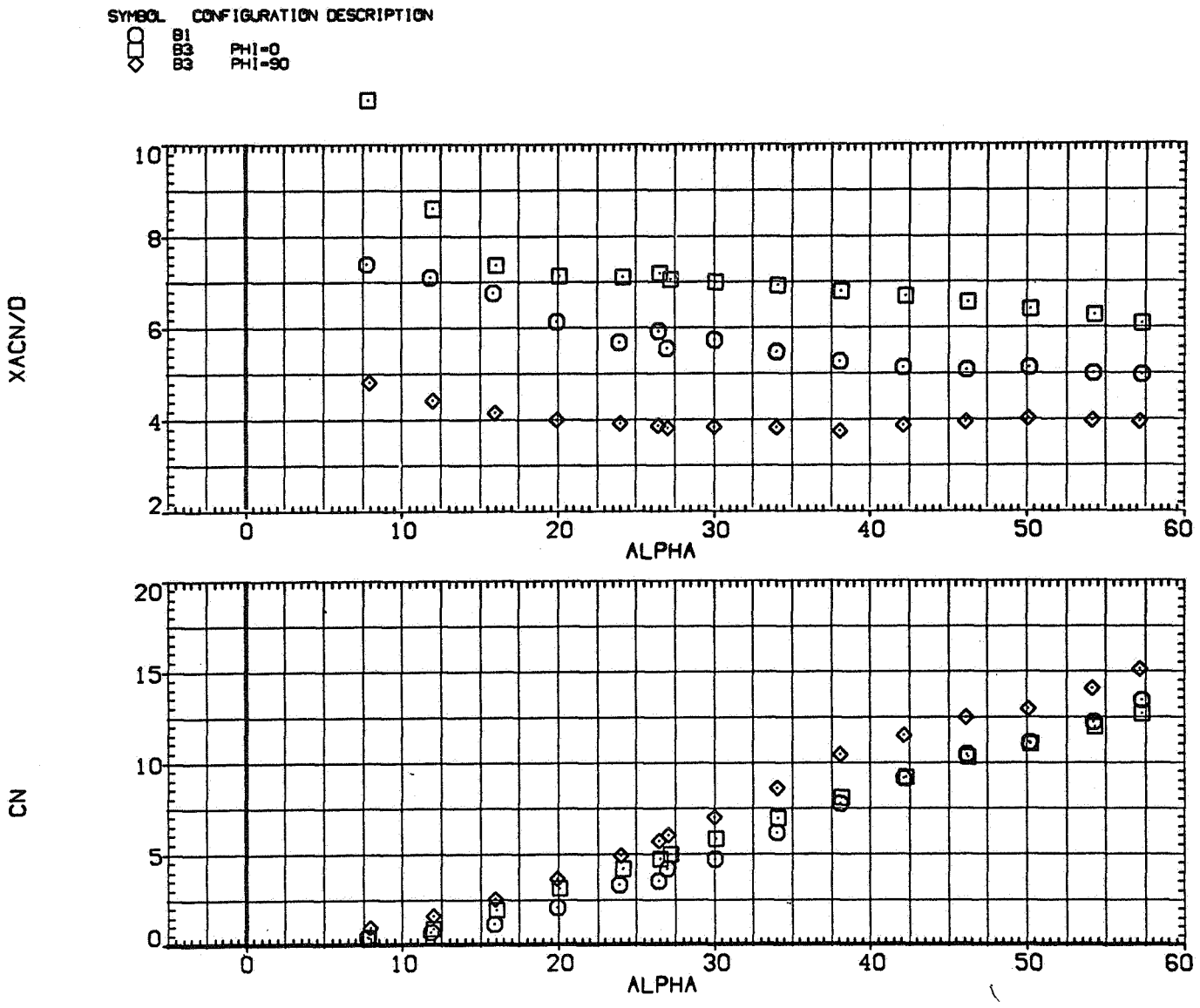

(a) x_{ac_N}/d and C_N versus α

Figure 10.– Effect of elliptic cross section with variable a/b; $M = 1.2$, $Re = 3.8 \times 10^5$.

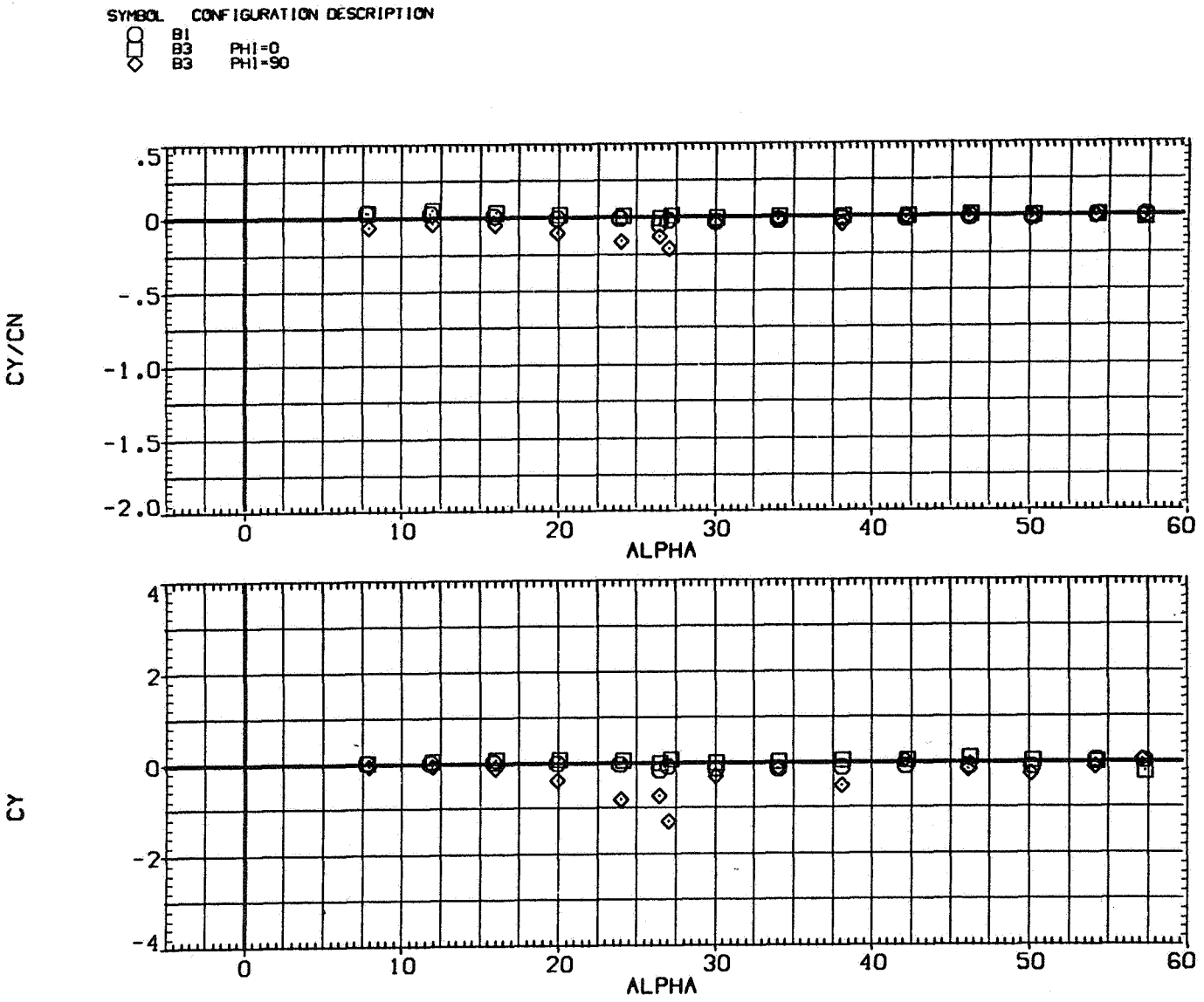

(b) C_Y/C_N and C_Y versus α

Figure 10.– Continued.

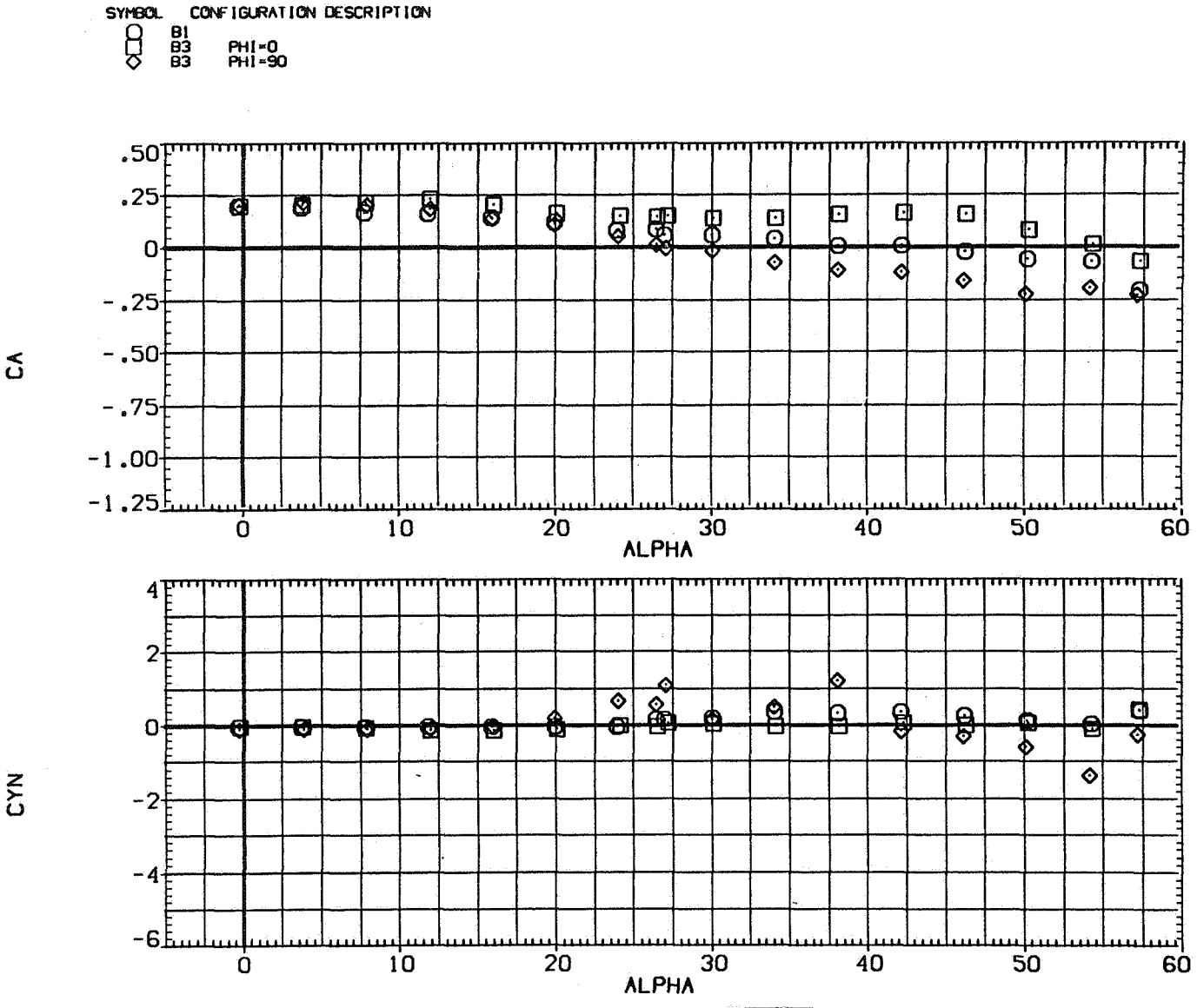

(c) C_A and C_n versus α

Figure 10.— Concluded.

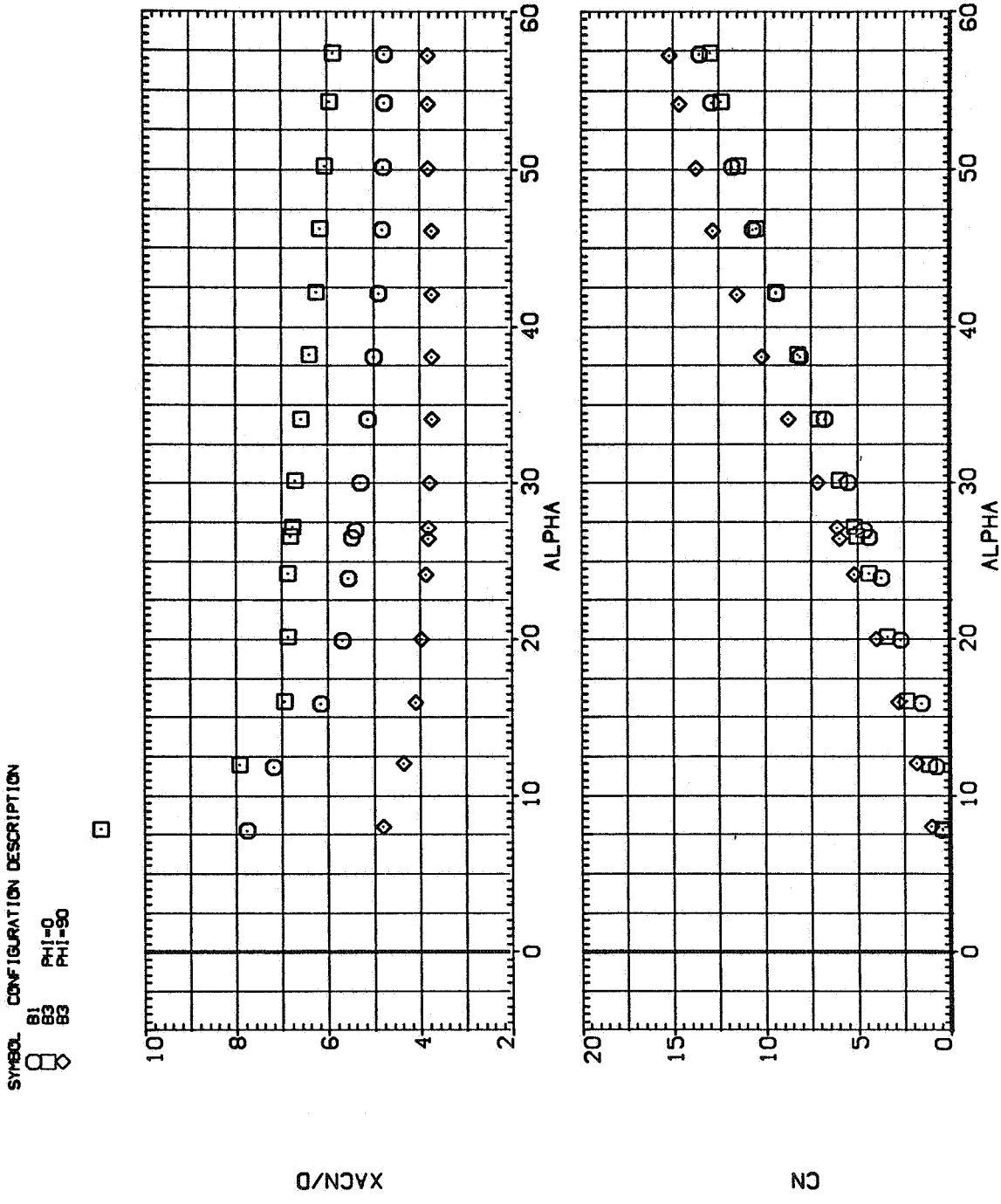

(a) x_{ac_N}/d and C_N versus α

Figure 11.— Effect of elliptic cross section with variable a/b; $M = 1.5$, $Re = 3.8 \times 10^5$.

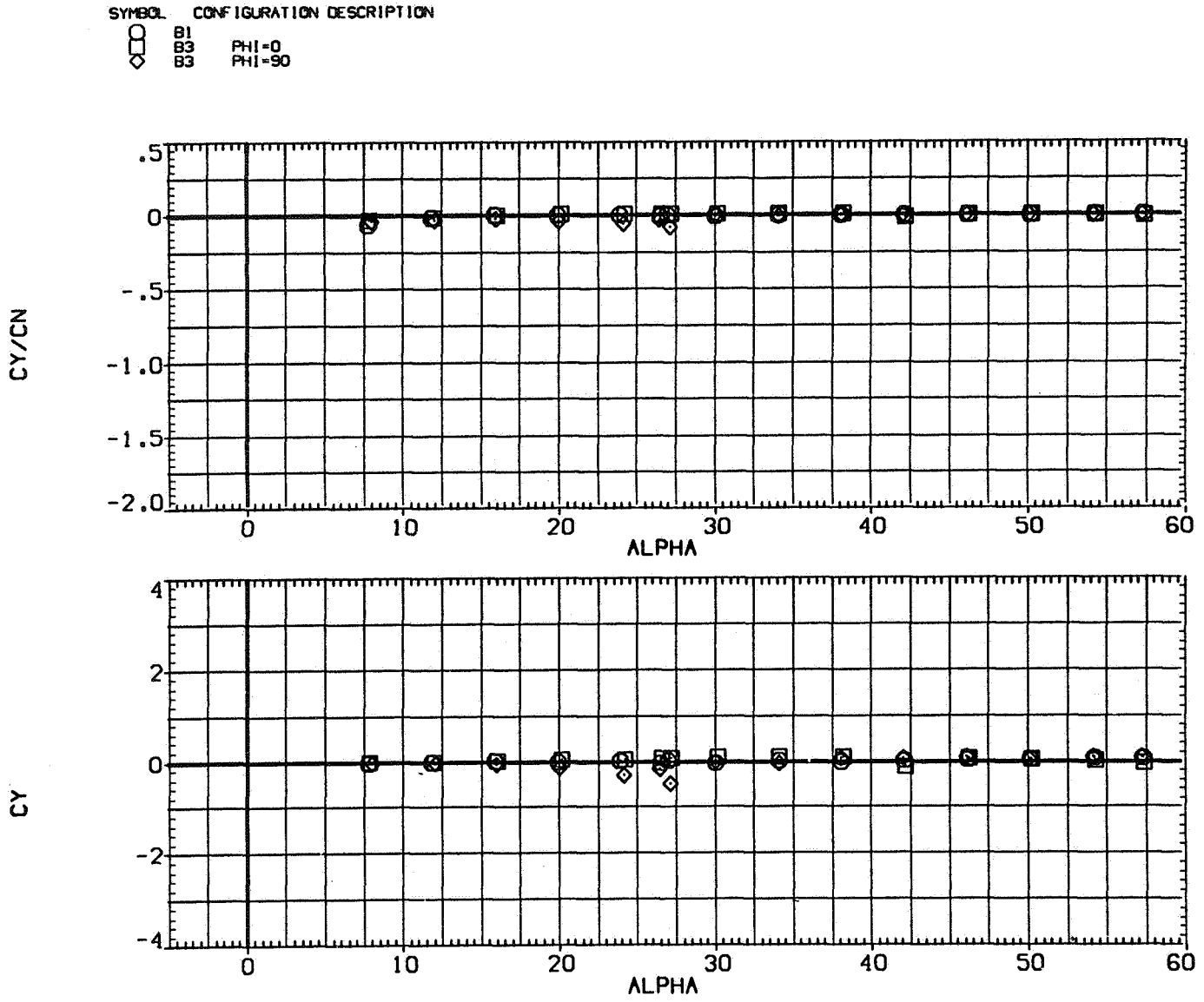

(b) C_Y/C_N and C_Y versus α

Figure 11.– Continued.

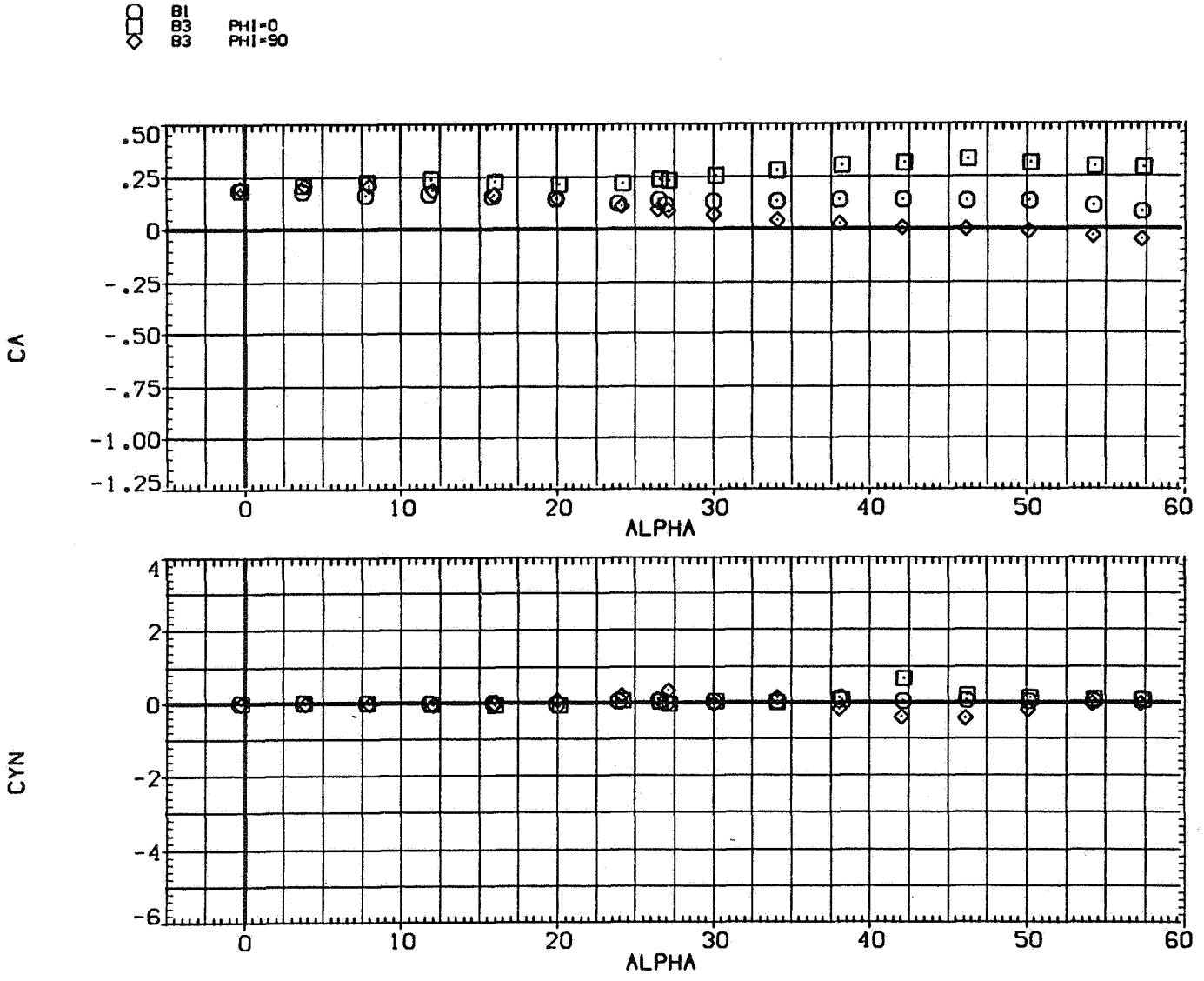

(c) C_A and C_n versus α

Figure 11.– Concluded.

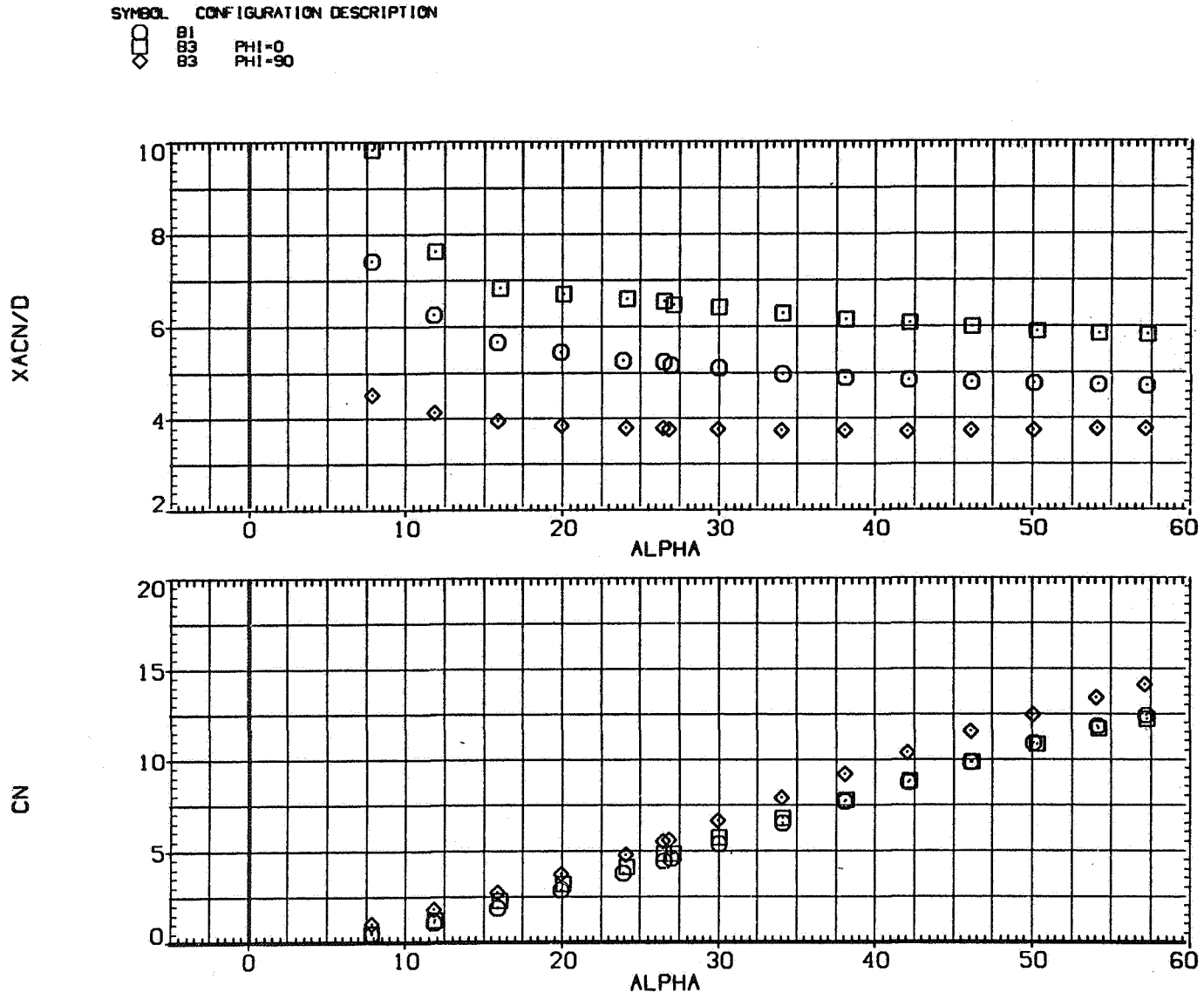

(a) x_{ac_N}/d and C_N versus α

Figure 12.– Effect of elliptic cross section with variable a/b; $M = 2.0$, $Re = 3.8 \times 10^5$.

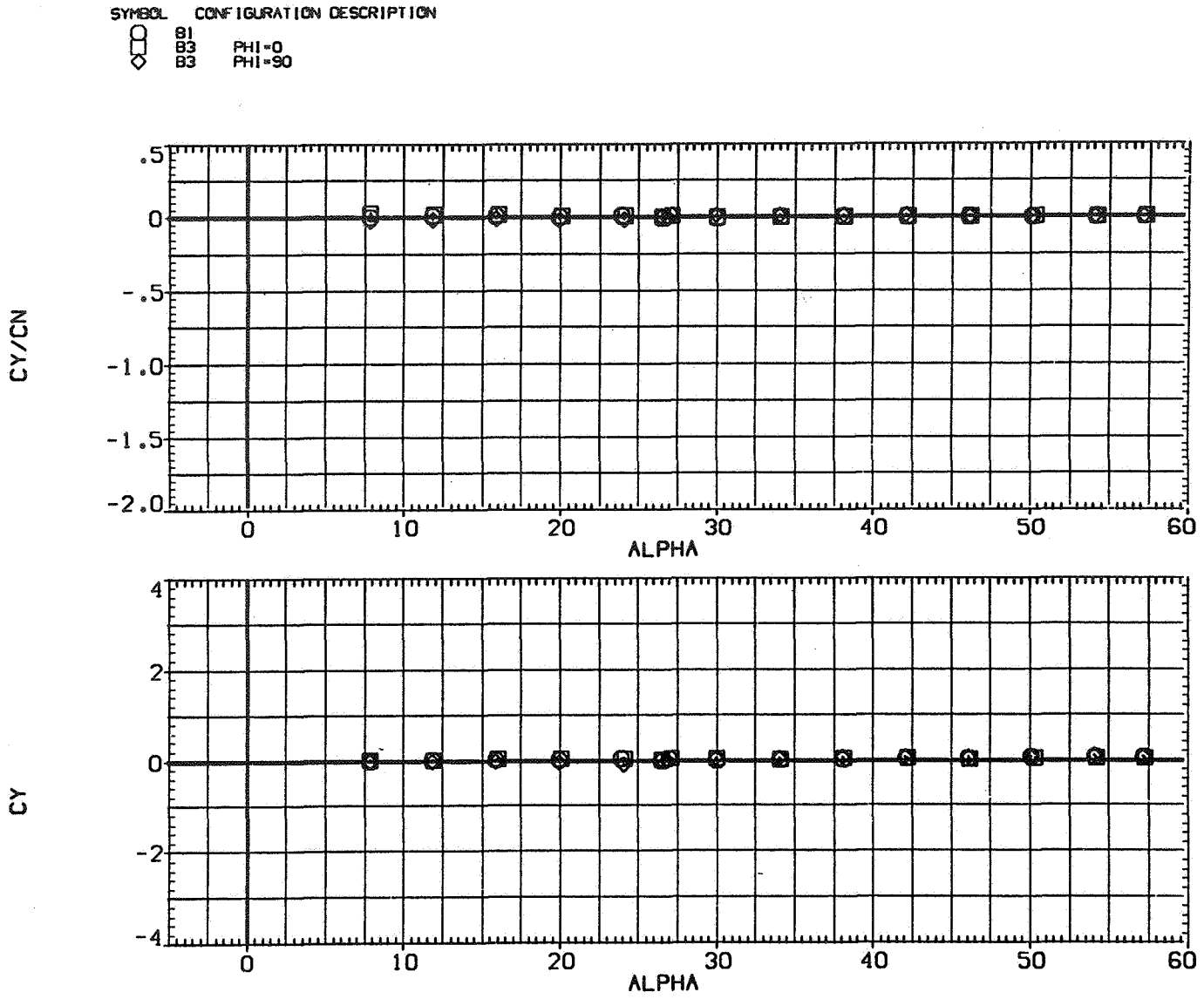

(b) C_Y/C_N and C_Y versus α

Figure 12.– Continued.

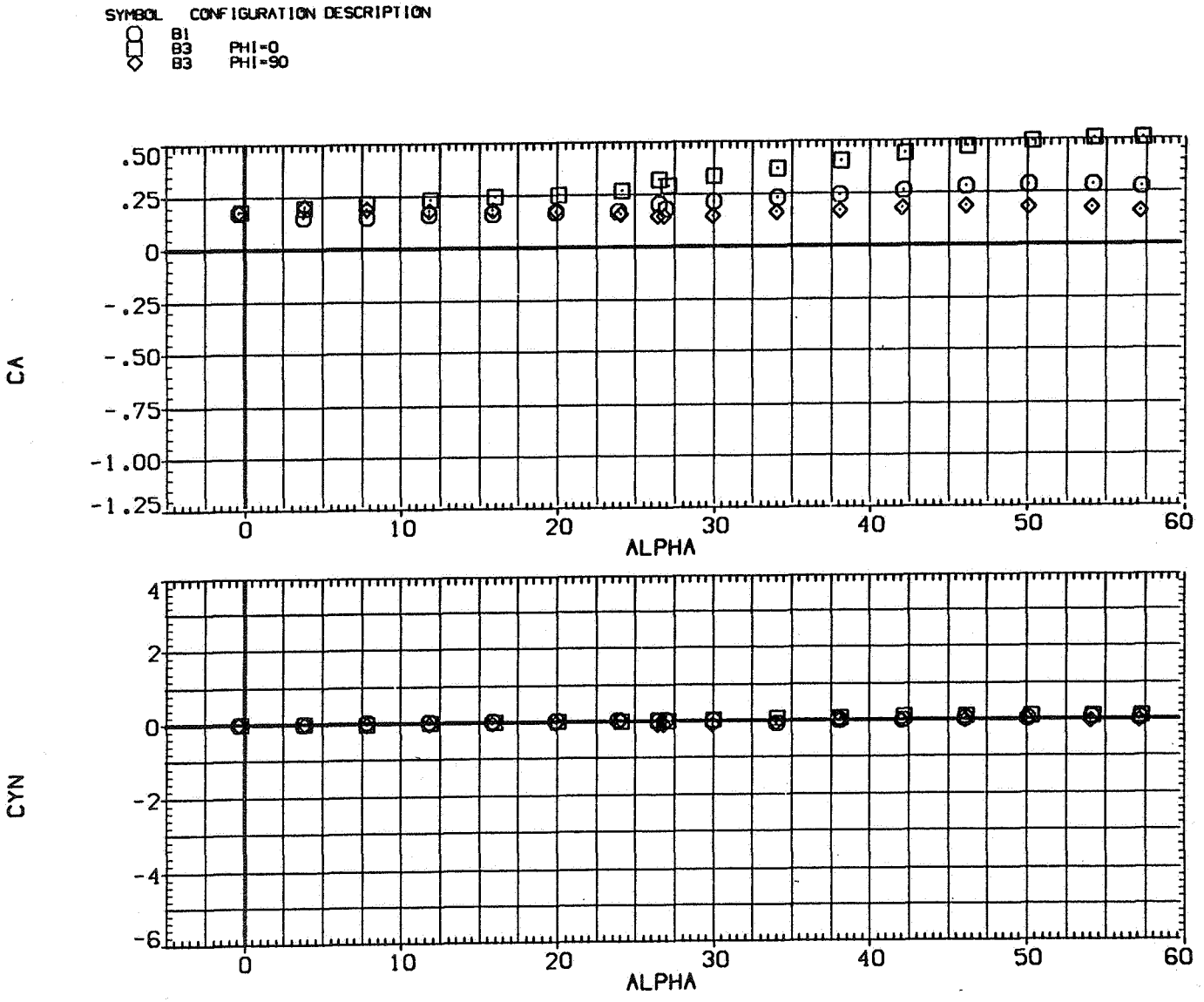

(c) C_A and C_n versus α

Figure 12.– Concluded.

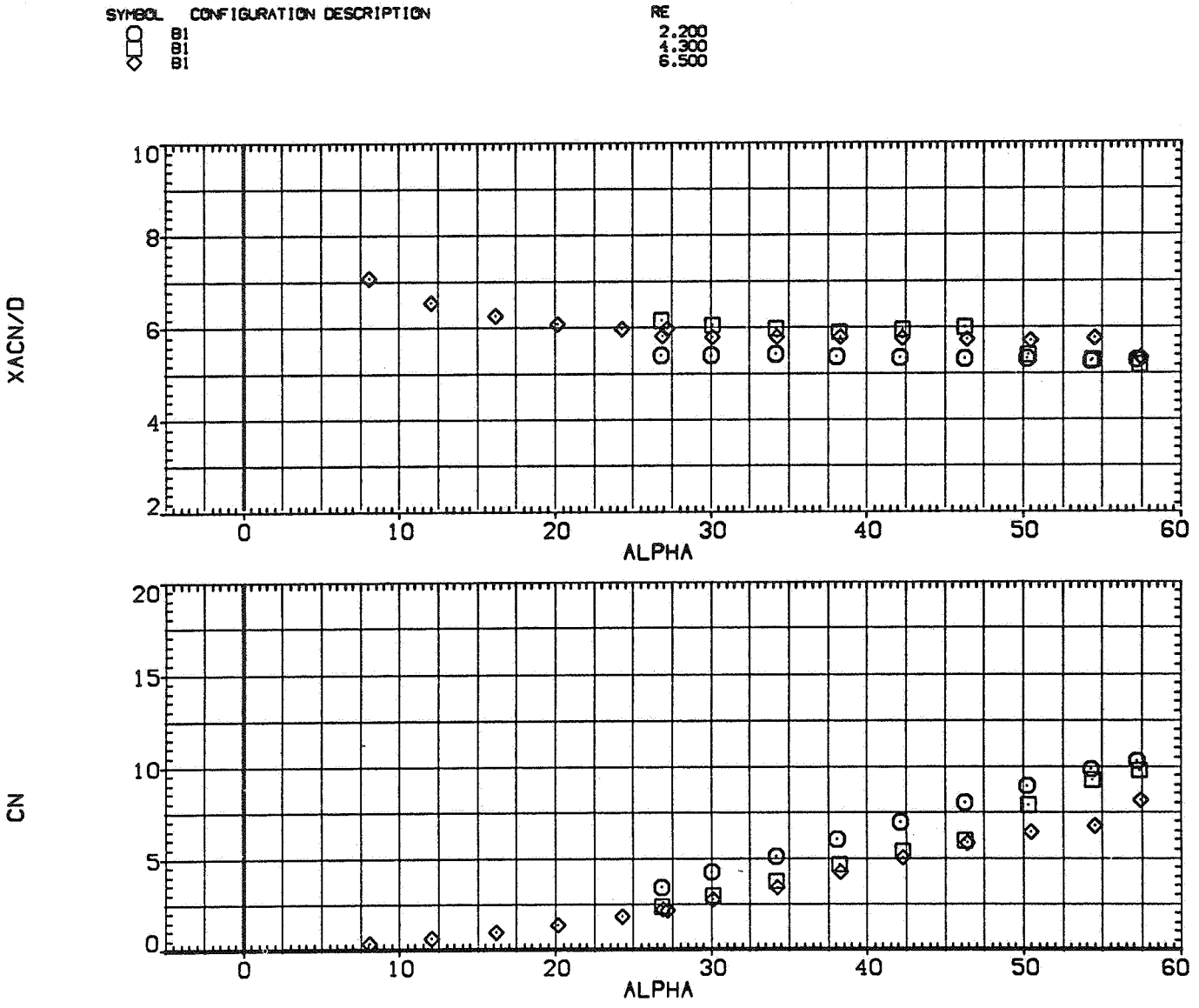

(a) x_{ac_N}/d and C_N versus α

Figure 13.– Effect of Reynolds number for B_1, $M = 0.6$.

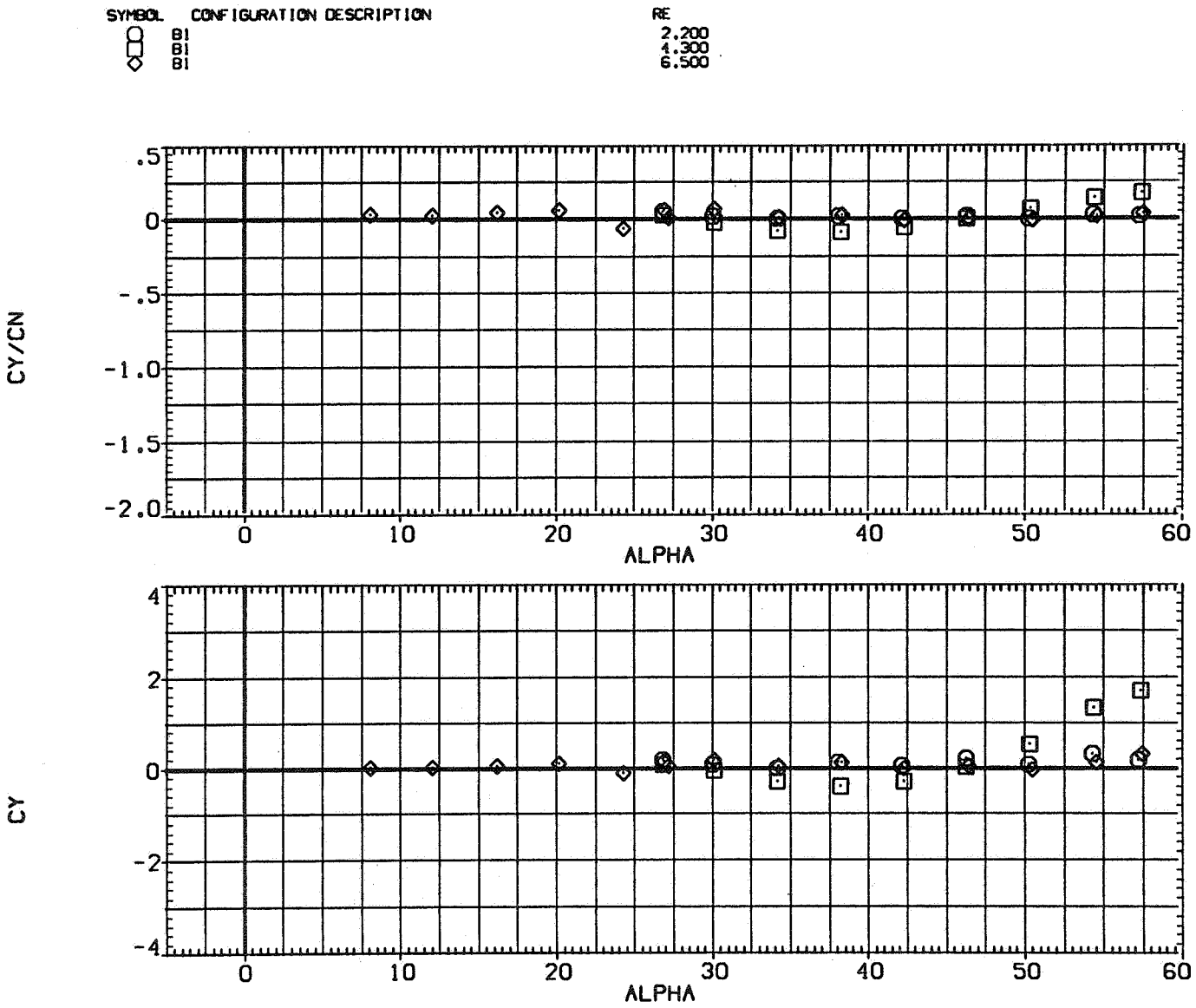

(b) C_Y/C_N and C_Y versus α

Figure 13.– Continued.

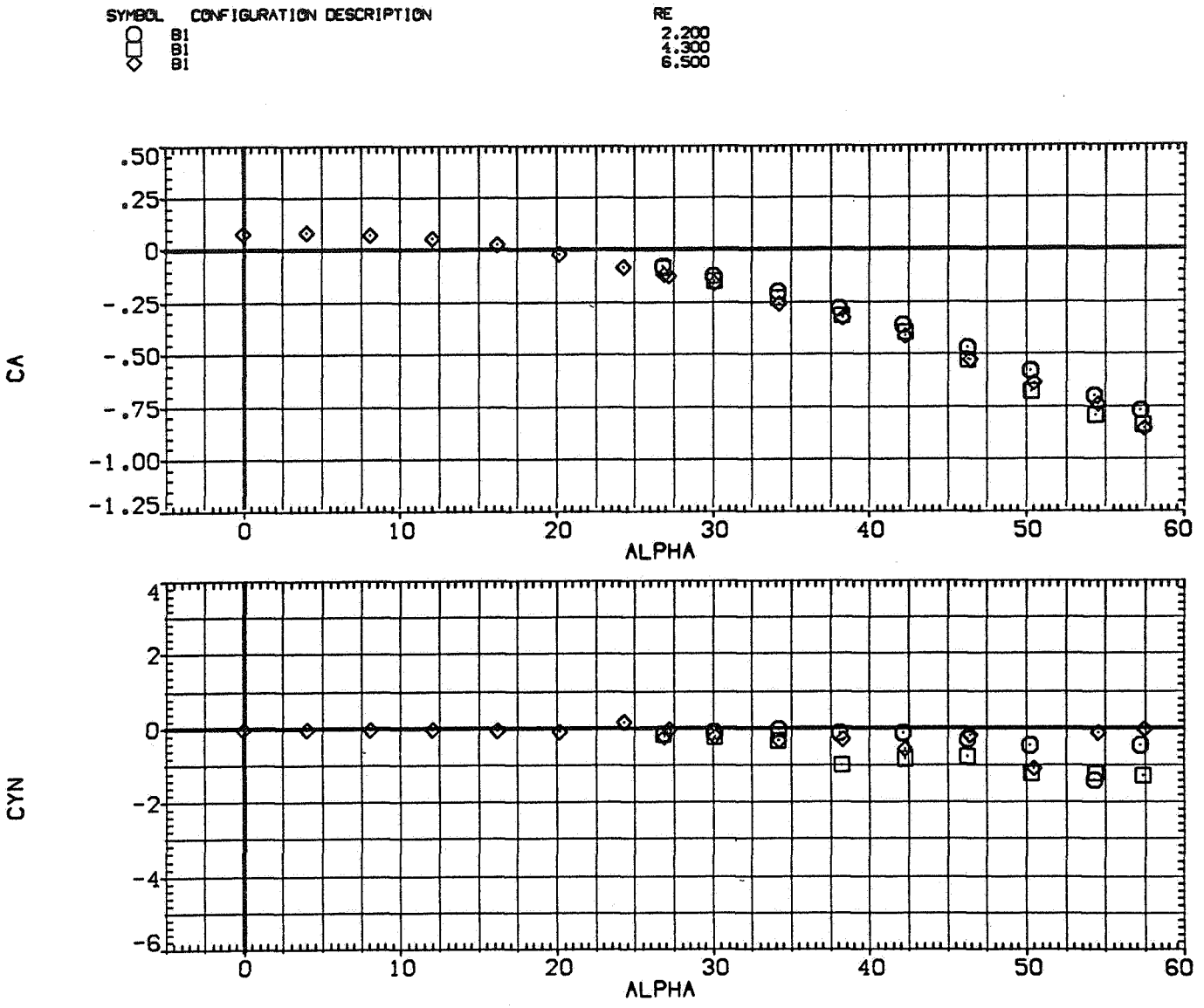

(c) C_A and C_n versus α

Figure 13.– Concluded.

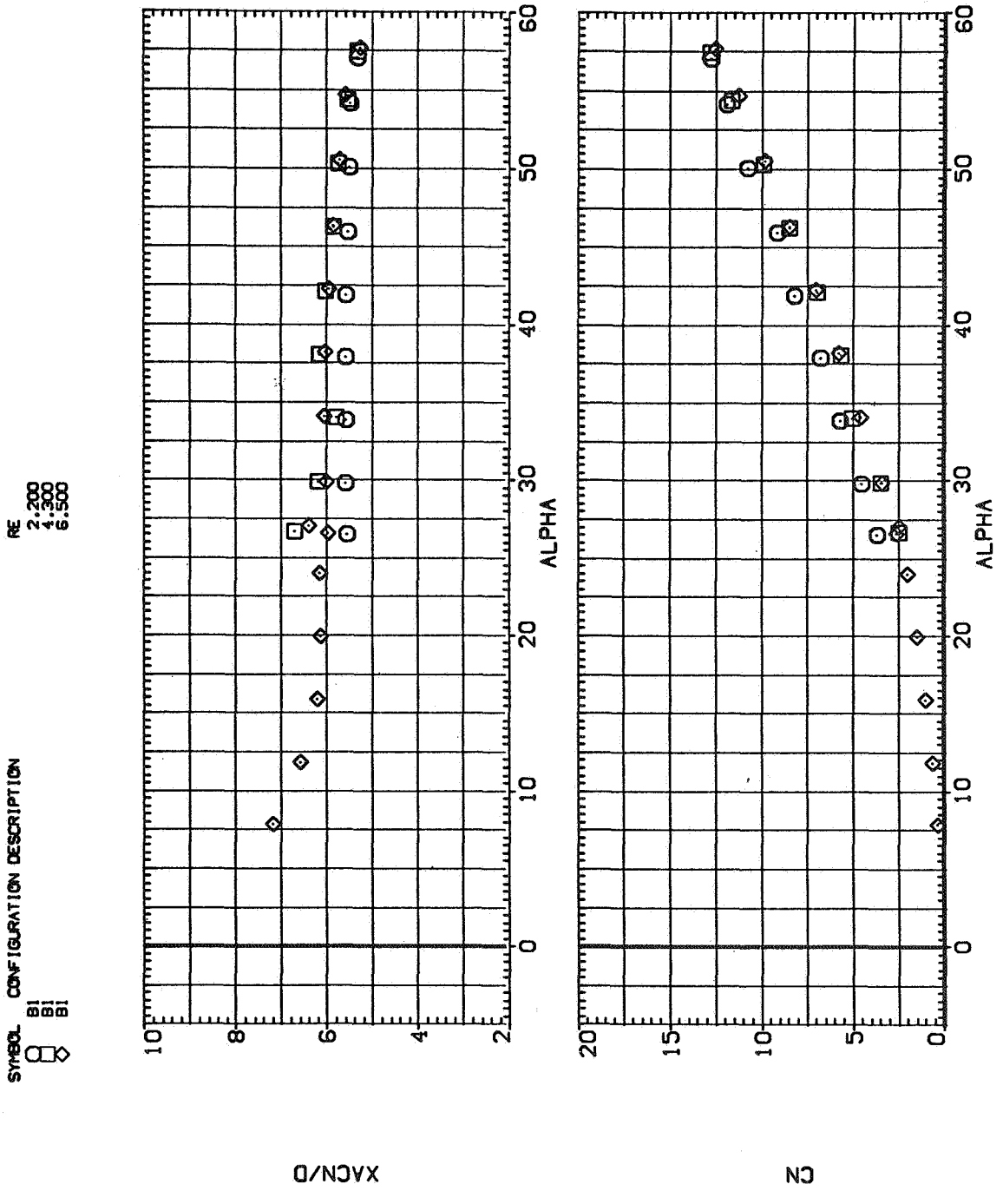

(a) x_{ac_N}/d and C_N versus α

Figure 14.– Effect of Reynolds number for B_1, $M = 0.9$.

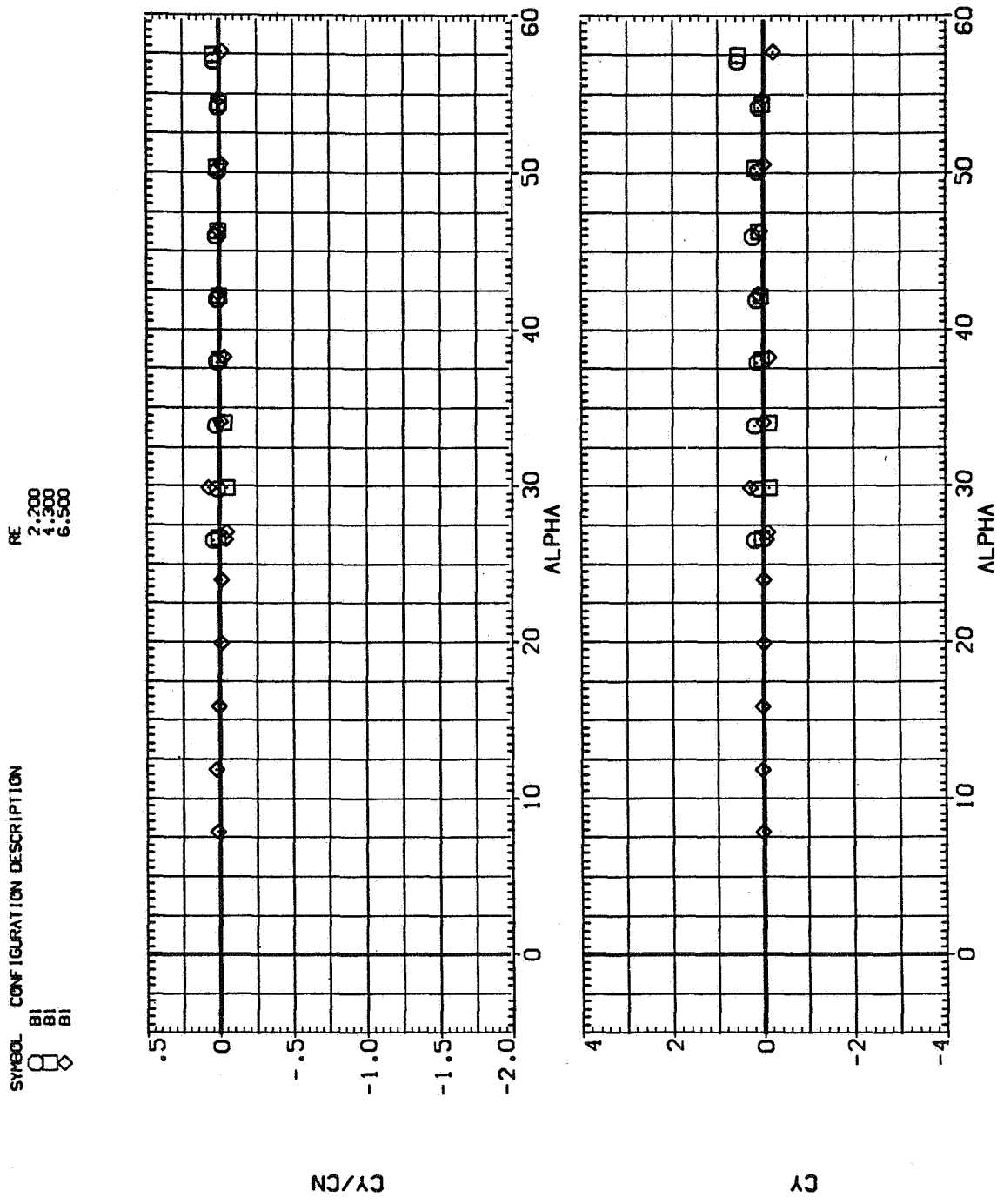

(b) C_Y/C_N and C_Y versus α

Figure 14.– Continued.

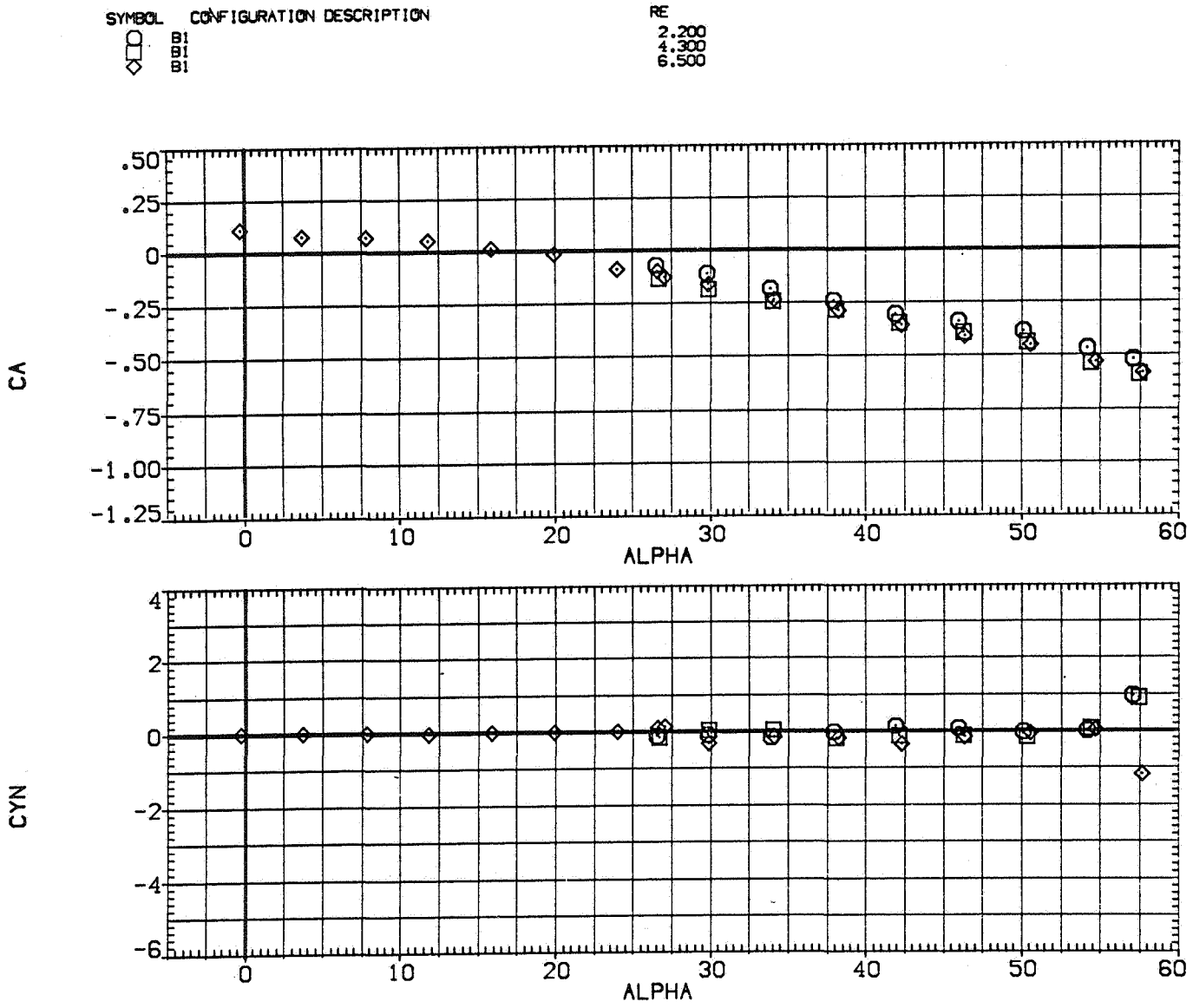

(c) C_A and C_n versus α

Figure 14.– Concluded.

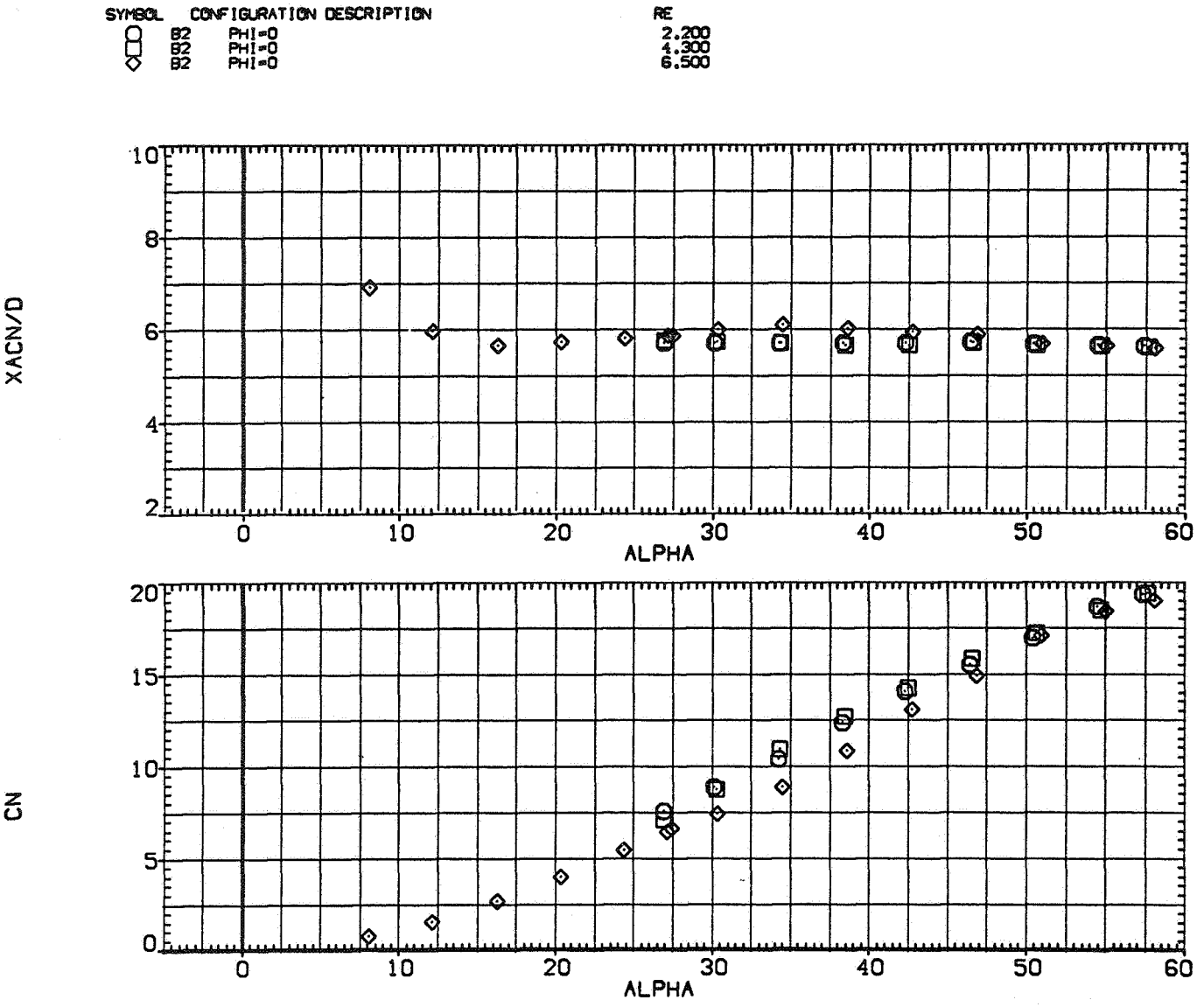

(a) x_{ac_N}/d and C_N versus α

Figure 15.– Effect of Reynolds number for B_2 ; $\phi = 0°, M = 0.6$.

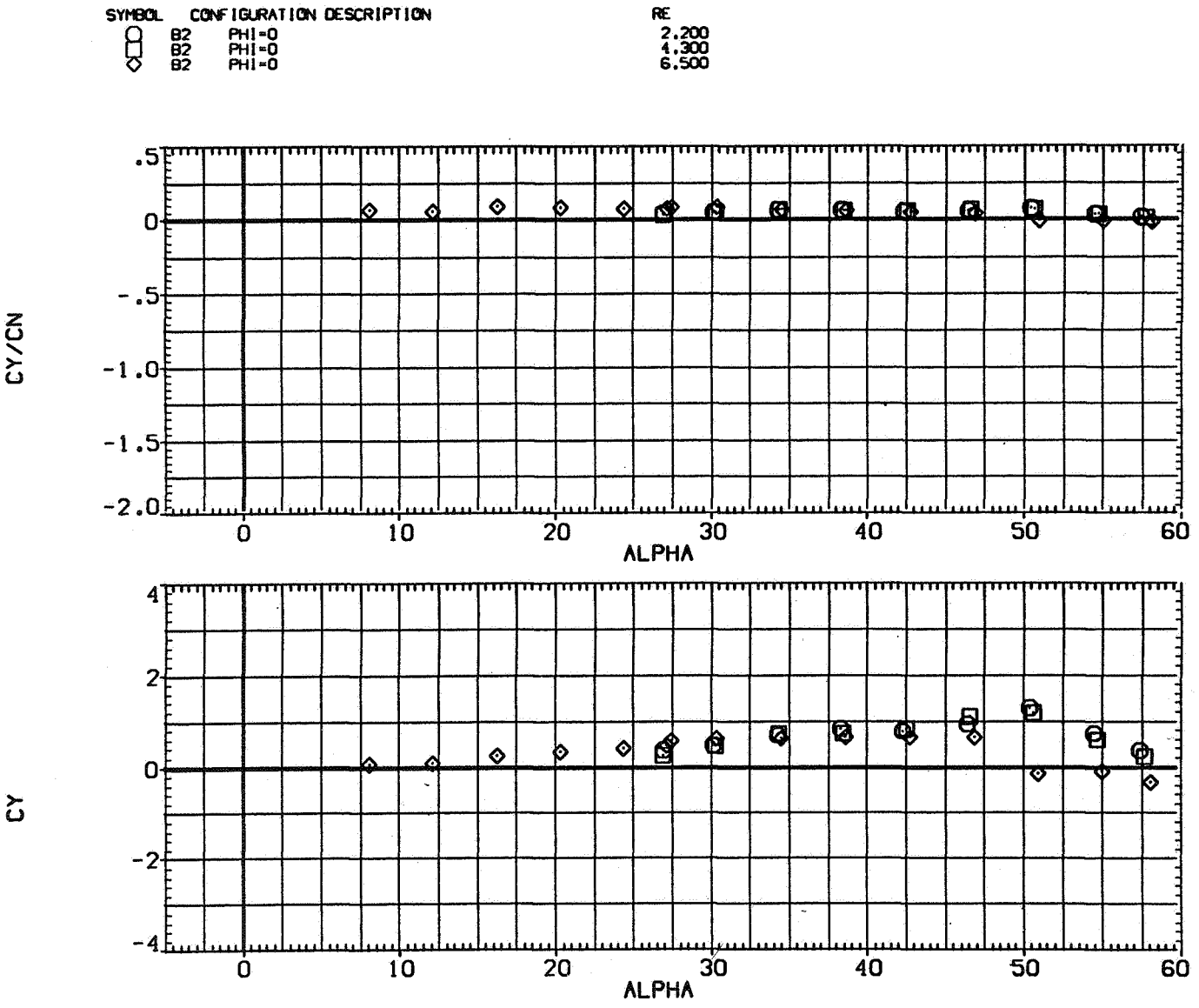

(b) C_Y/C_N and C_Y versus α

Figure 15.– Continued.

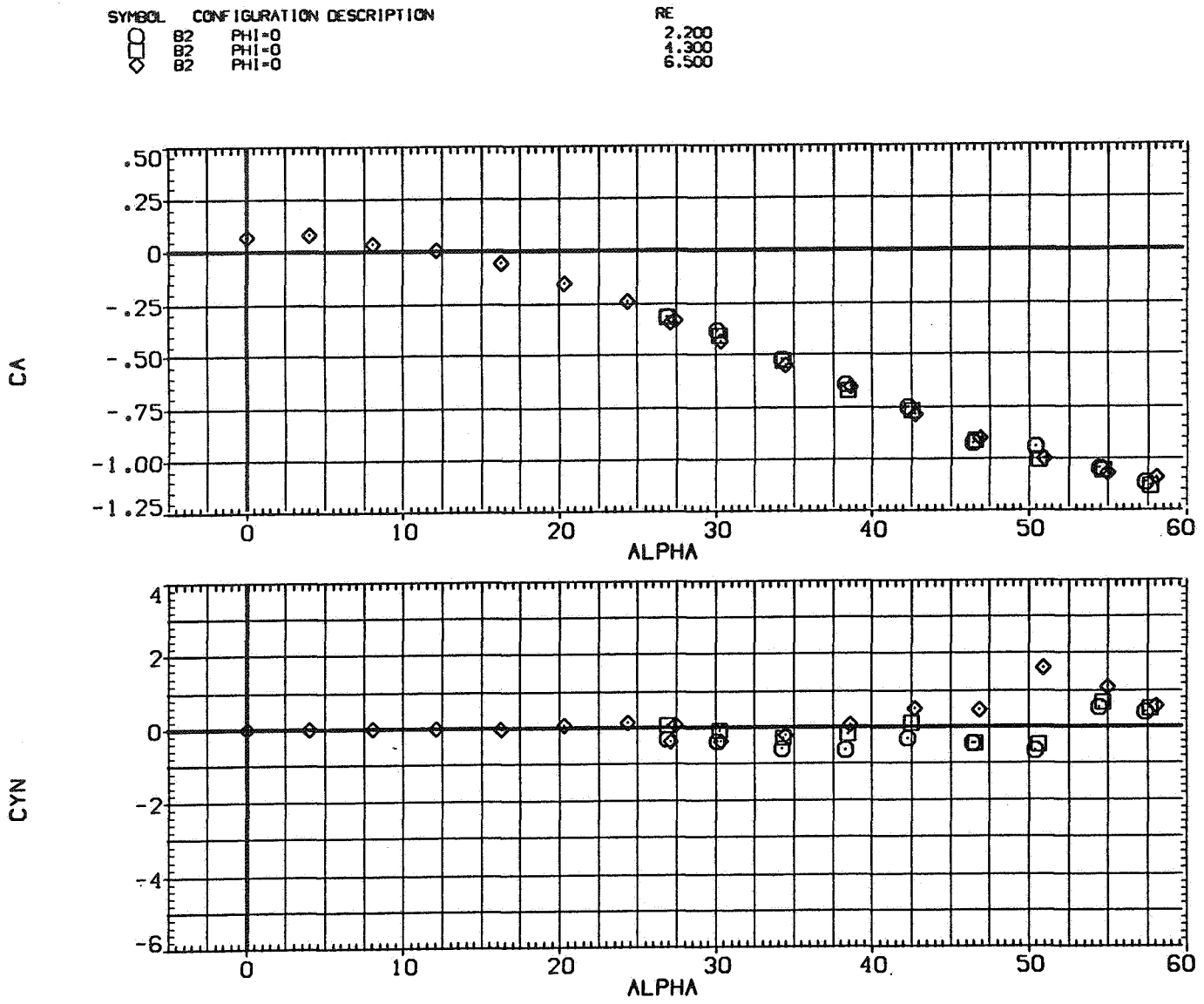

(c) C_A and C_n versus α

Figure 15.– Concluded.

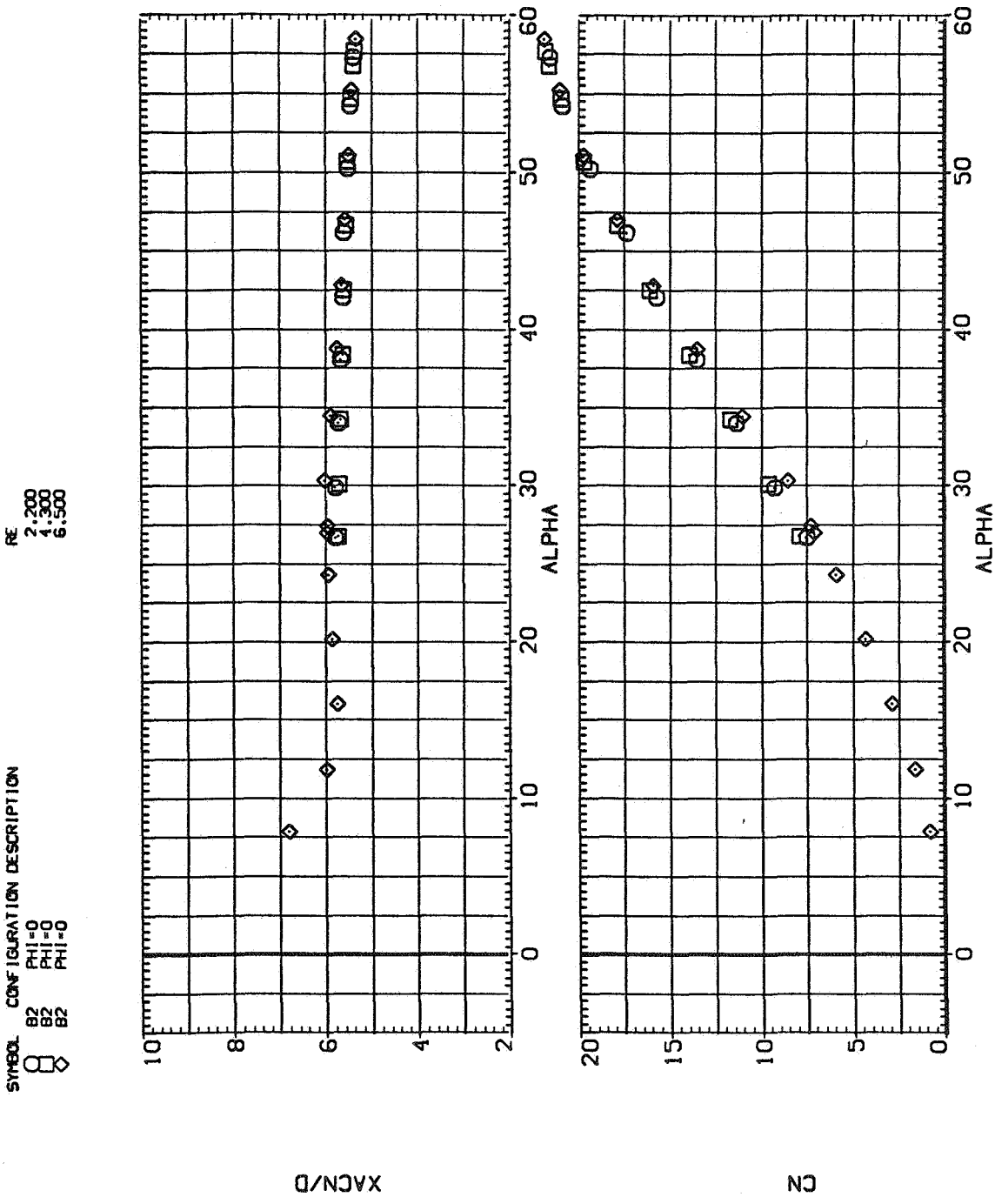

(a) x_{ac_N}/d and C_N versus α

Figure 16.– Effect of Reynolds number for B_2 ; $\phi = 0°$, $M = 0.9$.

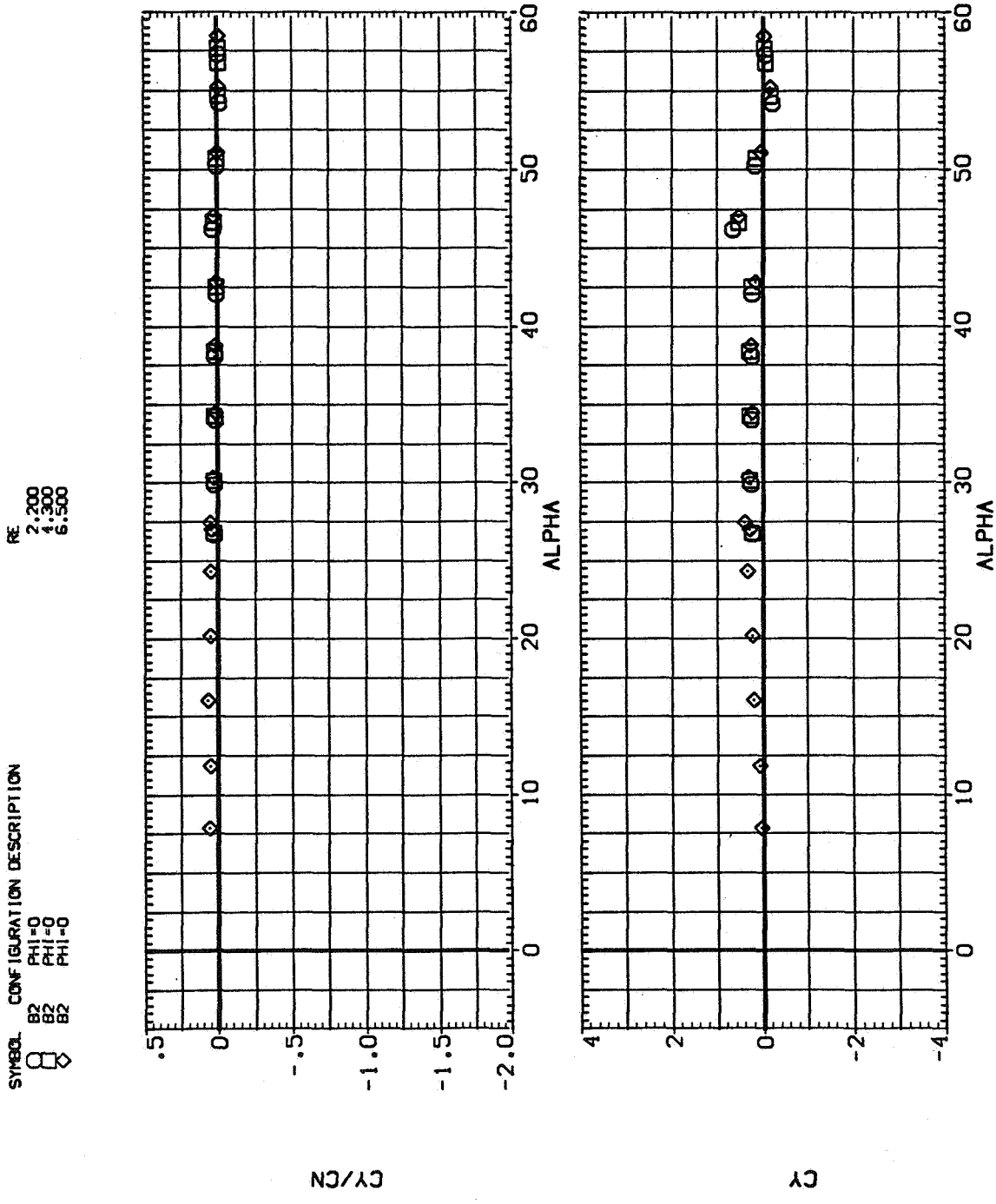

(b) C_Y/C_N and C_Y versus α

Figure 16.– Continued.

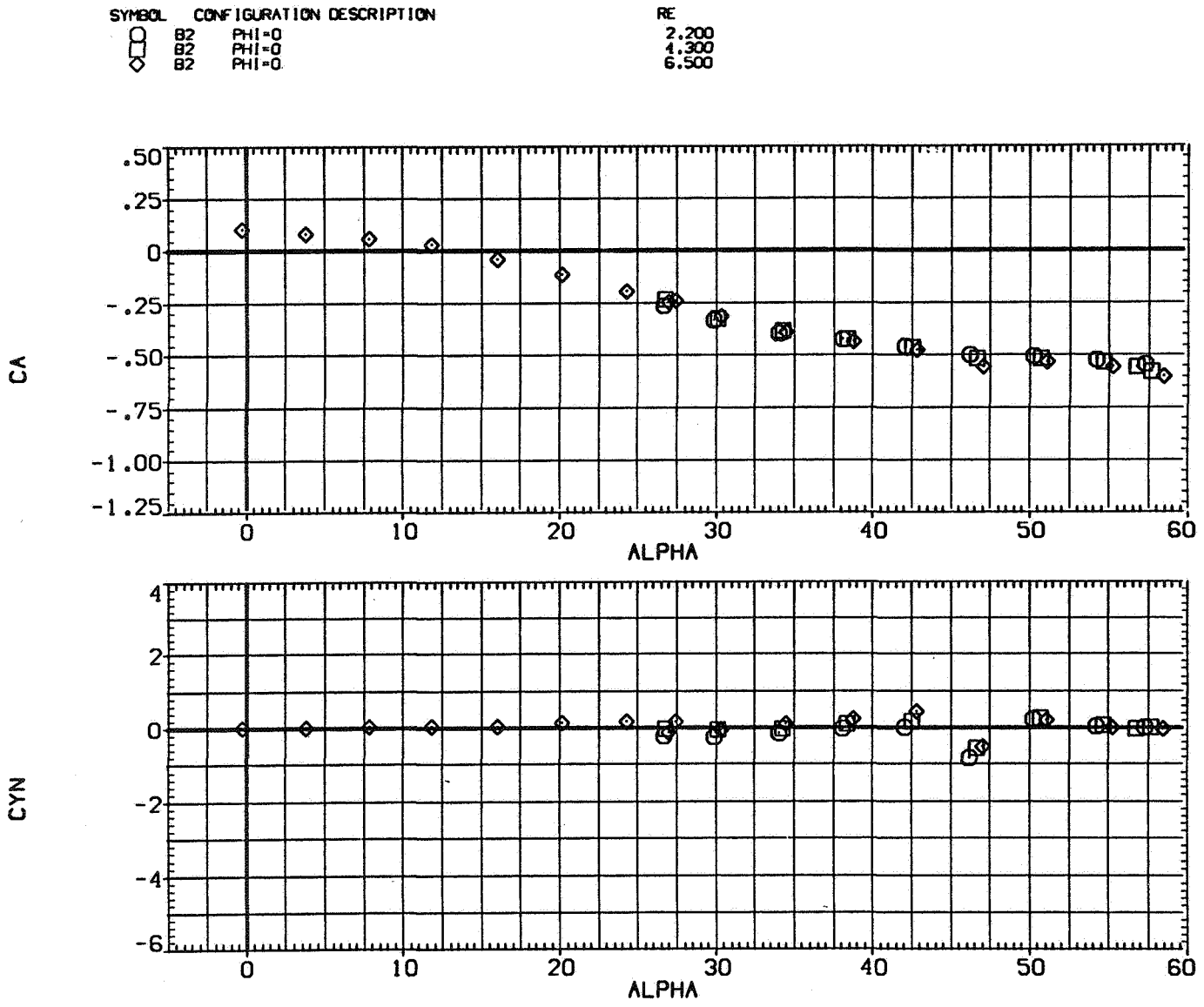

(c) C_A and C_n versus α

Figure 16.– Concluded.

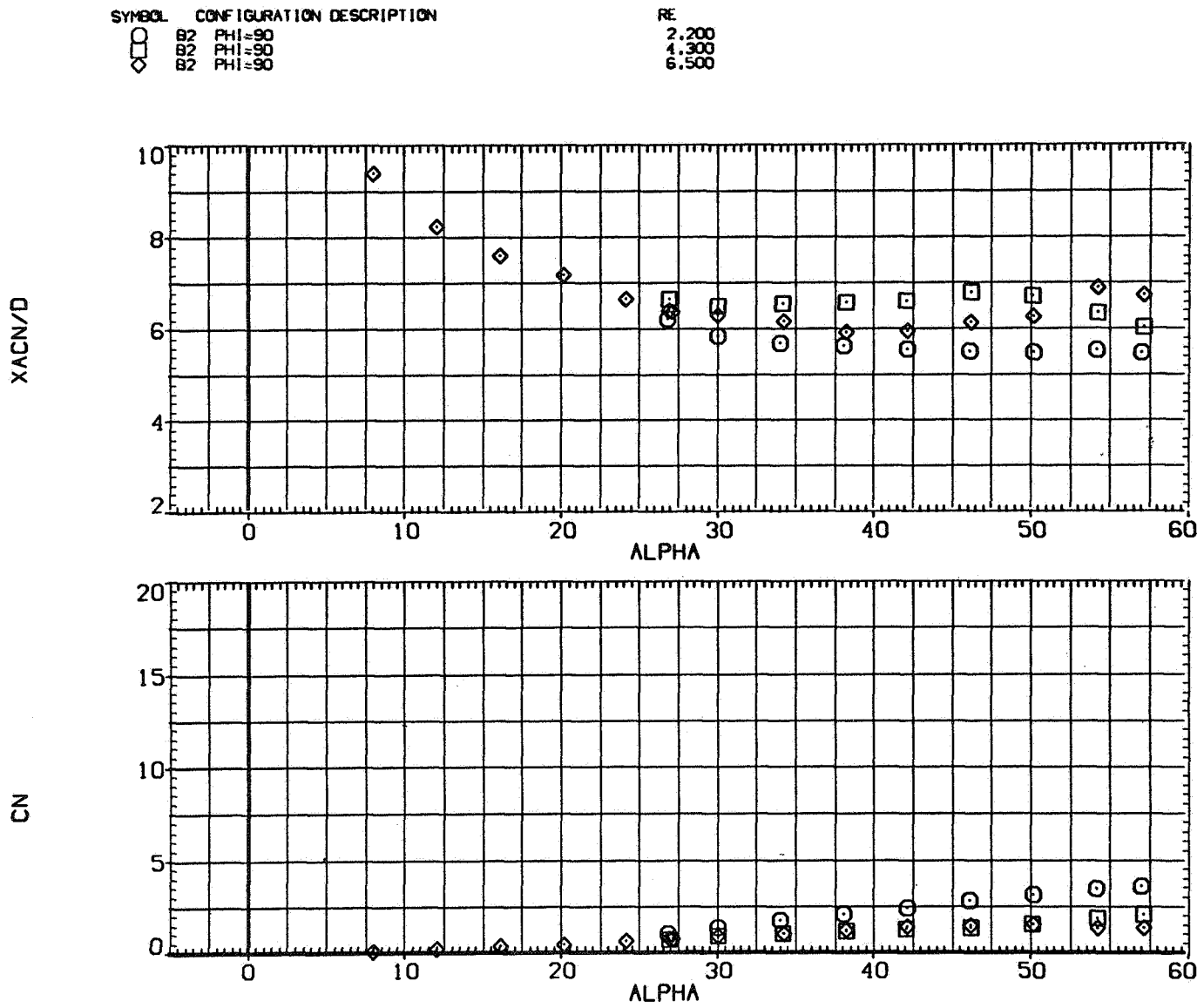

(a) x_{ac_N}/d and C_N versus α

Figure 17.– Effect of Reynolds number for B_2 ; $\phi = 90°$, $M = 0.6$.

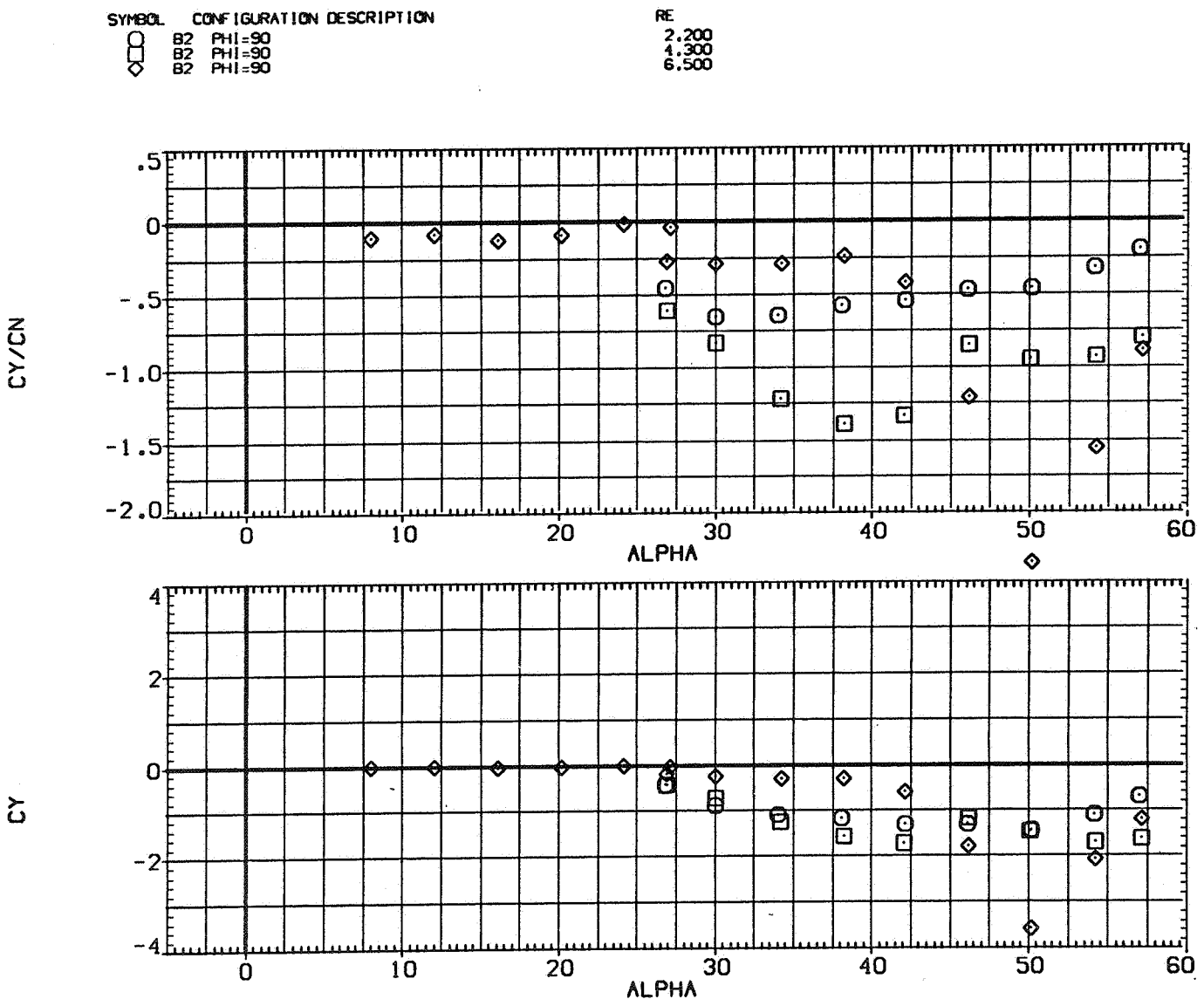

(b) C_Y/C_N and C_Y versus α

Figure 17.– Continued.

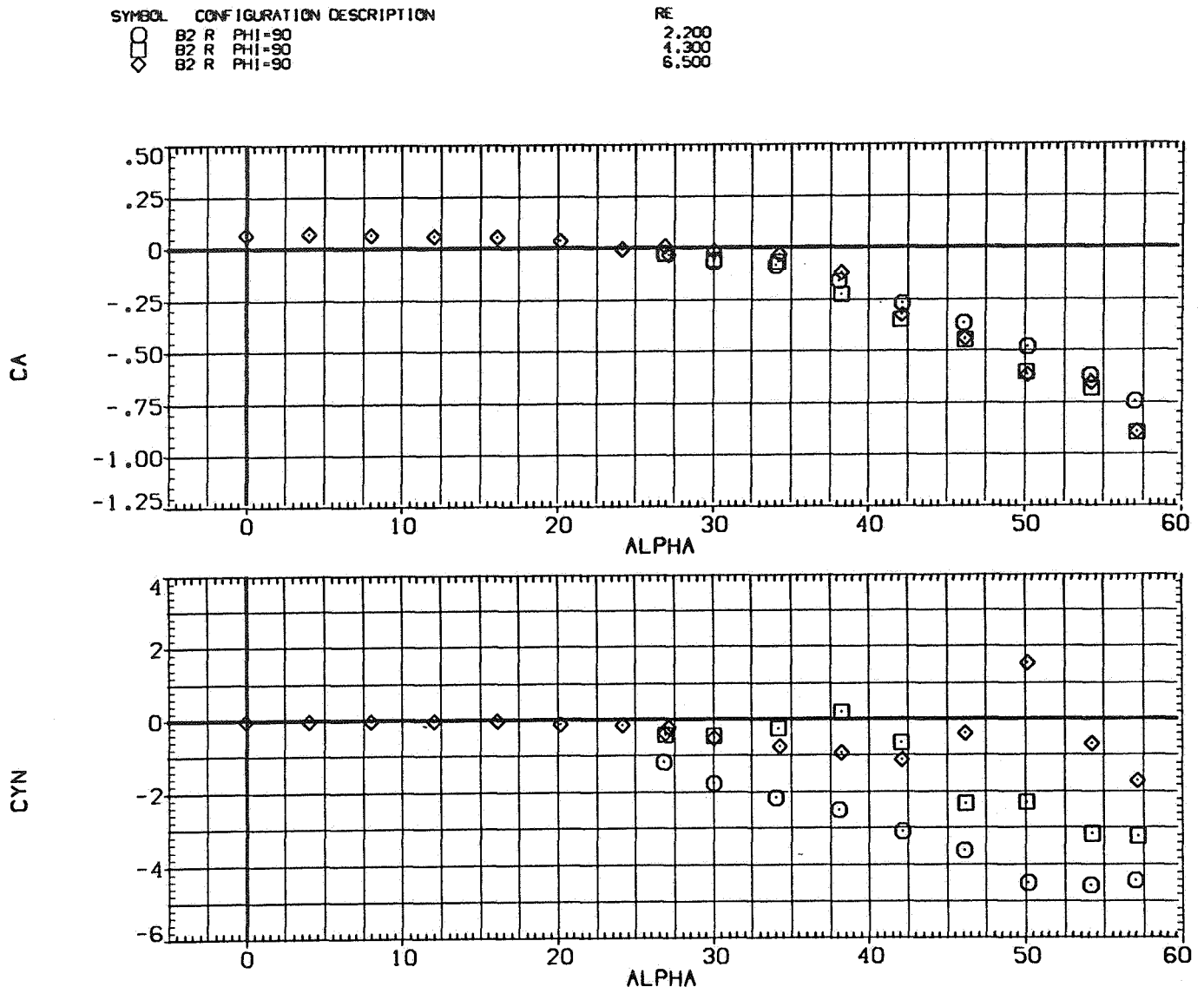

(c) C_A and C_n versus α

Figure 17.– Concluded.

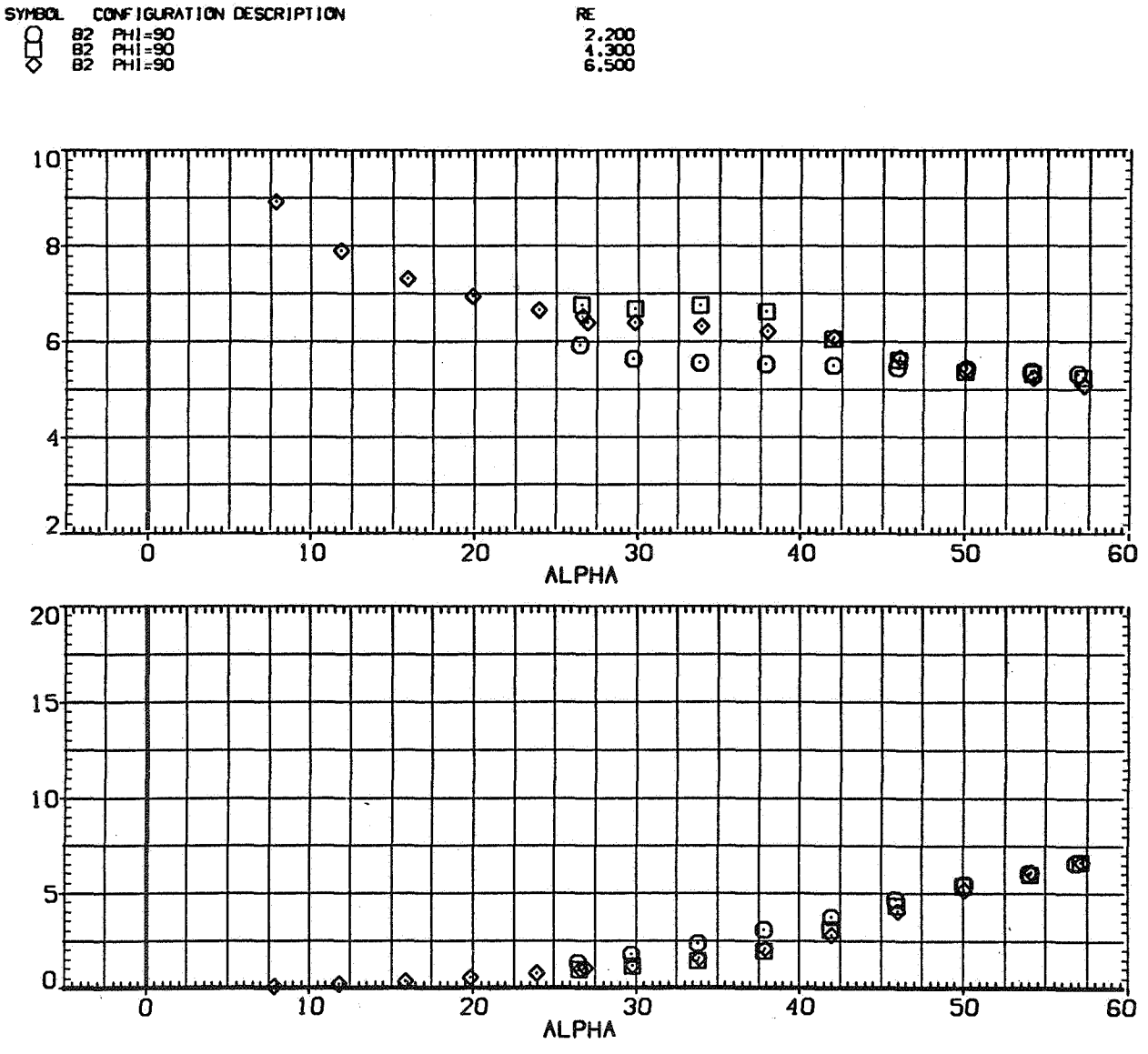

(a) x_{ac_N}/d and C_N versus α

Figure 18.– Effect of Reynolds number for B_2 ; $\phi = 90°, M = 0.9$.

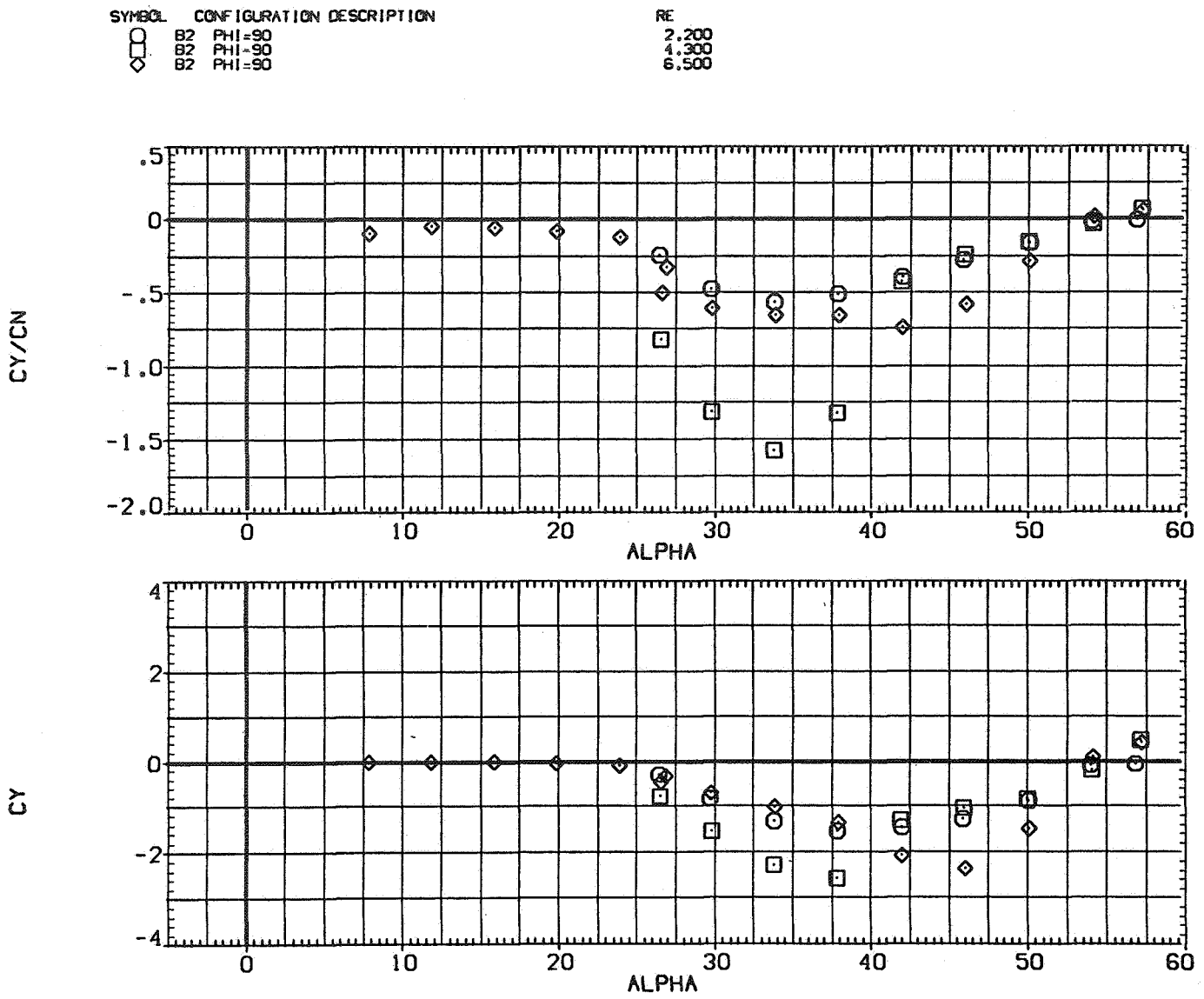

(b) C_Y/C_N and C_Y versus α

Figure 18.– Continued.

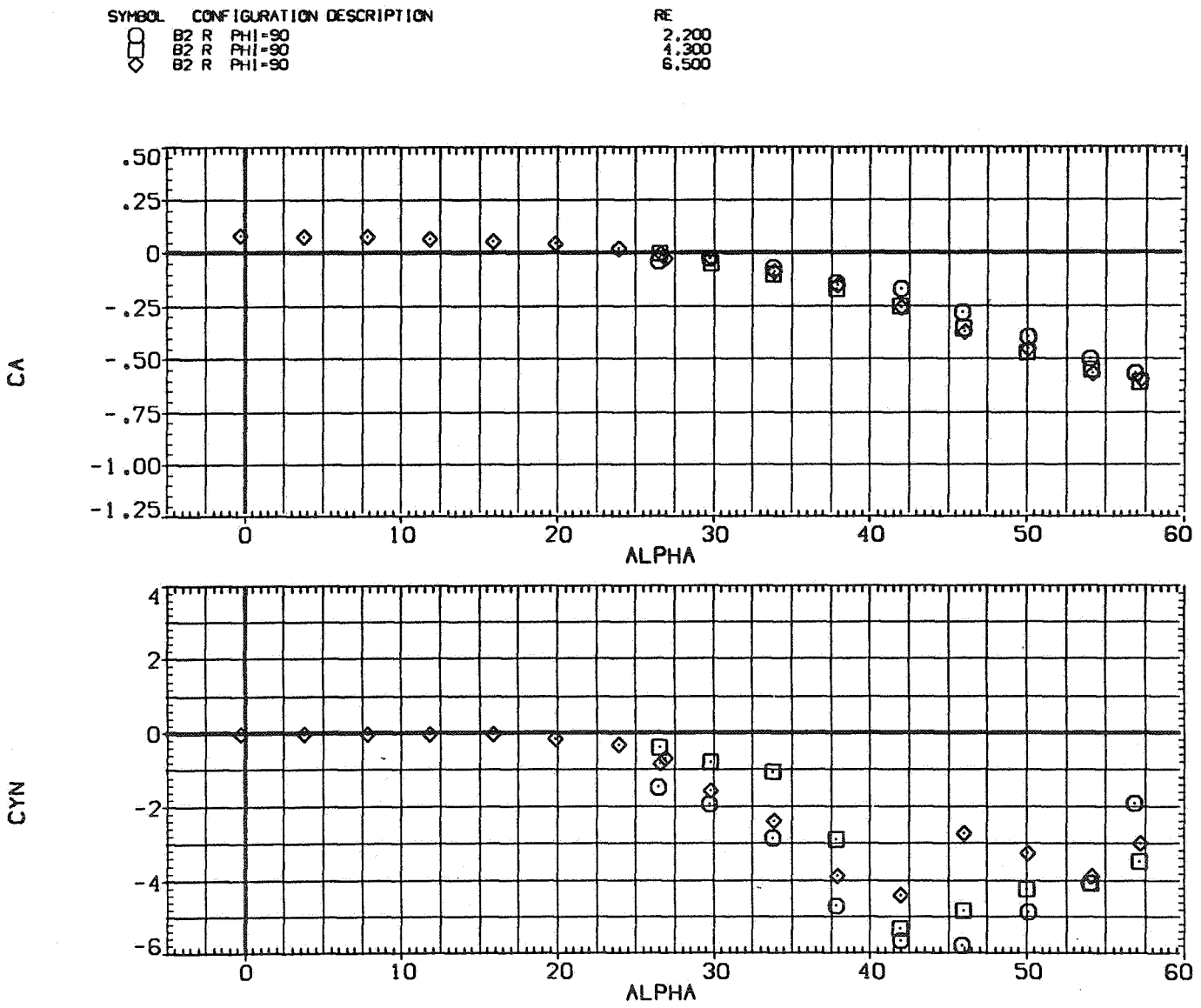

(c) C_A and C_n versus α

Figure 18.– Concluded.

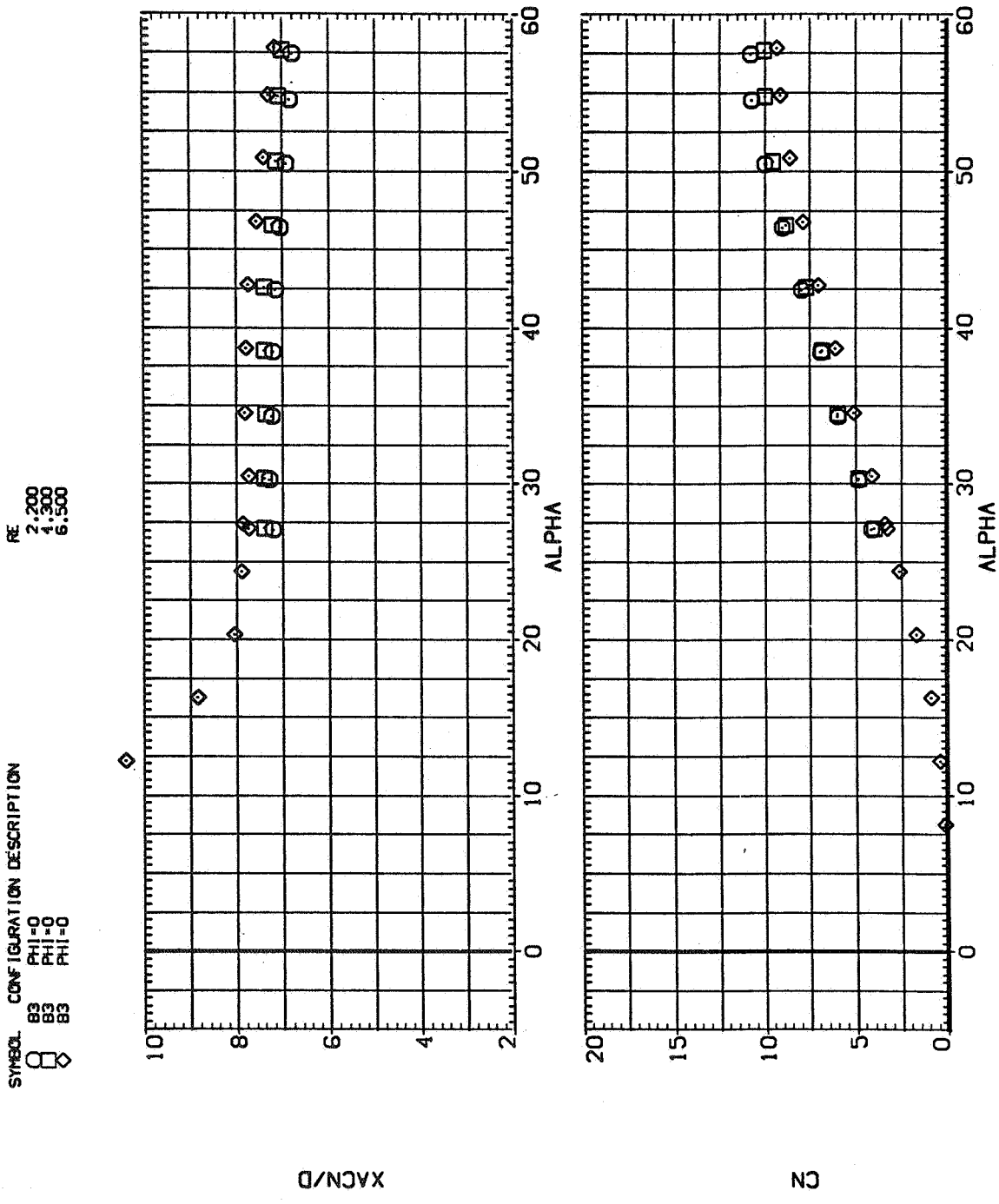

(a) x_{ac_N}/d and C_N versus α

Figure 19.– Effect of Reynolds number for B_3 ; $\phi = 0°$, $M = 0.6$.

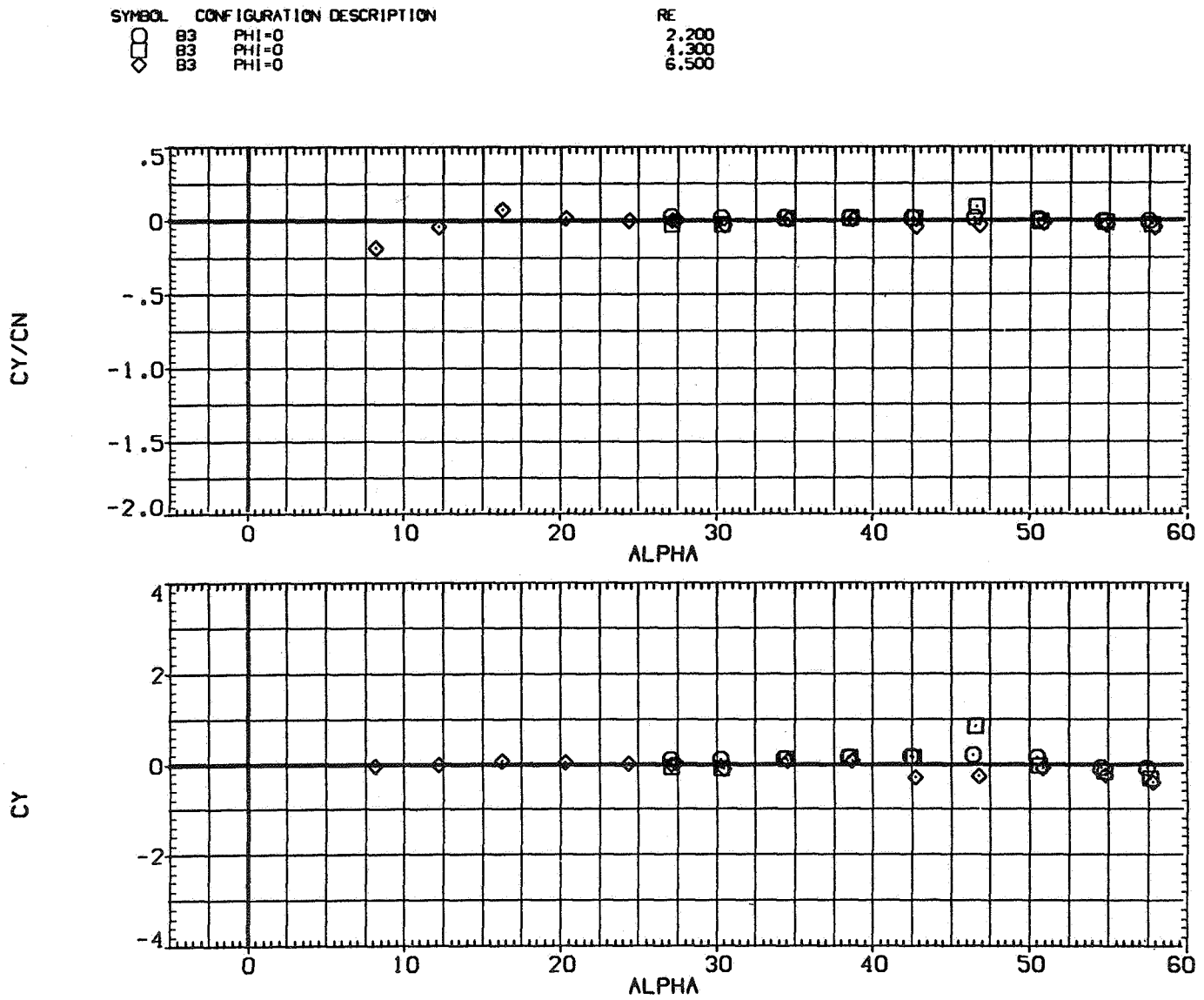

(b) C_Y/C_N and C_Y versus α

Figure 19.– Continued.

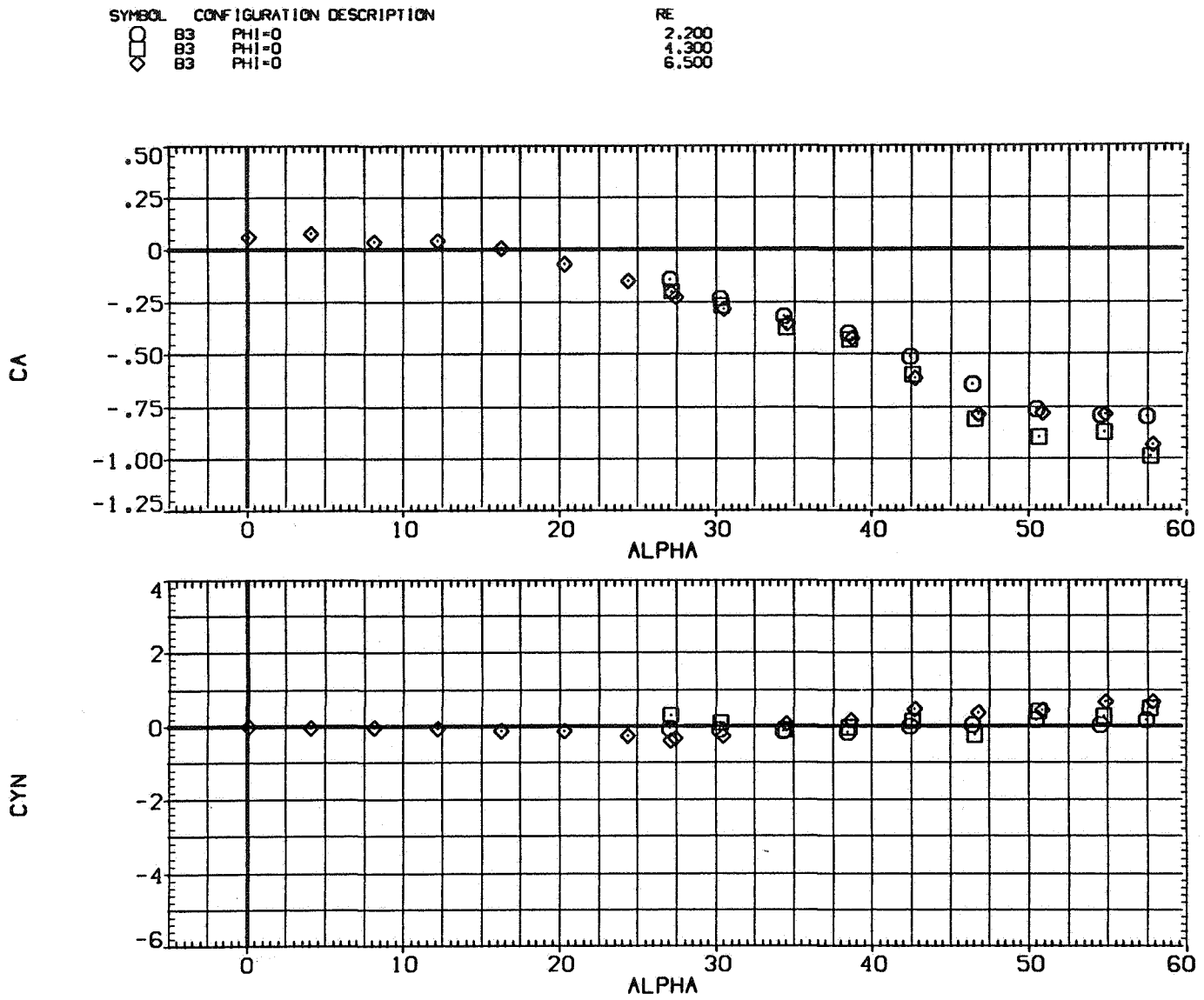

(c) C_A and C_n versus α

Figure 19.– Concluded.

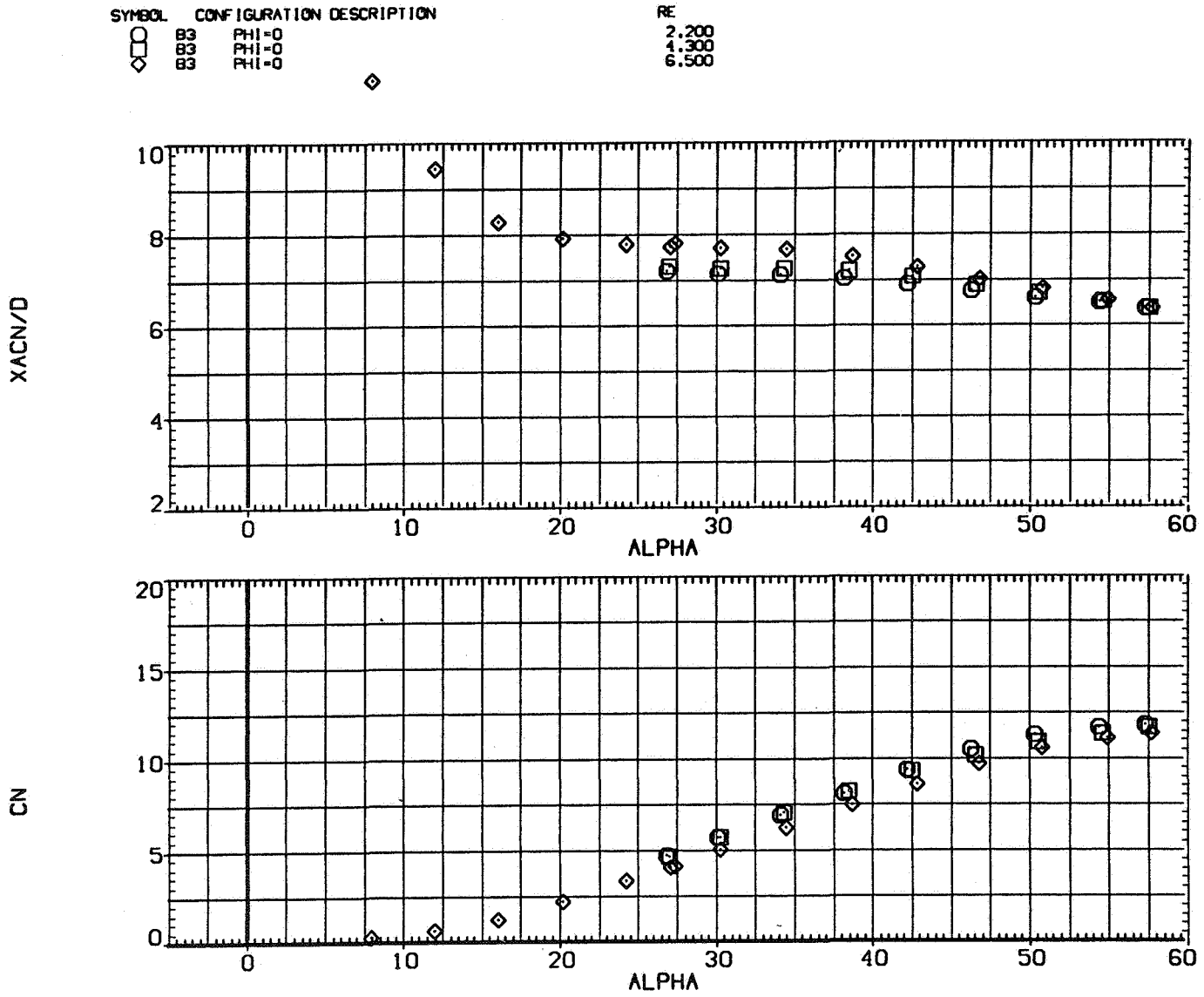

(a) x_{ac_N}/d and C_N versus α

Figure 20.– Effect of Reynolds number for B_3 ; $\phi = 0°, M = 0.9$.

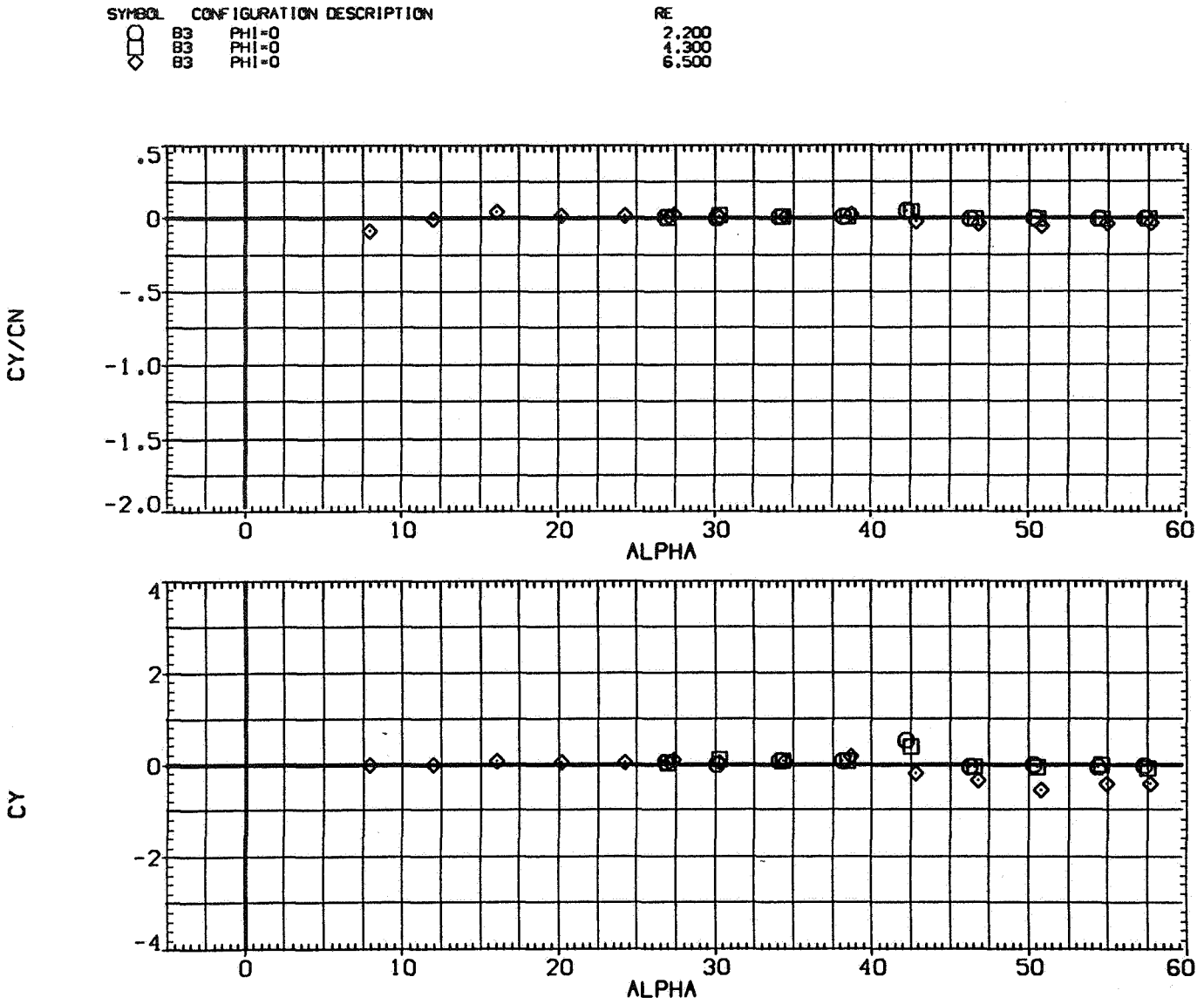

(b) C_Y/C_N and C_Y versus α

Figure 20.– Continued.

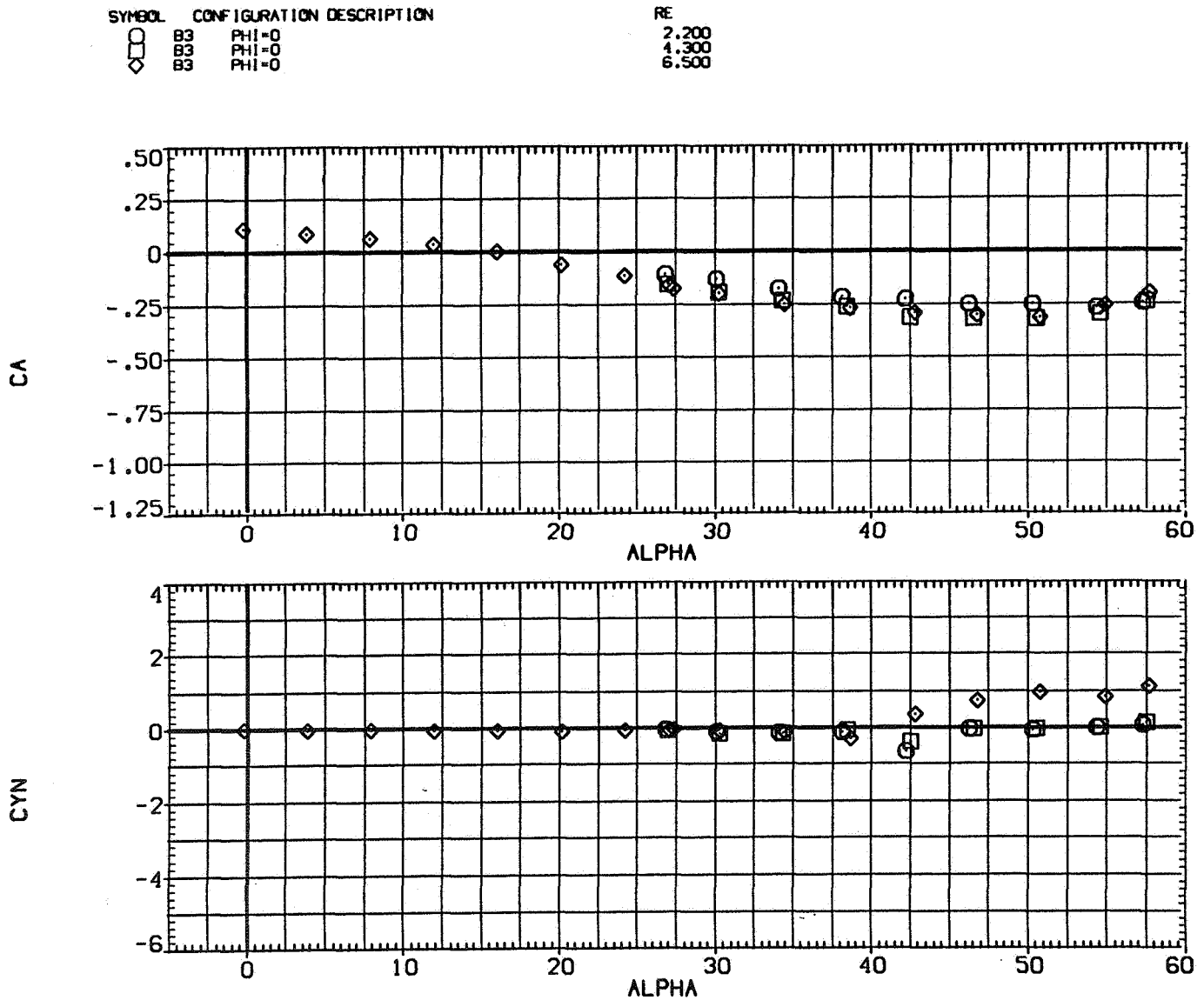

(c) C_A and C_n versus α

Figure 20.– Concluded.

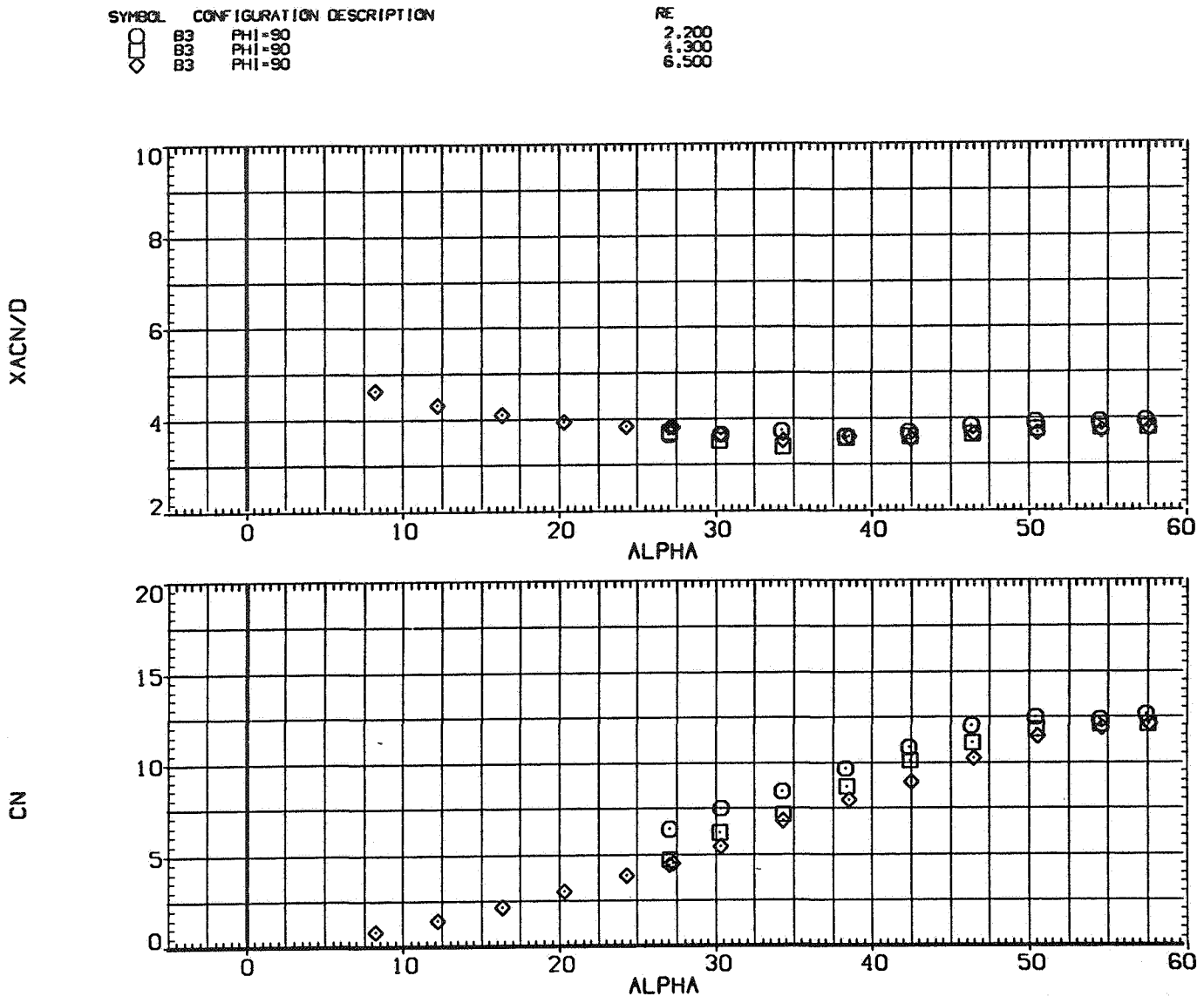

(a) $x_{ac_N}/\overline{d}$ and C_N versus α

Figure 21.– Effect of Reynolds number for B_3 ; $\phi = 90°$, $M = 0.6$.

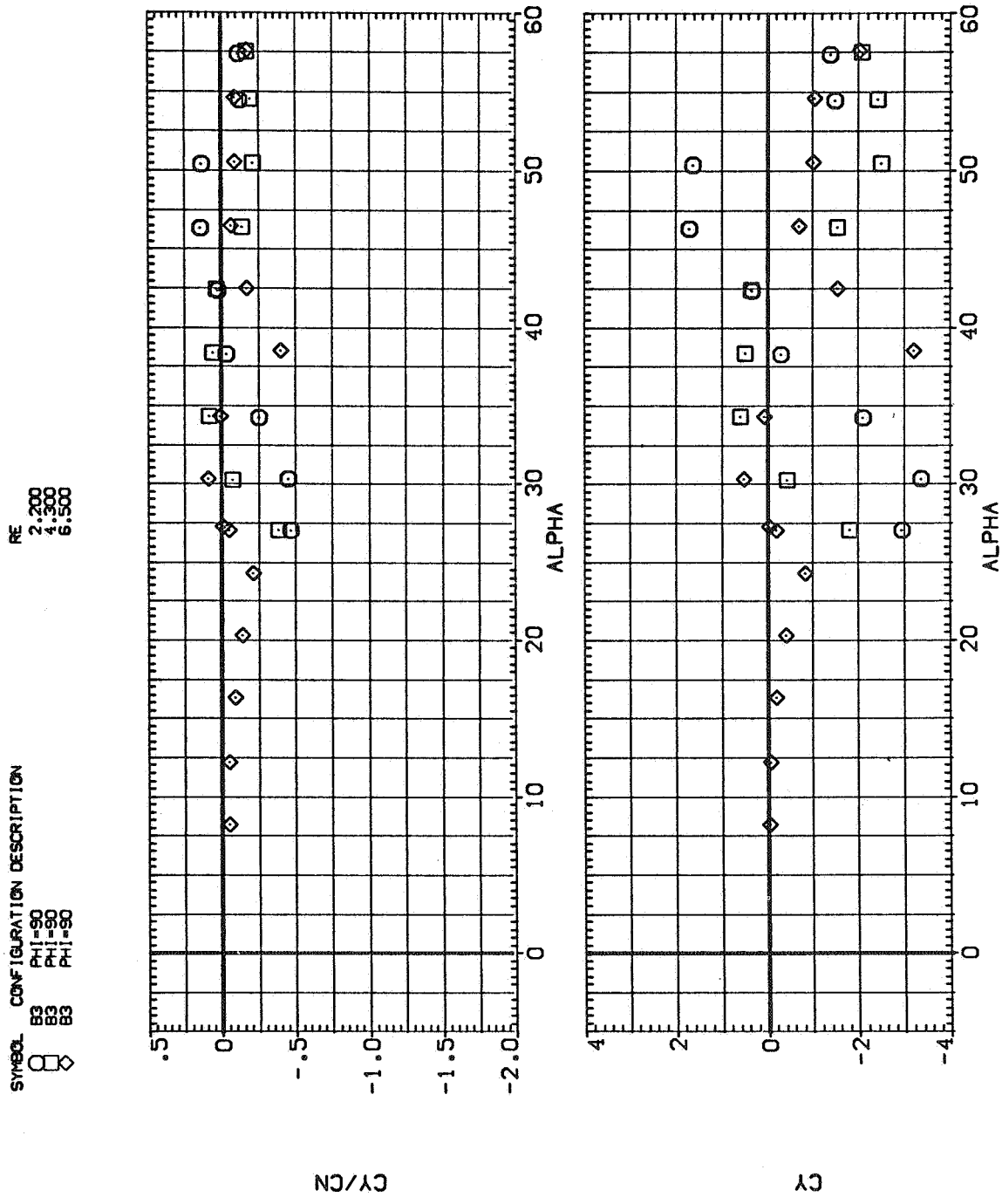

(b) C_Y/C_N and C_Y versus α

Figure 21.– Continued.

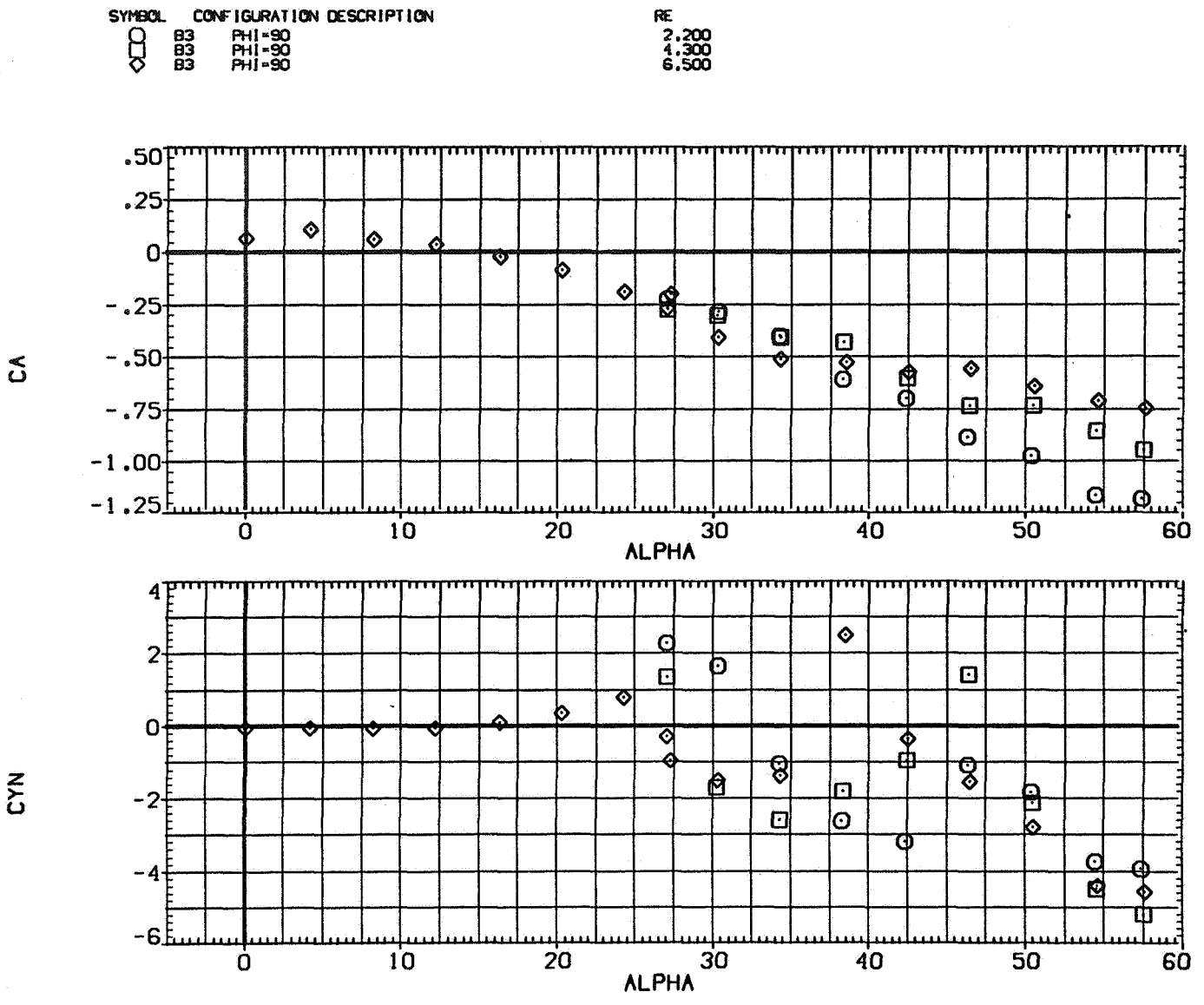

(c) C_A and C_n versus α

Figure 21.– Concluded.

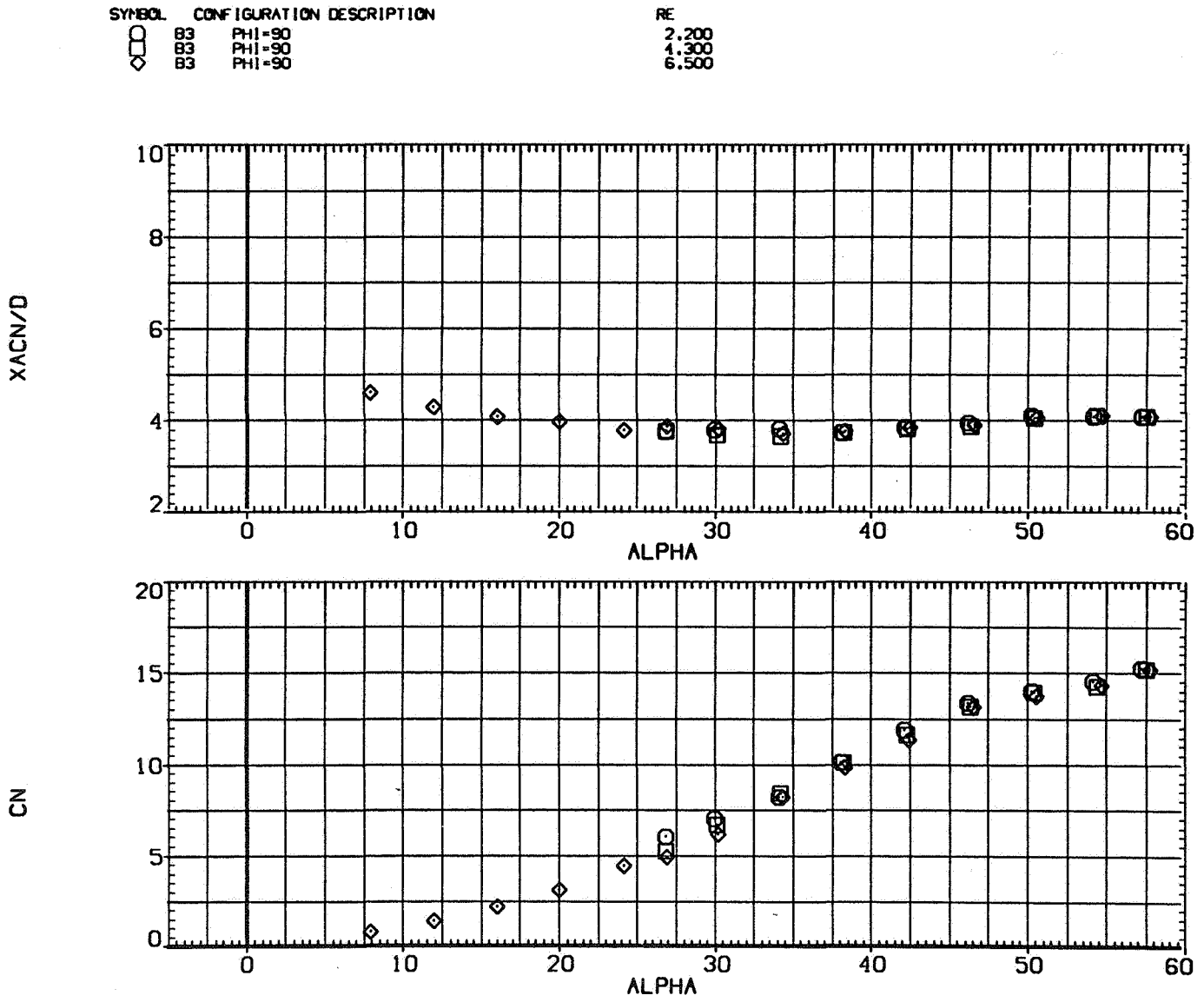

(a) x_{ac_N}/d and C_N versus α

Figure 22.– Effect of Reynolds number for B_3; $\phi = 90°, M = 0.9$.

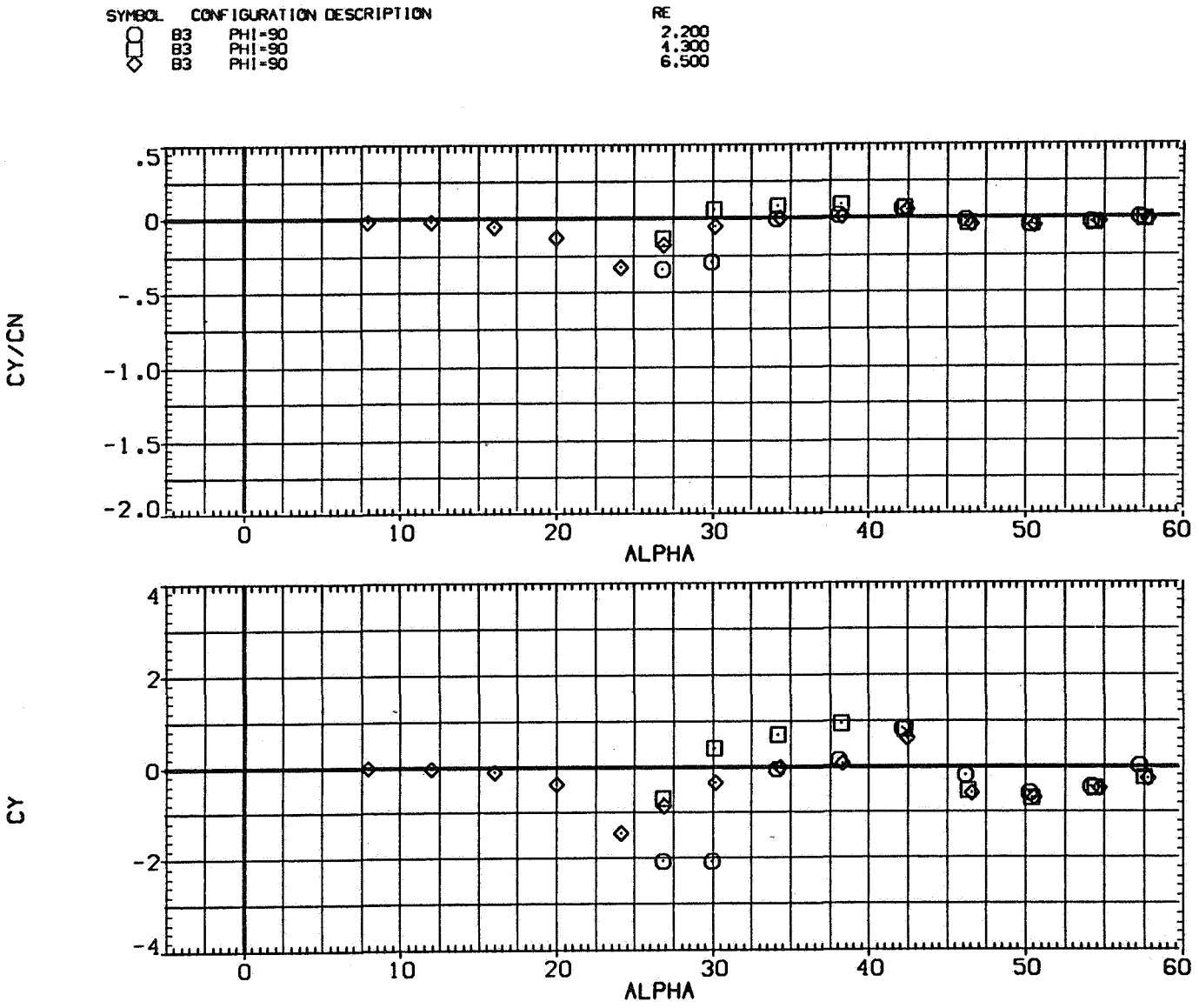

(b) C_Y/C_N and C_Y versus α

Figure 22.– Continued.

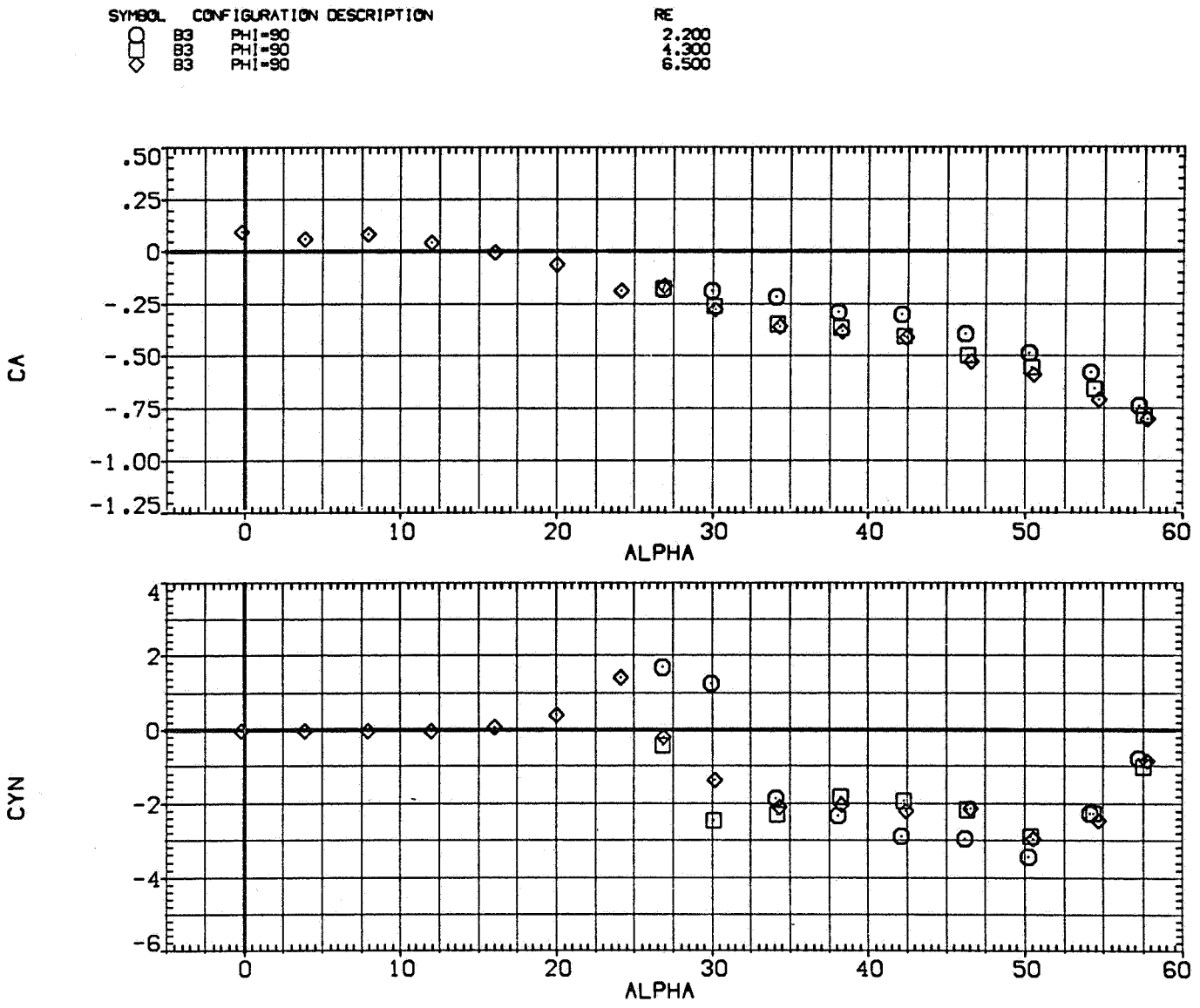

(c) C_A and C_n versus α

Figure 22.— Concluded.

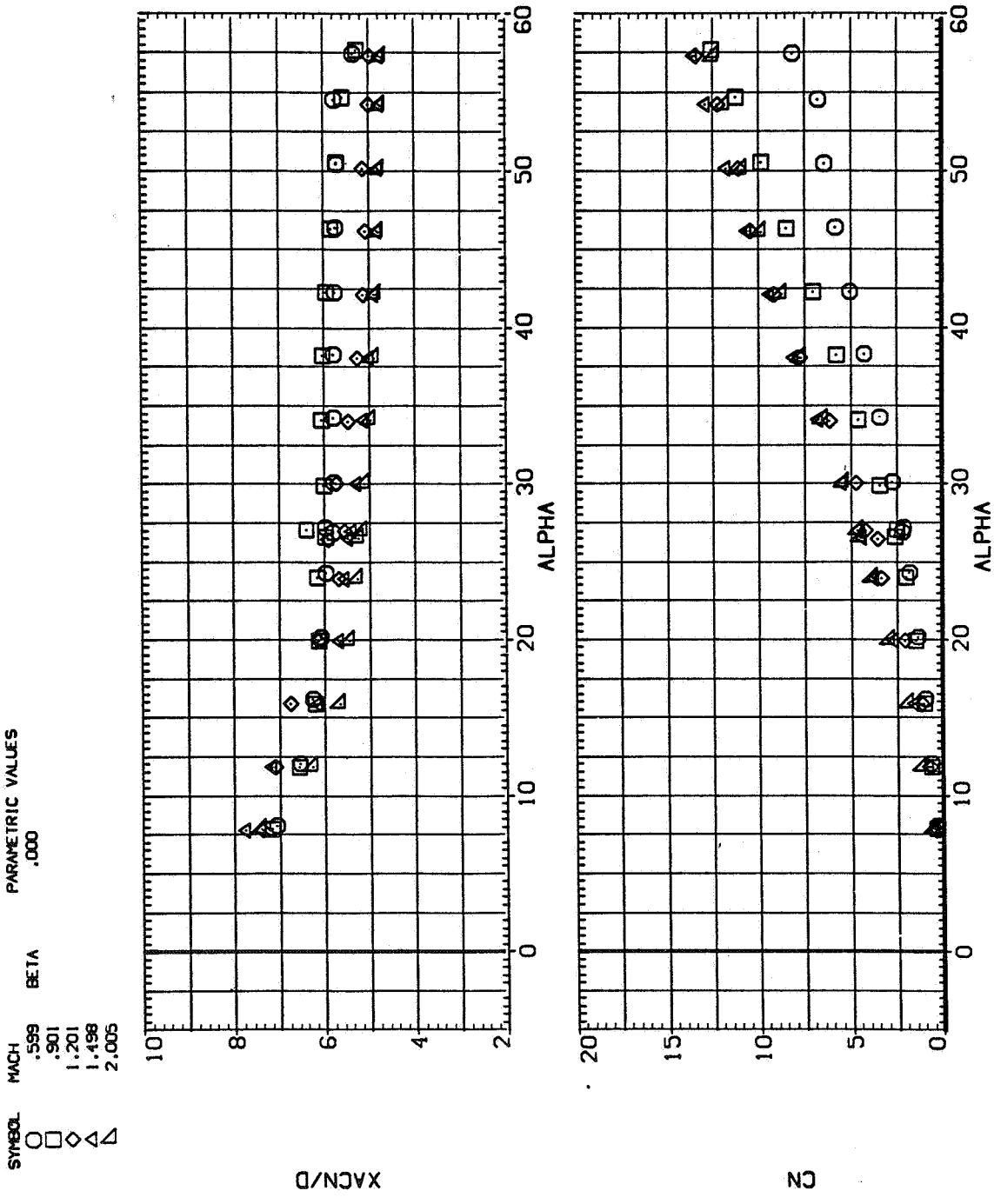

(a) x_{ac_N}/d and C_N versus α

Figure 23.– Effect of Mach number for B_1.

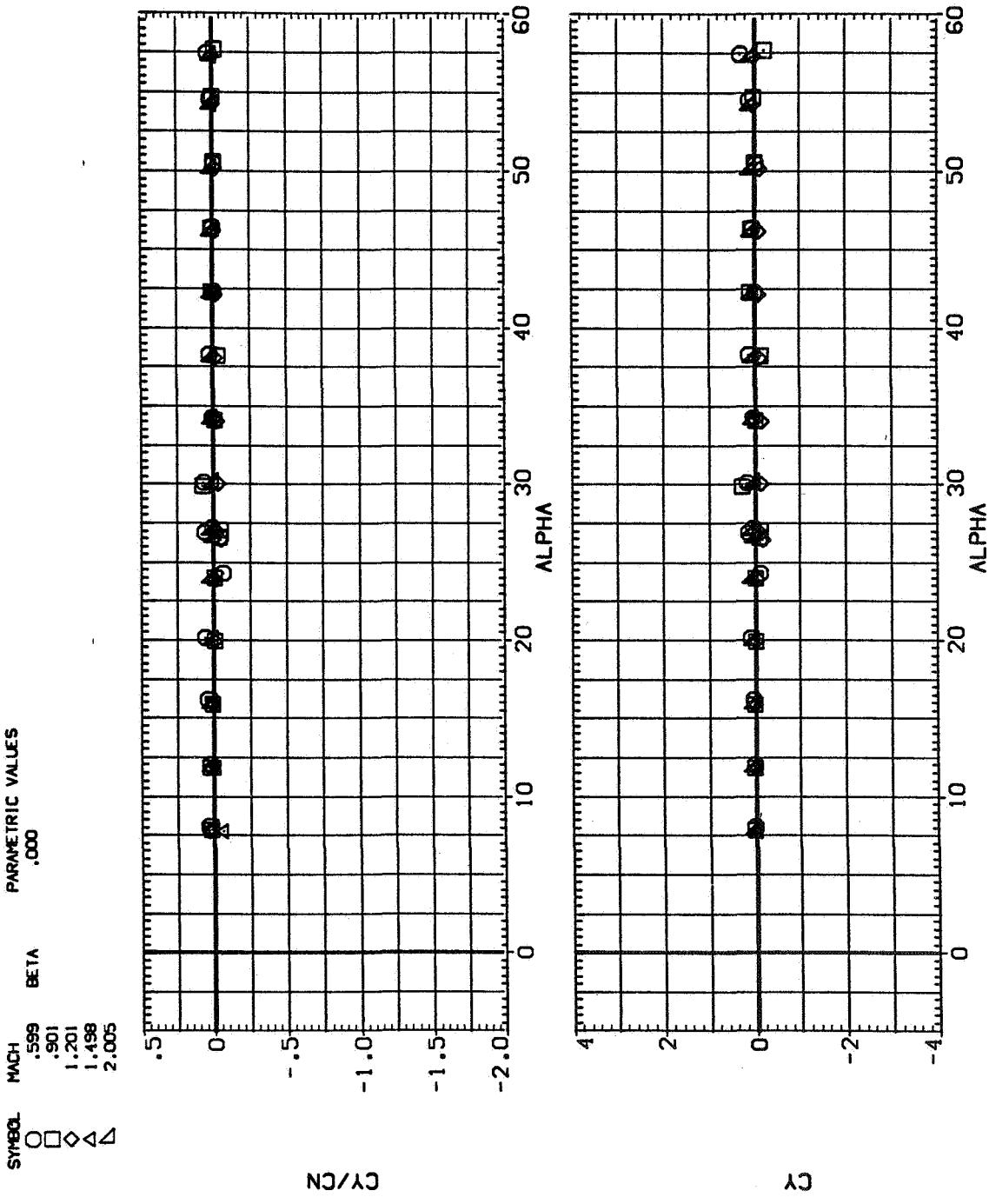

(b) C_Y/C_N and C_Y versus α

Figure 23.– Continued.

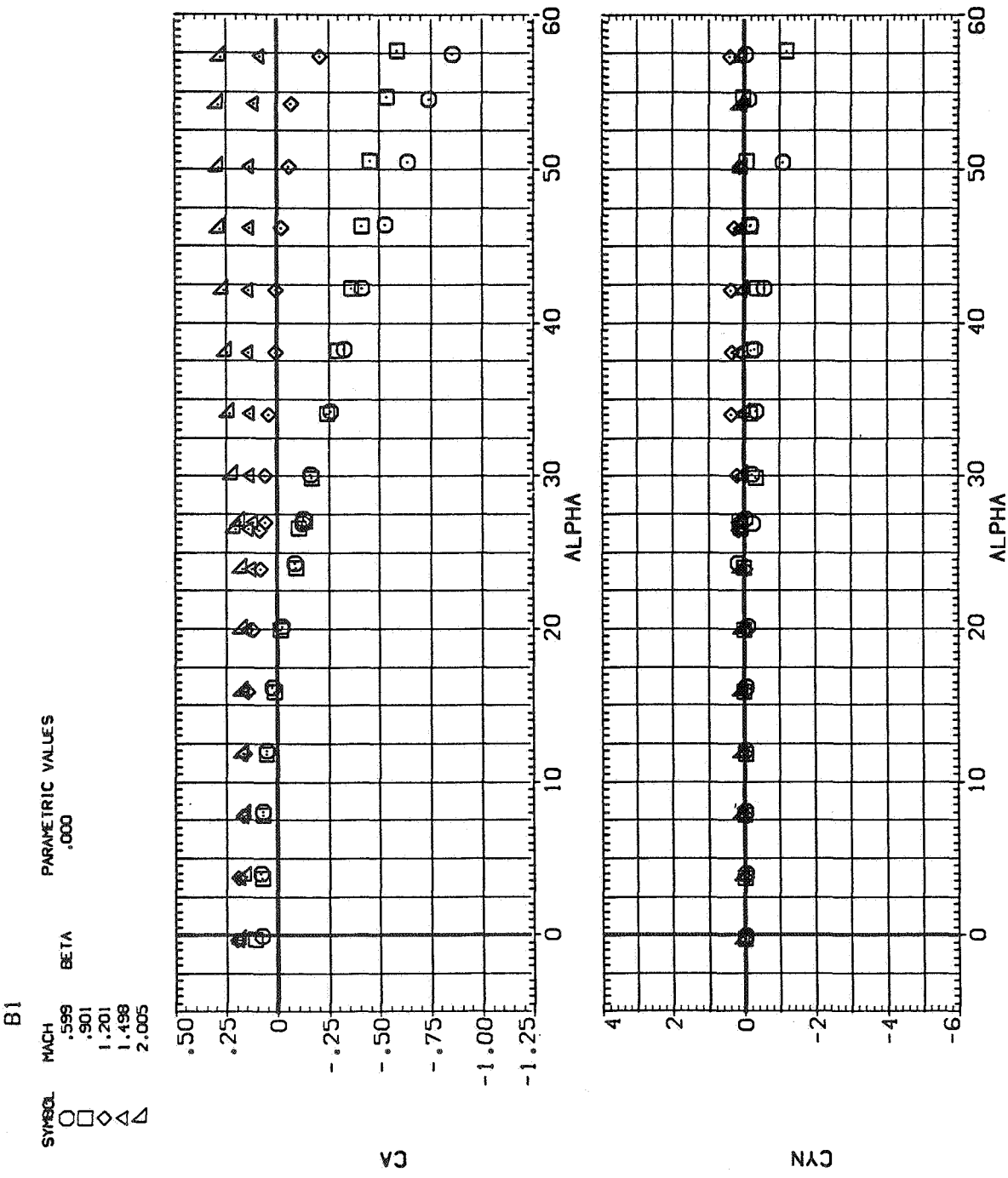

(c) C_A and C_n versus α

Figure 23.– Concluded.

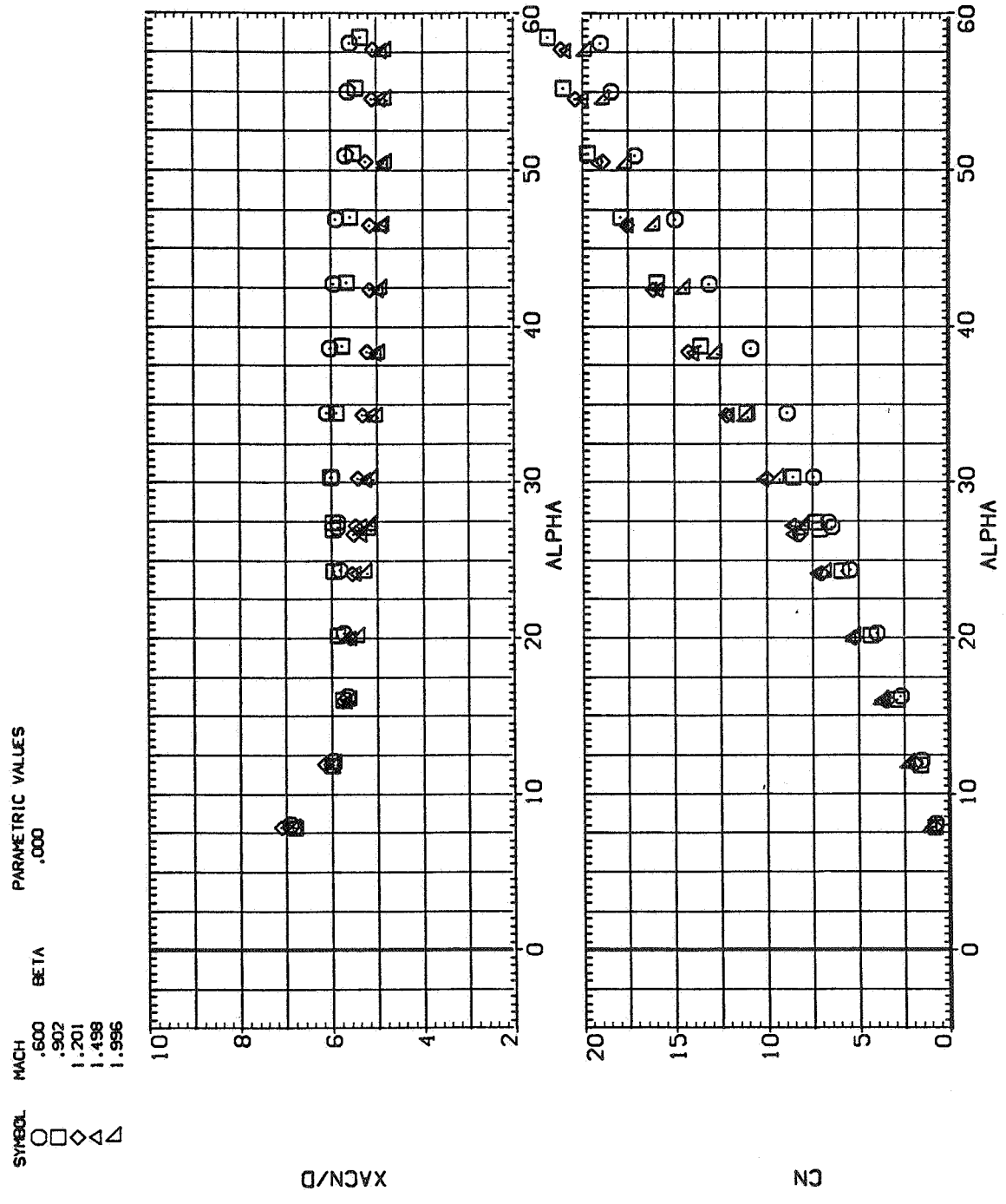

(a) x_{ac_N}/d and C_N versus α

Figure 24.– Effect of Mach number for B_2, $\phi = 0°$.

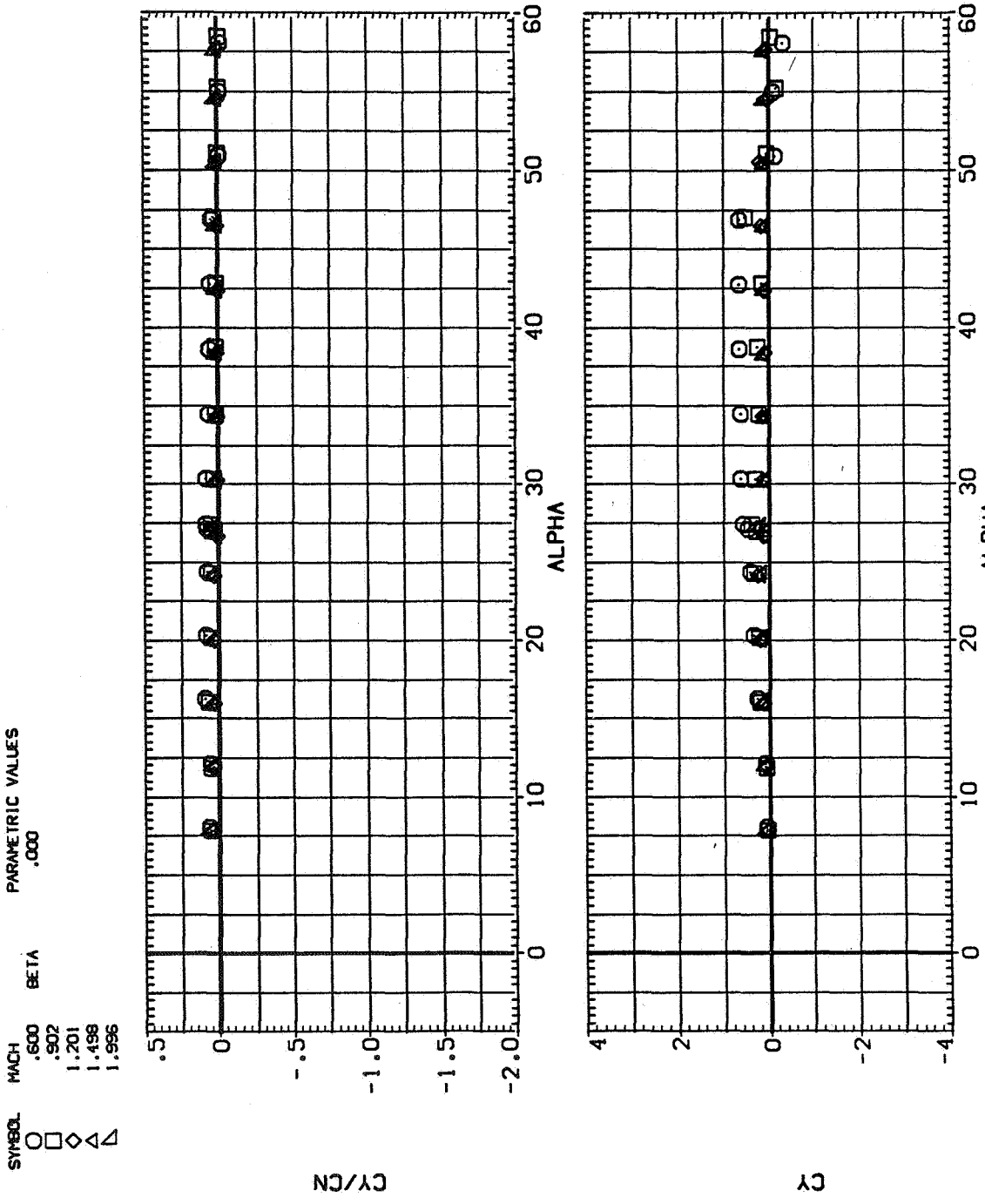

(b) C_Y/C_N and C_Y versus α

Figure 24.– Continued.

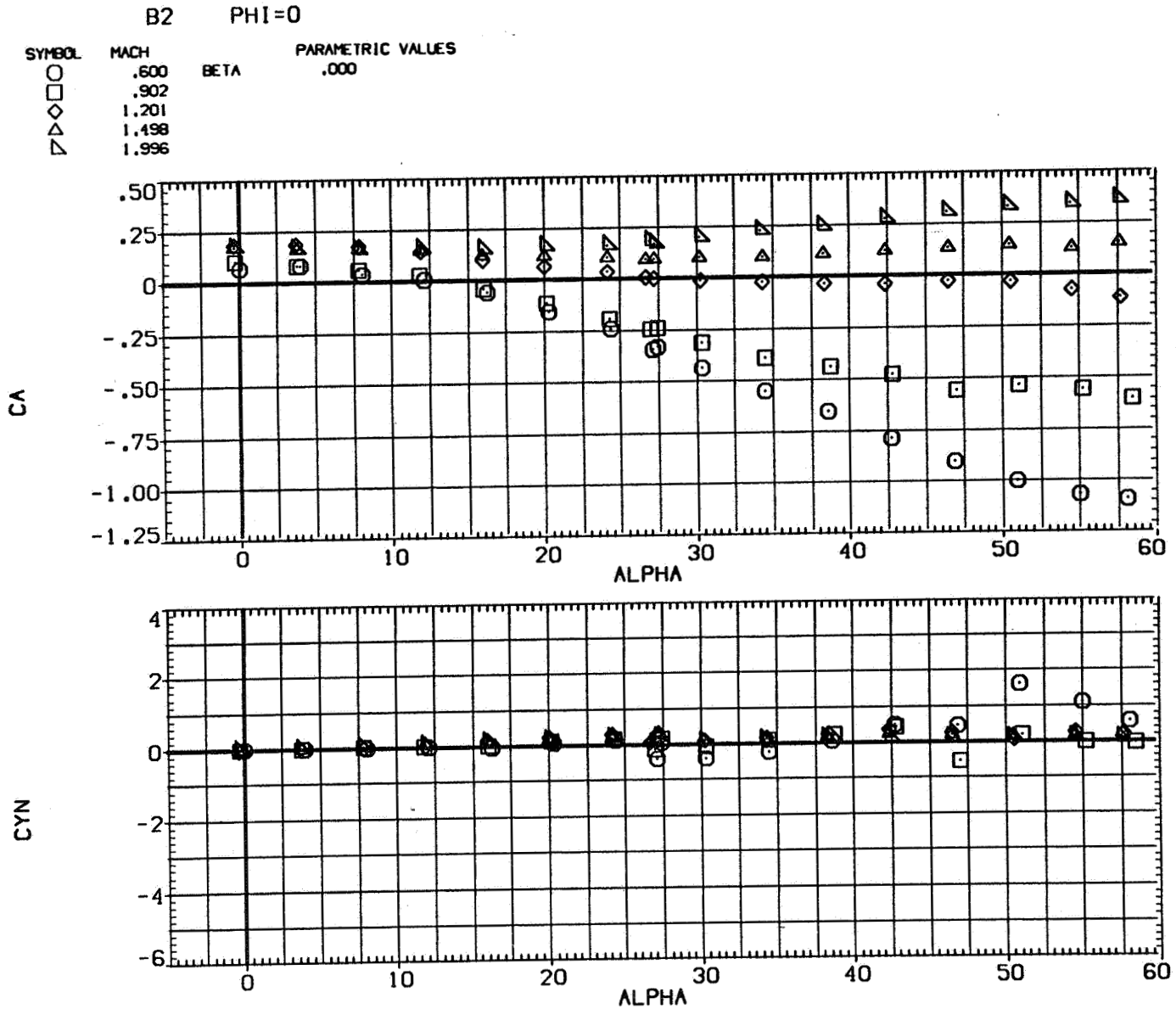

(c) C_A and C_n versus α

Figure 24.– Concluded.

NATIONAL AERONAUTICS AND SPACE ADMINISTRATION
WASHINGTON, D.C. 20546

OFFICIAL BUSINESS
PENALTY FOR PRIVATE USE $300

SPECIAL FOURTH-CLASS RATE
BOOK

POSTAGE AND FEES PAID
NATIONAL AERONAUTICS AND
SPACE ADMINISTRATION
451

U.S. MAIL

POSTMASTER: If Undeliverable (Section 158
Postal Manual) Do Not Return

"The aeronautical and space activities of the United States shall be conducted so as to contribute . . . to the expansion of human knowledge of phenomena in the atmosphere and space. The Administration shall provide for the widest practicable and appropriate dissemination of information concerning its activities and the results thereof."

—NATIONAL AERONAUTICS AND SPACE ACT OF 1958

NASA SCIENTIFIC AND TECHNICAL PUBLICATIONS

TECHNICAL REPORTS: Scientific and technical information considered important, complete, and a lasting contribution to existing knowledge.

TECHNICAL NOTES: Information less broad in scope but nevertheless of importance as a contribution to existing knowledge.

TECHNICAL MEMORANDUMS: Information receiving limited distribution because of preliminary data, security classification, or other reasons. Also includes conference proceedings with either limited or unlimited distribution.

CONTRACTOR REPORTS: Scientific and technical information generated under a NASA contract or grant and considered an important contribution to existing knowledge.

TECHNICAL TRANSLATIONS: Information published in a foreign language considered to merit NASA distribution in English.

SPECIAL PUBLICATIONS: Information derived from or of value to NASA activities. Publications include final reports of major projects, monographs, data compilations, handbooks, sourcebooks, and special bibliographies.

TECHNOLOGY UTILIZATION PUBLICATIONS: Information on technology used by NASA that may be of particular interest in commercial and other non-aerospace applications. Publications include Tech Briefs, Technology Utilization Reports and Technology Surveys.

Details on the availability of these publications may be obtained from:

SCIENTIFIC AND TECHNICAL INFORMATION OFFICE

NATIONAL AERONAUTICS AND SPACE ADMINISTRATION

Washington, D.C. 20546